REZA ZOMORRODI MOGHADDAM

INFLUENCE OF THE DENDRITIC MORPHOLOGY ON ELECTROPHYSIOLOGICAL RESPONSES OF THALAMOCORTICAL NEURONS

Thèse présentée
à la Faculté des études supérieures et postdoctorales de l'Université Laval
dans le cadre du programme de doctorat en physique
pour l'obtention du grade de Philosophiae Doctor (Ph.D)

DE DEPARTEMENT DE PHYSIQUE, DE GENIE PHYSIQUE ET D'OPTIQUE
FACULTÉ DES SCIENCES ET DE GÉNIE
UNIVERSITÉ LAVAL
QUÉBEC

2011

Résumé

Les neurones thalamiques de relai ont un rôle exclusif dans la transformation et de transfert de presque toute l'information sensorielle dans le cortex. L'intégration synaptique et la réponse électrophysiologique des neurones thalamiques de relai sont déterminées non seulement par l'état du réseau impliqué, mais ils sont également contrôlés par leurs propriétés intrinsèques tels les divers canaux ioniques voltage-dépendants ainsi que l'arborisation dendritique élaboré. Par conséquent, investiguer sur le profil complexe de morphologie dendritique et sur les propriétés dendritiques actives révèle des renseignements importants sur la fonction d'entrée-sortie de neurones thalamiques de relai.
Dans cette étude, nous avons reconstruit huit neurones thalamocorticaux (TC) du noyau VPL de chat adulte. En se basant sur ces données morphologiques complètes, nous avons développé plusieurs modèles multicompartimentaux afin de trouver un rôle potentiellement important des arbres dendritiques des neurones de TC dans l'intégration synaptique et l'intégration neuronale.

L'analyse des caractéristiques morphologiques des neurones TC accordent des valeurs précises à des paramètres géométriques semblables ou différents de ceux publiés antérieurement. En outre, cette analyse fait ressortir de tous nouveaux renseignements concernant le patron de connectivité entre les sections dendritiques telles que l'index de l'asymétrie et la longueur de parcours moyen (c'est-à-dire, les paramètres topologiques).
Nous avons confirmé l'étendue des valeurs rapportée antérieurement pour plusieurs paramètres géométriques tels que la zone somatique (2956.24±918.89 μm^2), la longueur dendritique totale (168017.49±4364.64 μm) et le nombre de sous-arbres (8.3±1.5) pour huit neurones TC. Cependant, contrairement aux données rapportées antérieurement, le patron de ramification dendritique (avec des cas de bifurcation 98 %) ne suit pas la règle de puissance de Rall 3/2 pour le ratio géométrique (GR), et la valeur moyenne de GR pour un signal de propagation est 2,5 fois plus grande que pour un signal rétropropagé. Nous avons également démontré une variabilité significative dans l'index de symétrie entre les sous-arbres de neurones TC, mais la longueur du parcours moyen n'a pas montré une grande variation à travers les ramifications dendritiques des différents neurones.

Nous avons examiné la conséquence d'une distribution non-uniforme des canaux T le long de l'arbre dendritique sur la réponse électrophysiologique émergeante, soit le potentiel Ca^{2+} à seuil bas (low-threshold calcium spike, LTS) des neurones TC. En appliquant l'hypothèse du «coût minimal métabolique», nous avons constaté que le neurone modélisé nécessite un nombre minimal de canaux-T pour générer un LTS, lorsque les canaux-T sont situés dans les dendrites proximales.

Dans la prochaine étude, notre modèle informatique a illustré l'étendue d'une rétropropagation du potentiel d'action et de l'efficacité de la propagation vers des PPSEs générés aux branches dendritiques distales. Nous avons démontré que la propagation dendritique des signaux électriques est fortement contrôlée par les paramètres morphologiques comme illustré par les différents paliers de polarisation obtenus par un neurone à équidistance de soma pendant la propagation et la rétropropagation des signaux électriques. Nos résultats ont révélé que les propriétés géométriques (c.-à-d. diamètre, GR) ont un impact plus fort sur la propagation du signal électrique que les propriétés topologiques. Nous concluons que (1) la diversité dans les propriétés morphologiques entre les sous-arbres d'un seul neurone TC donne une capacité spécifique pour l'intégration synaptique et l'intégration neuronale des différents dendrites, (2) le paramètre géométrique d'un arbre dendritique fournissent une influence plus élevée sur le contrôle de l'efficacité synaptique et l'étendue du potentiel d'action rétropropagé que les propriétés topologiques, (3) neurones TC suivent le principe d'optimisation pour la distribution de la conductance voltage-dépendant sur les arbres dendritiques.

Abstract

Thalamic relay neurons have an exclusive role in processing and transferring nearly all sensory information into the cortex. The synaptic integration and the electrophysiological response of thalamic relay neurons are determined not only by a state of the involved network, but they are also controlled by their intrinsic properties; such as diverse voltage-dependent ionic channels as well as by elaborated dendritic arborization. Therefore, investigating the complex pattern of dendritic morphology and dendritic active properties reveals important information on the input-output function of thalamic relay neurons.
In this study, we reconstructed eight thalamocortical (TC) neurons from the VPL nucleus of adult cats. Based on these complete morphological data, we developed several multi-compartment models in order to find a potentially important role for dendritic trees of TC neurons in the synaptic integration and neuronal computation.

The analysis of morphological features of TC neurons yield precise values of geometrical parameters either similar or different from those previously reported. In addition, this analysis extracted new information regarding the pattern of connectivity between dendritic sections such as asymmetry index and mean path length (i.e., topological parameters). We confirmed the same range of previously reported value for several geometric parameters such as the somatic area (2956.24±918.89 μm^2), the total dendritic length (168017.49±4364.64 μm) and the number of subtrees (8.3±1.5) for eight TC neurons. However, contrary to previously reported data, the dendritic branching pattern (with 98% bifurcation cases) does not follow Rall's 3/2 power rule for the geometrical ratio (GR), and the average GR value for a forward propagation signal was 2.5 times bigger than for a backward propagating signal. We also demonstrated a significant variability in the symmetry index between subtrees of TC neurons, but the mean path length did not show a large variation through the dendritic arborizations of different neurons.

We examined the consequence of non-uniform distribution of T-channels along the dendritic tree on the prominent electrophysiological response, the low-threshold Ca^{2+} spike (LTS) of TC neurons. By applying the hypothesis of "minimizing metabolic cost", we

found that the modeled neuron needed a minimum number of T-channels to generate low-threshold Ca^{2+} spike (LTS), when T-channels were located in proximal dendrites.

In the next study, our computational model illustrated the extent of an action potential back propagation and the efficacy of forward propagation of EPSPs arriving at the distal dendritic branches. We demonstrated that dendritic propagation of electrical signals is strongly controlled by morphological parameters as shown by different levels of polarization achieved by a neuron at equidistance from the soma during back and forward propagation of electrical signals. Our results revealed that geometrical properties (i.e. diameter, GR) have a stronger impact on the electrical signal propagation than topological properties.

We conclude that (1) diversity in the morphological properties between subtrees of a single TC neuron lead to a specific ability for synaptic integration and neuronal computation of different dendrites, (2) geometrical parameter of a dendritic tree provide higher influence on the control of synaptic efficacy and the extent of the back propagating action potential than topological properties, (3) TC neurons follow the optimized principle for distribution of voltage-dependent conductance on dendritic trees.

Foreword

This Ph.D. thesis contains five chapters, presented in from of a general introduction, conclusion and scientific articles (that either published or under final preparation for publication in international peer-reviewed journals). The first chapter is consisted of two parts: first section is a brief summary of theoretical neuroscience and computational methods used in our research and second part is a general review of the thalamus and thalamocortical neurons. Chapters two through four are composed of published articles or soon-to-be published article. All references related to articles are presented at the end of the corresponding paper. The bibliography used for both introduction and conclusion is listed at the very end of the thesis.

The completion of this thesis would not have been possible without the help, advice, and encouragement of my supervisor, Dr. Helmut Kroger and my co-supervisor, Dr. Igor Timofeev.

I am heartily thankful to Dr. Kroger, whose inspiration, guidance and support to help me to start my research in the neuroscience field and accomplish this work. It has been an honor to be his Ph.d student.

I want to express my sincere gratitude to Dr. Timofeev, for his endless help, support, encouragement and patience during all these years of my study. He has taught me, both consciously and unconsciously, how to be a good scientist. I appreciate all his contributions of time, ideas, and funding to make my Ph.d.

I am grateful to Dr. Alex S. Ferecskó and Dr. Krisztina Kovács, for their excellent work on extracting morphological data of thalamocortical neurons.

I am especially thankful to Dr. Kalatin Toth for proof-reading the thesis and for her useful comments on the manuscript; Josée Seigneur for his generous help for the translation of abstracts to French.

I would like to appreciate my colleagues in Dr. Timofeev's research group, who have been a source of friendships as well as good advice and collaboration. Especially, I like to thank Josée Seigneur, Sylvain Chauvette, Eliane Proulx, Sînziana Avramescu, Dragos Nita, Maxime Lemieux, Courtney Pinard, and Laszlo Grand. I am also thankful to my colleagues in physics department, who worked together; Jean-Francois Laprise and Ahmad Hosseinizadeh.

Most importantly, my heartfelt gratitude goes to my loving, supportive, encouraging, and patient wife Sahar for her faithful support during my study. Without her emotional and spiritual support, completion of this PhD degree might have been impossible.

Last but not least, I would like to thank my family, who, even being far away, were always there to support me with their endless love. I owe them all my achievements.

When you can measure what you are speaking about, and express it in numbers, you know something about it; but when you cannot measure it, your knowledge is of a meager and unsatisfactory kind; it may be the beginning of knowledge, but you have scarcely in your thoughts advanced to state of Science, whatever the matter may be. Lord Kelvin [PLA, vol. 1 "Electrical Units of Meaurment",1883-05-03]

Table of Contents

List of tables

List of figures

List of abbreviations

Asym_index	asymmetry index
BP-AP	back propagation of action potential
C_m	membrane capacitance
d	diameter of dendritic segment
$d_{1,2}$	diameter of daughters at branching point
d_p	diameter parent at branching point
E_{ion}	equilibrium potential
EPSP	excitatory postsynaptic potential
FP	forward propagation
GABA	gamma-amino butyric acid
$\overline{G}_{ion}$	maximum of an ionic conductance
G_{ion}	ionic conductance
G_k	potassium conductance
G_L	leak conductance
G_{Na}	sodium conductance
GR	geometrical ratio
HH model	Hodgkin-Huxley model
I_A	fast transient potassium current
I_h	hyperpolarization-activated cation current
I_{inj}	injected current
I_{ionic}	ionic currents
$I_{k[ca]}$	calcium- dependent potassium current
I_{km}, I_{ks}	Slow transient potassium currents
I_L	high-voltage Ca^{2+} current
$I_{Na(p)}$	persistent Na^+ current
I_T	transient Ca^{2+} current
I_{total}	total current
L	length of dendritic segment
LGN	lateral geniculate nucleus
LTS	low-threshold Ca^{2+} spike
MPL	mean path length
NMDA	N-methyl-D-aspartate
N^{thr}	threshold number of channel
N^{tota}	total number of channel
P_{ca}	permeability of Ca^{2+} channel
R_a	axial resistivity
r_i	intracellular resistivity
R_{in}	input resistance
r_m	membrane resistance
RTN	reticular thalamic nucleus
TC	thalamocortical
T-channel	low-threshold Ca^{2+} channel
V_m	membrane potential

$V_m(x,t)$	membrane potential for a specific moment (t) and location (x)
VPL	ventral posterolateral
VPM	ventral posteromedial
Y_{ion}	gating particle for an ionic channel
α_s, β_s	voltage-dependent rate constants
λ	space constant or DC length
λ_f	frequency-dependent space constant
τ	time constant

Introduction

1.1 A brief review on computational neuroscience

After long but successful efforts by human beings to establish scientific tools and logic (Popper, 2002), to dig out the principal rules and building blocks that regulate and fabricate our matter-energy world, scientists challenge their knowledge to face the most complex system: The Brain.

Between different scientific approaches that study structures and functions of the brain, computational neuroscience employs mathematical tools, physical theory and engineering technique in order to understand the unique performance of the brain by comparing its operation with the most complex human made machine: The computer.

Physical science demonstrated that no matter how complex an observed system is, its average dynamic can be described by a set of simple laws that are formulated with the precise language of mathematical equations. Nevertheless, applying the same approach to investigate performance of the brain gives rise to several basic questions: Are there any simple mathematical laws that may capture the rules that govern the operation of neural systems? Will we one day be able to understand the brain to a similar degree as we now understand the material world? If so, can we quantitatively predict the complicated cognitive behaviors underlying arbitrary external and internal conditions and build good brain emulators, very much as the trajectory of an asteroid or design a bridge with a given safety level (Tsodyks, 2008)?. Although the ultimate goal of computational neuroscience has been challenged by philosophical questions and has been looked at with some skepticism by the experimental neuroscience community, this multidisciplinary field created a thriving branch in brain research (De Schutter, 2008; Destexhe and Crunelli, 2008; Tsodyks, 2008).

Theoretical or computational neuroscience started with purely mathematical and engineering procedures by considering the brain as a biological counterpart of an advanced

computing machine. This approach leads to extensive use of computer science methods to analyze input-output function of the brain. In this point of view, scientists are looking for an algorithm for a programmable machine that illustrates, roughly, the same performance of the brain for a specific task. Artificial neural networks, reinforcement theory, computer vision and Bayesian brain are some successful examples of this approach. Despite significant achievements, this approach still appears to be largely detached from more biological inspired modeling (De Schutter, 2008; Tsodyks, 2008).

However, in recent years, close collaborations between computational and experimental neuroscientists have resulted in a remarkable growth of models that can directly use experimental data and, consequently, refine our understanding of brain functions or its malfunctions. In this approach, computational models may not apply only to predict or analyze experimental observations (Abbott, 2008; Destexhe and Crunelli, 2008; Tsodyks, 2008), but they also may directly deduce from the data using sophisticated fitting techniques (Hecht-Nielsen and McKenna, 2003; Feng, 2004; De Schutter, 2010). The model may even interact directly with living neurons (i.e., dynamic clamp protocol, which introduced in 1992 by Sharp et al.), that was beyond belief a few decades ago (Sharp et al., 1992; Markram, 2006; Druckmann et al., 2007; Jolivet et al., 2008).

Theoretical approach brought several advantages to the field of neuroscience. Expressing our thoughts about a phenomenon in terms of mathematical equations gives a precise, complete and self-consistent model that provides an opportunity to test hypotheses before an experiment or prompts new ideas, generalizes the model and provides new ways of thinking (Robinson and Kawai, 1993; Sharp et al., 1993; Hughes et al., 1998; Brette et al., 2008; Destexhe and Crunelli, 2008; Milescu et al., 2008; Economo et al., 2010).

1.1.1 First computational model of neurons

Presence of the mathematical model to explain neurophysiological data could be traced to some early works of integrate-and-fire model (Lapicque, 1907; Grossberg, 1982; Hopfield, 1982; Amit et al., 1985; Gerstner et al., 1996; Koch, 1999; Koch and Leisman, 2000;

Dayan and Abbott, 2005). However, the Hodgkin-Huxley (HH) model considered as root and groundwork of the field that came after the pioneer experimental and analytical work by Kenneth Cole to describe membrane potential of the squid giant axon (Cole and Hodgkin, 1939; Cole and Baker, 1941; Cole and Curtis, 1941; Sejnowski et al., 1988; Koch, 1999). Combination of a primarily theoretical and computational model by Andrew Huxley and delicate experimental design by Alan Hodgkin gave them power to analyze data and summarize them in an astonishing set of equations which, after 50 years are still used in their original form (Hodgkin, 1937; Hodgkin and Huxley, 1945, 1947; Huxley and Stampfli, 1949; Hodgkin and Huxley, 1952c). In addition, the HH model created a framework for other excitable membranes (Hodgkin and Huxley, 1952b). They won the Noble Prize in 1963.

Using a method, later named the voltage clamp, and pharmacological current blocker, they manipulate the voltage of the axon membrane and measure the resultant current that flowed through its ion channels. They demonstrated that current could be carried through the membrane either by charging the membrane capacitance or by movement of ions through the resistances in parallel with the capacity. Therefore, total transmembrane current can be expressed as:

$$I_{total} = I_{ionic} + c_m \frac{dV_m(t)}{dt} \tag{1-1}$$

Where I_{total} is total current, I_{ionic} indicates ionic currents, c_m and V_m are membrane capacitance and potential, respectively. Hodgkin and Huxley postulated the following phenomenological model of events underlying the generation of action potential in the squid giant axon (Jack et al., 1983; Rinzel, 1990):

(1) Two major ionic conductances, sodium (G_{Na}) and potassium (G_k) are sufficient to generate the action potential and explain the threshold, the refractory period and anode break (action potential after offset a hyperpolarized current). These conductances are time and voltage-dependent and operate independent of each

other. They also find another smaller leak conductance (voltage independent) that passes through the membrane. Hence,

$$I_{ionic} = I_{Na} + I_K + I_{leak}$$

(1-2)

(2) The ionic current (I_{ion}) is equal to the conductance (G_{ion}) multiplied by the difference between the membrane potential (V_m) and the equilibrium potential for the given ion (E_{ion}).

$$I_{ion} = G_{ion}(V_m(t),t)\,(V_m(t) - E_{ion})$$

(1-3)

The equilibrium potential, E_{ion}, is given by Nerst's equation (Hodgkin and Huxley, 1952b; Johnston and Wu, 1995; Koch, 1999).

(3) The ionic conductances are controlled by gating particles and G_{ion} can be written as the product of gating particles ,$Y_{ion}(V_m,t)$, and maximum conductance, $\overline{G}_{ion}$, as follow

$$G_{ion} = \overline{G}_{ion}\, Y_{ion}(V_m,t)$$

(1-4)

Indeed, gating particle refers to the fraction of the open channels and varies between 0 and 1.

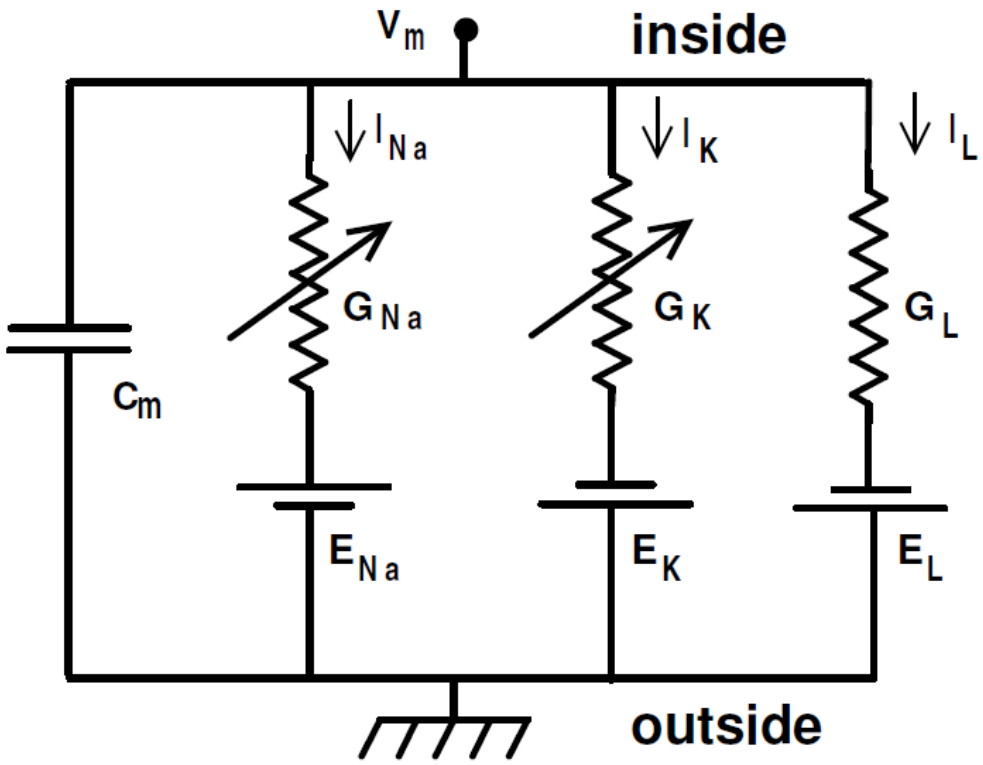

Figure 1-1 Illustration of the electrical equivalent circuit for membrane of the squid giant axon. Hodgkin-Huxley proposed that membrane potential could be simulated by an equivalent RC-circuit of the membrane. The variable resistances represent voltage-dependent conductances (G_{ion}), reversal potential (E_{ion}), ionic current (I_{ion}), membrane capacitance (C_m) and V_m indicates membrane potential (Hille, 2001).

1.1.2 Ion Channels Underlying Action Potentials

Hodgkin and Huxley found out that the delayed onset and exponential decay of ionic conductance upon a step depolarization current could not be described by a simple differential equation. To overcome to this problem, they proposed a first-order kinetics mechanism (Hodgkin and Huxley, 1952b). Although, today's measurement of a single channel could be described more precisely by stochastic model (Weiss, 1996; Jones, 2006), nonetheless, introducing gating state and attribute activation and inactivation state to an ionic conductance provided an efficient explanation of ionic channel kinetics and their contribution to neural activity.

1.1.2.1 Activation and inactivation state

In the Hodgkin-Huxley model of ionic conductance, the flow of ions through a channel are controlled by the gate state (Hodgkin and Huxley, 1952b). An individual gate can be in one of two states; active or inactive, which means the channel is permeable or non-permeable for ionic flow. When all channel gates are in the active state, ions can pass through the channel and the channel is open. While if any of these gates is in the inactive state, ions cannot flow and the channel is closed.

By considering two available states for a gating variable, with probability of ***S*** being in active and ***1-S*** in the inactive sate and assuming that a first-order-kinetics law governs the transition between two states, we can write the following reaction scheme:

$$S \underset{\alpha_s}{\overset{\beta_s}{\rightleftarrows}} 1 - S \tag{1-5}$$

Where α_s is a voltage-dependent rate constant, which indicates the transition rate between closed to open and β_s express transition rate from the active (open) to inactive (close) state. In the HH model by considering a large number of channels instead of a single channel, ***S***

and ***1-S*** may interpret as the fraction of channels in the open and close state, respectively. This first order reaction model can be expressed by a first order differential equation,

$$\frac{dS}{dt} = \alpha_s (1 - S) - \beta_s (S)$$

(1-6)

According to this model, a channel could have its maximum conductance when the gate is open and gains zero value when the gate is closed. Therefore, for a population of channels total conductances will be proportional to probability of the opening state of all gates,

$$G_{ion} \propto \prod_i S_i$$

$$G_{ion} = \overline{G}_{ion} \prod_i S_i$$

(1-7)

Where G_{ion} is defined as the maximum possible conductance when all the channels are open.

1.1.2.2 Potassium current

Voltage clamp experiments to identify conductance of the potassium current revealed that only a fourth power of an exponential function could be fitted to the experimental data. Therefore, Hodgkin-Huxley proposed the following mathematical description (Hodgkin and Huxley, 1952b) for potassium current,

$$I_k = \overline{G}_k \, n^4 \, (V_m - E_k)$$

$$\frac{dn}{dt} = \alpha_n \, (1-n) - \beta_n \, n$$

(1-8)

It was assumed that four similar gating particles controlled the potassium current across the membrane. **n** represents the proportion of the particles in an open (active) state and **1- n** represents the proportion that is in the close (inactive) state. Hodgkin and Huxley approximate (Hodgkin and Huxley, 1952b) the voltage dependencies of rate constant, $\alpha_{..}$ $\beta_{..}$, by

$$\alpha_n(V) = \frac{10 - V}{100\,(e^{(10-V/10)} - 1)}, \quad \beta_n(V) = 0.125\, e^{-V/80}$$

(1-9)

1.1.2.3 Sodium current

Voltage clamp data illustrated complex dynamics for sodium conductance. In order to fit a mathematical model to data, Hodgkin-Huxley postulated the existence of two gating particles, which are responsible for activation (m) and inactivation state (h). Hence, they proposed the following equation for sodium current,

$$I_{Na} = \overline{G}_k \, m^3 h \, (V_m - E_{Na})$$

$$\frac{dm}{dt} = \alpha_m \, (1-n) - \beta_m \, n$$

$$\frac{dh}{dt} = \alpha_h \, (1-n) - \beta_h \, n$$

(1-10)

Empirically, they derived the following equations for the rate constant:

$$\alpha_m = \frac{25-V}{10(e^{(25-V)/10} - 1)}, \qquad \beta_m = 4e^{-V/18}$$

$$\alpha_h = 0.07e^{-V/20}, \qquad \beta_h = \frac{1}{e^{(30-V)/10} + 1}$$

(1-11)

1.1.3 Hodgkin-Huxley model

In computational neuroscience, researchers refer to Hodgkin-Huxley type of equations as the conductance-based model. In this approach, the electrical activity of a neuron is simulated by an equivalent circuit of the form shown in Fig. 1-1, which has a time- and voltage- dependent conductance (or resistance) and its corresponding ionic battery (reversal potential) for the specific ionic current in the membrane of the neuron. HH model can be summarized by following set of differential equation,

$$Cm\frac{dV}{dt} = \sum_{ion} \overline{G}_{ion}\ P_{ion}^{a}\ Q_{ion}^{b}(E_{ion} - V) + G_L(E_L - V) + I_{inj}$$

$$\frac{dS_{ion}}{dt} = \alpha_{S_{ion}}(1 - S_{ion}) - \beta_{S_{ion}}(S_{ion}), \qquad S = P, Q$$

(1-12)

Where P and Q show the activation and the inactivation gate, a and b indicate required number of activation or inactivation particles to control the ionic conductance, G_L is leak conductance and I_{inj} indicates injected current into the membrane.

HH model consists of a nonlinear equation for the membrane that is accompanied with several linear differential equations for kinetics of gating particles. Increasing the number of ionic conductances in the model raises the computational cost to implement this model and consequently, makes it difficult to employ it for a large network of spiking neurons (Izhikevich, 2004). However, today's advance supercomputers create a possibility to use HH model for a large network of spiking neurons (Markram, 2006; Ananthanarayanan et al., 2009).

Using simple mathematical models in order to investigate the input-output function of the brain with analytical and feasible computational tools lead to the development of several simpler mathematical models such as different forms of integrate-and-fire, FitzHugh-Nagumo, Morris-Lecar, Hindmarsh-Rose, Wilson, Rulkov, Izhekevich and etc. (Izhikevich, 2004; Rulkov et al., 2004). These models are preferable for analytical study and constructing a large network, but mostly they are abstract mathematical models with non-biological parameters in their equations and most of them are designed to reproduce specific firing patterns seen in electrophysiological recordings.

Employing HH model to investigate the electrophysiological behavior of a single neuron has two main advantages: first, this model can regenerate the most prominent neuronal

firing patterns and second, its parameters are biophysically meaningful and experimentally measurable.

In the early computational simulation based of HH model, only temporal aspect of the input-output function of a neuron was under investigation. In this approach, soma was the main and the only section in a neuron that performed decoding and coding process. Therefore, independent of complex arborization of a neuron, mathematical equations were describing only a reduced morphological shape of a neuron, which represented as an isopotential sphere.

This phenomenological model was; (a) acceptable for experimentalists, since they had assumption that currents were mostly confined at the soma and (b) plausible for theoretical work since the describing equation for input-output function had a relatively simple form. However, results of more precise experimental data using intracellular recordings revealed the importance of dendritic trees (Koch, 1999; Gerstner and Kistler, 2002; Izhikevich, 2003; Feng, 2004; Dayan and Abbott, 2005; De Schutter, 2010). The interpretation of new experimental data needed a model that assigns an important role for the spatial distribution of synaptic inputs on dendritic arborizations. Such models require not only a temporal domain, but also a spatial domain in order to consider propagation of the electrical signal or the interaction of synaptic activity over a dendritic tree.

1.1.4 Cable theory

In order to show the significance of dendritic arborization for neuronal input-output function, Wilfirid Rall proposed a cable theory to involve the complexity of morphological and biophysical properties of a neuron. In this theory, Rall revealed the influence of dendritic morphology on synaptic integration and attenuation electrical potential on dendritic trees (Rall et al., 1995).

Developing cable theory stands on several basic assumptions:

1- Generated magnetic field by ionic movements during the action potential is negligible and can be excluded from a mathematical model. The impact of magnetic field associated with ionic currents during an action potential on electric field is in order of 10^{-9} (Rosenfalck, 1969).

2- Ohm's law is adequate to describe an electrical current within the axon or dendritic membrane. Only in thin fibers (< 1μm), longitudinal current due to ionic concentration gradient may play a role, that will need another equation than Ohm's law, in order to describe the relation between electric current and electric field (Koch, 1999).

3- A dendritic segment is considered as a cylindrical object with uniform electrical properties. However, today's precise 3D reconstruction from successive EM section illustrated that the cross section of dendritic segment is elliptical rather than circular (Kubota et al., 2009).

4- The transmembrane resistance is much higher than intracellular resistivity and the dominant fraction of ionic currents flows in parallel to its longitudinal axis. Therefore, the equation that describes propagation of an electrical signal along the dendritic segment is a one-dimensional equation. Rall showed that the radial and angular membrane potential typically decays 1000 times faster than the component along the axis (Rall, 1969).

5- The extracellular domain is a homogeneous environment (isopotential space) with zero resistivity. Electrical charge in the cytoplasm (inside or outside) relaxes in a matter of microseconds. Therefore, any capacitive effects can be ignored in this time scale or longer time, and intra or extra-cellular environment can be approximated only by Ohmic resistance environment. In addition, small extracellular potential and its

decay distance compare to diameter of the fiber, implies the extracellular space can be considered as a homogenous dielectric, averaging over local inhomogeneities(Koch, 1999).

Considering these assumptions, Rall derived a one-dimensional partial differential equation (Rall, 1959, 1962b, a) that describes the dynamic of electrical potential along a cylindrical dendritic segment, $V_m(x,t)$, with passive property (e.g., no voltage- dependent ionic conductances),

$$\frac{r_m}{r_i}\frac{\partial^2 V_m(x,t)}{\partial x^2} = r_m c_m \frac{\partial V_m(x,t)}{\partial t} + (V_m(x,t) - V_{rest}) + r_m I_{inj}(x,t) \tag{1-13}$$

Where r_m and r_i indicate the membrane and intracellular resistivity per unit length. c_m shows membrane capacitance per unit length.

Mathematically, this is a parabolic type of a partial differential equation that can be solved analytically for a transient current input into a class of dendritic trees that are equivalent to unbranched cylinders. This equation has a straightforward solution for a few geometrical features such as infinite, semi-infinite or finite length (x=L) with different boundary conditions such as Neumann ($\frac{\partial V\ x}{\partial x}|_{x=L} = 0$) or Dirichlet ($V\ x\ |_{x=L} = 0$) (Johnston and Wu, 1995; Koch, 1999; Gerstner and Kistler, 2002).
Several algorithms proposed to find an analytical solution for an arbitrary branching structure or current injection, but these methods become very complex and computationally expensive by considering synaptic inputs and voltage-depended conductances (Johnston and Wu, 1995; Koch, 1999; Gerstner and Kistler, 2002).

The linear cable equation, Eq.1-13, only determines the time-space dependency of the membrane potential on an unbranched dendritic segment with a constant diameter. Obviously, applying this approach to a real neuron creates a serious obstacle.

The basic assumptions that considered a dendritic tree, as an unbranched cylindrical object with uniform biophysical properties cannot represent all features of input-output function of a neuron. A realistic model of a neuron should include the presence of non-uniform electrical properties and highly branched dendritic trees. Therefore, one needs a completely new model or new technique to apply the cable theory approach.

Fortunately, mathematicians had already developed several numerical techniques to solve a one-dimensional partial differential equation with linear or nonlinear terms. However, the complexity of dendritic arborization and presence of different active properties needs a new approach to apply these techniques for a real neuron. Although, several numerical algorithms and even analytical solutions were proposed for special conditions, the general solution for a real neuron with complex dendritic arborization and active membrane is not a feasible mathematical task (Rinzel and Rall, 1974; Tuckwell and Walsh, 1983; Koch and Poggio, 1985; Bluman and Tuckwell, 1987; Agmon-Snir and Segev, 1993; Cao and Abbott, 1993).

1.1.5 Compartmental Model

To apply cable theory and overcome the problem of non-uniform membrane properties and complex structure of the dendritic tree, Rall proposed a new technique, which is called the compartmental method (Rall et al., 1995). In this method, the membrane potential of the dendritic tree is estimated by several small consecutive cylindrical compartments with an approximately uniform membrane potential. Each compartment has its own passive or active properties and connects to neighboring compartments with a longitudinal resistance (Fig. 1-2). In this manner, the non-uniform geometrical and electrical properties and difference in membrane potential occurs between compartments rather than within them. Therefore, with the appropriate differential equations for each compartment, we can model the behavior of each compartment as well as its interactions with neighboring compartments. Mathematically, the compartmental approach is a discrete approximation to

the non-linear differential equation (Rall, 1959; Rall and Rinzel, 1973; Bower and Beeman, 1995; Rall et al., 1995; Carnevale and Hines, 2005).

In the compartmental model, each compartment must be made small enough to be at approximately the same electrical potential. Applying the concept of the compartment in a computation algorithm requires specification of the number of compartments that are needed to capture the dynamic of membrane potential along a dendritic tree. One has to determine whether thousands of compartments or only several representative compartments can reproduce a good approximation of membrane dynamics.

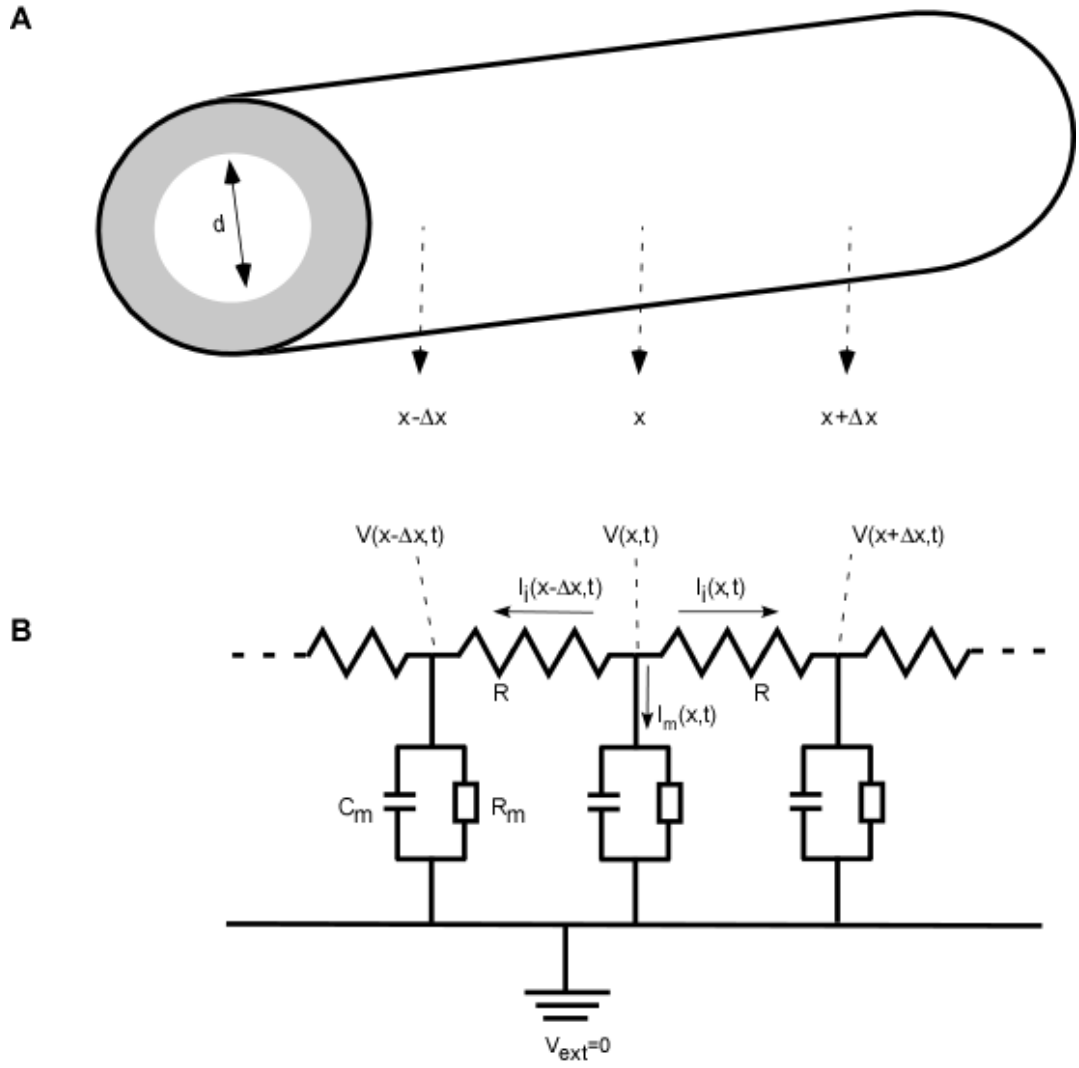

Figure 1-2. Electrical structure for passive dendritic section. (A) In cable theory, a dendritic segment is represented by a cylinder with a constant diameter (e.g., *d*), and for a dendritic section with passive membrane, (B), the dynamic of membrane potential analog dendritic section is characterized by a liner first order differential equations (Eq. 1-13). Current per unit length across the membrane, is indicated by $i_m(x,t)$ for a specific time(t) and location (x). C_m and R_m show membrane capacitance and resistance, respectively.

1.1.5.1 Spatio-temporal grid

Theoretically and computationally, selecting an appropriate number of compartments to capture electrical activity of a neuron with complex dendritic morphology is a challenge in computational neuroscience (Carnevale and Hines, 2005). The numerical analysis technique transfers the cable equation from a continuous time-space into a discreet domain. Therefore, one needs to define the optimal grid size of time-space variable in order to have a good estimation of exact solution.

1.1.5.1.1 Temporal grid

Selecting a short time step for temporal integration of the cable equation keeps the membrane potential dynamic very close to behavior in a continues time domain. However, a very short time step dramatically increases the computational time and even may cause instability or artifact in numerical integration of the nonlinear cable equation (De Schutter and Bower, 1994). On another side, the size of the time step should not be longer than the fastest dynamic in the system such as the time constant of synaptic conductance or period, 1/frequency, of external stimuli.

Moreover, it has been shown that for a partial differential equation, the size of the time step and spatial grid are not independent of each other (Morton and Mayers, 2005).

1.1.5.1.2 Spatial grid

A short time step alone does not guarantee good temporal precision. If propagation of electrical or chemical signal involves a significant delay, then spatial grid also plays an important role. For instance, Hines and Carnevale (Crank, 1979) illustrated this problem by considering the dynamic of membrane potential on a dendritic tree in response to a fast synaptic input. In this case, the solution of the cable equation for a short time step, but coarse spatial grid, cannot reproduce a rapid change in membrane potential at site of

synaptic inputs. This error could change the whole dynamic of the system if one expects to investigate the activation of an ionic conductance by a fast synaptic event.

1.1.6 Number of compartments

Besides the mathematical method to find an appropriate spatiotemporal grid for the numerical solution of cable theory, computational neuroscientists looked back to the original idea of the cable theory to find a criterion for size of grid or number of compartment. They showed that the accuracy depends on the morphological and biophysical complexity of the neuron (Hines and Carnevale, 2001).

As the first approximation, number of compartments can be determined from steady-state signal propagation on a cable with constant diameter and passive properties. In this case, cable equation, Eq.13 finds the following form,

$$V = \frac{r_m}{r_i}\frac{d^2V}{dx^2} \qquad (1\text{-}14)$$

Where r_m and r_i indicate the membrane and intracellular resistivity per unit length. The solution of Eq. 14 in response to a constant (DC) current injected at $x=0$ is given by $V = V_0\, e^{-x}{}_{\lambda}$. Where, $V(x=0) = V_0$ and $\lambda = \sqrt{\frac{r_m}{r_i}}$. Inspection of this steady-state signal propagation shows that when $x=\lambda$, membrane potential attenuated to 0.37 of the value at the site of the input. This value defined as space constant or DC length of the cable. Instead of resistance per unit length, characteristic length can be expressed as $\lambda = \sqrt{\frac{R_m}{R_i}\frac{d}{4}}$, where d is the diameter of dendritic segment, R_m and R_i ,respectively, indicate transmembrane and intracellular resistivity.

Adjusting the size of spatial grid or length of compartment in the range of a small fraction of space constant can be a good approximation for the proposed definition of compartment by Rall that requested an equal membrane potential along the length of compartment.

The space constant or DC length provides only the upper limit for compartment length. This approach does not involve a fast dynamic event (e.g. high frequency input) or impact of a low-pass filtering effect of dendritic membrane (Koch and Segev, 1998). Thus, the immediate way to solve this problem begins with the upper limit, which reduces the size of spatial grid (i.e, increase the number of compartments) until the further increase cause no significant difference in simulation results. This is a practical solution, but computationally is expensive and time consuming.

Hines and Carnevale proposed d-lambda strategy, based on frequency-dependent space constant (Fortune and Rose, 1997; Koch, 1999; Hines and Carnevale, 2001). In this method, they derived a formula for space constant at a frequency where membrane resistance (R_m) can be neglected. In this formula, the distance over which an *e*-fold attenuation occurs is

$$\lambda_f \approx \frac{1}{2}\sqrt{\frac{d}{\pi f\, R_i\, C_m}} \qquad (1\text{-}15)$$

Thus, the upper limit for the maximum length of compartment should be λ_f. This algorithm implemented in NEURON simulation environment, and has been used for all numerical simulations in following chapters (Hines and Carnevale, 1997).

Once we found an optimal grid for the numerical solution of the cable equation in the spatio-temporal domain, some or all compartments can be equipped with nonlinear ion channels. In this way, we can study the membrane potential dynamics under the effect of different voltage/time dependent conductance and synaptic inputs along a complex dendritic tree.

1.1.7 Reduced model

Developing a realistic model faces two major problems. First, the complexity of membrane properties and second, morphological details. The complexity of membrane features consisted of wide range of time and voltage dependent ionic conductances as well as different forms of synaptic inputs over dendritic trees. In addition, more advanced methods for staining and full reconstruction of a neuron provides more morphological details, which should be included in the model.

Even if for the sake of simplicity, all nonlinear ionic conductances were confined to the soma and only passive properties (i.e., leak current) assigned to the dendrites, the compartmental model encounters a practical problem. This challenge arises from a growing number of compartments and consequently, complexity of the underlying mathematical equations. In addition, we have to note that the compartmental approach is complementary for the analytical model, and many insightful and key parameters can be obtained by first applying the analytical methods to simplify and idealized approximation of a neuron (Johnston and Wu, 1995; Koch, 1999; De Schutter, 2010). Therefore, it is quite beneficial to develop a method that can reduce the complexity of the neuron while preserving the essential input-output characteristics of the full model. Moreover, such reduced model can then be serve as the building block for large neuronal networks (Segev and Burke, 1998).
A great simplification model suggested by Wilfrid Rall (Rall et al., 1995). Rall proposed "Equivalent cylinder model" which reduces the complex branched dendrites to a single equivalent cylinder that one does not need to solve numerous sets of differential equations (Koch and Segev, 1998; Evans, 2000).

To represent a branching dendrite by an equivalent cylinder, several conditions should hold (Rall, 1962b, a, 1964):

(1) The dendritic diameters of daughters (d_1 and d_2) and parent (d_p) at each branching point must hold the following relation (Rall's 3/2 rule),

$$d_p^{3/2} = d_1^{3/2} + d_2^{3/2} \tag{1-16}$$

(2) Membrane resistance and intracellular resistivity must be spatially uniform within the branching structures.

Rall initially examined this method for cat α-motoneuron, and illustrated that the input resistance and transient responses in the full tree are the same as in the corresponding equivalent cylinder (Rall, 1960). In addition, this approach successfully reproduced the extracellular field potential in the olfactory bulb and predicted the dendro-dendritic excitatory synaptic contacts on mitral cells, which later were found in experimental data (Rall et al., 1966; Rall and Shepherd, 1968).

The equivalent cylinder model provides an opportunity for analytical analysis and simply examines the influence of geometrical and biophysical properties on input-output function of a neuron (Mainen and Sejnowski, 1996). In addition, it affords the main insights regarding the behavior of voltage and summation of postsynaptic potentials in dendritic trees.

While, following Rall's 3/2 rule is not a law in nature and only with a few exceptions most neurons violate the constrain required to apply the equivalent dendrite model, its beneficial approach leads to develop other reduction algorithms (Schierwagen, 1989; Poznanski, 1991; Bush and Sejnowski, 1993; Cao and Abbott, 1993; Ohme and Schierwagen, 1998; Kellems et al., 2010).

What will happen to the dynamics and propagation of electrical signals if neurons do not follow Rall's power law?

1.1.8 Geometrical ratio

In order to study the dynamic of a propagating action potential along a branched axon, using Hodgkin-Huxley type of equation and cable theory, Goldstein and Rall pointed out that only a single parameter (geometrical ratio) would influence the electrical potential propagation upon branching points (Goldstein and Rall, 1974). By assuming uniform membrane properties for sections before and after branching points, they defined the geometrical ratio as follow,

$$GR = \frac{d_1^{3/2} + d_2^{3/2}}{d_p^{3/2}} \tag{1-17}$$

Where $d_{1,2}$ and d_p are diameter of daughters and parent at branching point. Indeed, GR indicates the ratio of the input impedance at branching point.

Analytical and modeling investigation (Goldstein and Rall, 1974; Parnas and Segev, 1979; Manor et al., 1991) illustrated that for a branching point with (a)- GR=1 the amplitude of propagation signal passes the branching point without any alteration, (b)- GR<1 cause transient increases in amplitude while (c)- Branch points with GR > 1 cause transient decreases in amplitude. As long as GR < 10 the propagation at branching point is assured (although with some delay). If GR > 10, conduction block occurs simultaneously at both branches, since the electrical load of the daughters has increased beyond the capacity of the electrical current from the parent branch to initiate a spike in the daughter branches (Parnas and Segev, 1979; Koch, 1999).

1.1.9 Details: God or Evil

Irrelevancy of details in the study of a complex system is always the place of debate. In the brain research field, some neuroscientists suggest that details of brain function have nothing to do with cognitive functions, and even most of the rhythmic or spontaneous activity of the

brain can be reproduced by a simple network model of spiking neuron (Fodor and Pylyshyn, 1988; Izhikevich and Edelman, 2008; Buzsaki, 2010). On another side, some neuroscientists trace high cognitive functions (i.e. consciousness) to level of a single neuron and consider a crucial role for each intermediate process (Koch and Segev, 2000; Timofeev et al., 2001; Euler et al., 2002; Crick and Koch, 2003; Koch, 2004; London and Hausser, 2005; Crochet and Petersen, 2006; Sevush, 2006; Buzsaki, 2010; London et al., 2010; Wang, 2010).

Advanced recordings and imaging techniques, shed light on unknown features and provided more details of an underlying mechanism that controls information processing and prominent parameters that control the behavior of a signal neuron or activity of a network (Stuart and Hausser, 2001; Vetter et al., 2001; Schaefer et al., 2003; Williams and Stuart, 2003; van Pelt and Schierwagen, 2004; Rossi et al., 2007; Sjostrom et al., 2008; Weaver and Wearne, 2008; Fellin et al., 2009; Remy et al., 2009; Economo et al., 2010; Henneberger et al., 2010). In addition, computational modeling not only illustrates how each detailed mechanism may influence the input-output function of a single neuron or a neuronal network, but it also provides new methods to estimate parameters that cannot easily be determined by experimental techniques (i.e., ionic conductances on dendrites, synaptic properties, network connectivity or even statistical estimation of dendritic arborization) (Prinz et al., 2003; Makarov et al., 2005; Achard and De Schutter, 2006; Huys et al., 2006; Mikula and Niebur, 2006; Cuntz et al., 2007; Donohue and Ascoli, 2008; Moran et al., 2008; Huys and Paninski, 2009; Keren et al., 2009; Pospischil et al., 2009; Wen et al., 2009).

While one can develop a computational model for roughly every individual experimental data, building up a realistic model that can embed all experimental facts and predict the dynamic of even a small network is close to impossible. One side of this difficulty is unknown influential parameters or missing information on exact properties of a network (i.e., pattern of connectivity, type of synapse, and synaptic distribution on the target neurons) or neurons performing a specific task (i.e., morphological and biophysical

properties). On the other side, the interpretation and analysis the influence of each factor or their complex interaction from a large set of parameters is ambiguous.

Nevertheless, struggling to implement all experimental details and build a realistic model that completely represents brain activity of a cat required another cat model (Vasku et al., 1999; Mazarati, 2007). Therefore, an important step to develop an accurate model for a complex dynamics is to identify the minimum set of parameters needed to account. In this form of simulation, an acceptable model might not be accurate in all details, but it must capture the wide range of the phenomena operating in neural circuits. This is the current approach, which is extensively used in computational neuroscience (Abbott, 2008).

1.2 Thalamus

The word “thalamus” comes from ancient Greece for "chamber" (thálamos), is an egg-shaped structure consisted of a relatively small group of neurons and located between the midbrain and the forebrain. We perceive everything about the environment and even ourselves through the brain. All sensory information (except olfaction) passes through the thalamus, which is a centrally located brain structure and responsible for controlling the flow of information to the cortex. Understanding the function of the cortex as the ultimate controlling and information-processing center will depend on understanding the function of the thalamus.

The classical view considers the thalamus as a relay of ascending messages to the cortex. This approach was suspected by several questions such as why the ascending inputs do not go straight to the cortex and what is the function of the thalamus if it has little or no effect on content of transmitted information (Sherman and Guillery, 2002)?

However, later experimental data suggested that the thalamus has a more important role than a simple relay system. These data demonstrated a crucial role for the thalamus in perceptual and cognitive functions that have been previously described by corticocortical interaction. Thalamus, by forming the thalamocortical circuits, controls network activity in the cortex (Jones, 2002b), regulates the state of sleep and wakefulness (Steriade and Llinas, 1988), produces epileptic discharges (Huguenard and Prince, 1997; McCormick and Bal, 1997), and even believed thalamus has a crucial role in consciousness (Llinas et al., 1998). Therefore, the thalamus cannot be viewed as an isolated structure that is merely engaged in the transmission of sensory messages from the periphery to the centers for perception in the cerebral cortex (Sherman and Guillery, 2002; Castro-Alamancos, 2003; Steriade, 2004).
While it has been shown that the passing message to the cerebral cortex depends on the state of vigilance (Steriade, 1997, 2000, 2001; Steriade and Timofeev, 2003), it is also subject to a variety of modulatory inputs that modify the way the information is passed to the cortex. Investigating the structural and functional organization of thalamic neurons, the

afferent and efferent pathways, synaptic and membrane as well as morphological properties, provides us a better view about the thalamic function.

1.2.1 Major divisions of the thalamus

The thalamus is the largest structure in the diencephalon that can be divided to Epithalamus, Ventral and Dorsal thalamus based on their fundamentally different connectional relationships (Steriade et al., 1997). Figure 1-3 shows the same thalamic nuclei in a simplified schematic. This division can also be subdivided into several nuclei, which are characterized by the type of efferent inputs and afferent output to the functionally corresponding area of the cerebral cortex. In the next sections, we briefly review major components of the thalamus.

1.2.1.1 Dorsal thalamus

Dorsal thalamus is the largest part of the diencephalon and consisted of various nuclei that project to the cerebral cortex or to the striatum (Steriade et al., 1997; Jones, 2007). Most of the dorsal thalamic nuclei have afferent connections to neocortex (Leonard, 1972; Jones, 2002a) and only a few nuclei (e.g., intralaminar nuclei) project to the striatum (Cowan and Powell, 1956; Gimenez-Amaya et al., 1995).The intralaminar nuclei are consisted of several subgroups (i.e., rhomboid, central medial, centeral lateral, paracentral, center median and posterior). Although it has been shown that a significant number of intralaminar nuclei may also project to the cerebral cortex (Jones and Leavitt, 1974). Other thalamic nuclei that send projection to the cerebral cortex are named principal relay nuclei. The major group of principal nuclei consisted of (Steriade et al., 1997):

a) Anterior nuclei: receive inputs from the mamillary hypothalamic nuclei and projects to the cingulate gyrus**.** They represent the thalamic target for feedback from hippocampal formation.

b) Medial nuclei: receive inputs from the amygdala, substantia nigra and temporal neocortex and reciprocally connected to the prefrontal cortex**.**

c) Lateral posterior and pulvinar nuclei: receive the major input from the visumotor region of the midbrain (pretectum and superior colliculus). The cortical output projects to the area of parieto-temporo-occipital cortex, intercalated zone between the primary somatosensory, auditory and visual area.

d) Ventral nuclei:

- **i)** Ventral anterior, which input from globus pallidus and substantia nigra and projects to prefrontal, orbital and premotor cortices**.**
- **ii)** Ventral lateral: input from cerebellum, globus pallidus, and substantia nigra and projects to motor and supplementary motor cortices
- **iii)** Ventral posterior: Ventral posterolateral (VPL) receives input from the spinothalamic tracts and the medial lemniscus and projects to the somatosensory cortex. Ventral posteromedial (VPM) recieves the trigeminal lemniscus inputs and projects to the soamtosensory cortex.

e) Dorsal lateral geniculate nuclei: almost exclusively derived from the field of view, and the cortical output is focused on striate area**.**

f) Medial geniculate nuclei: can be sub-classified as ventral, dorsal and medial nuclei. Ventral nucleus is the most direct relay from contralateral ear to the primary auditory cortex. Dorsal medial geniculate nuclei receive diffusely originating auditory brainstem inputs and projects to auditory areas around the primary auditory area. Medial nuclei receive mixed auditory, vestibular and somatosensory inputs and many of its cells project rather diffusely on the auditory and surrounding non-auditory areas of the cortex.

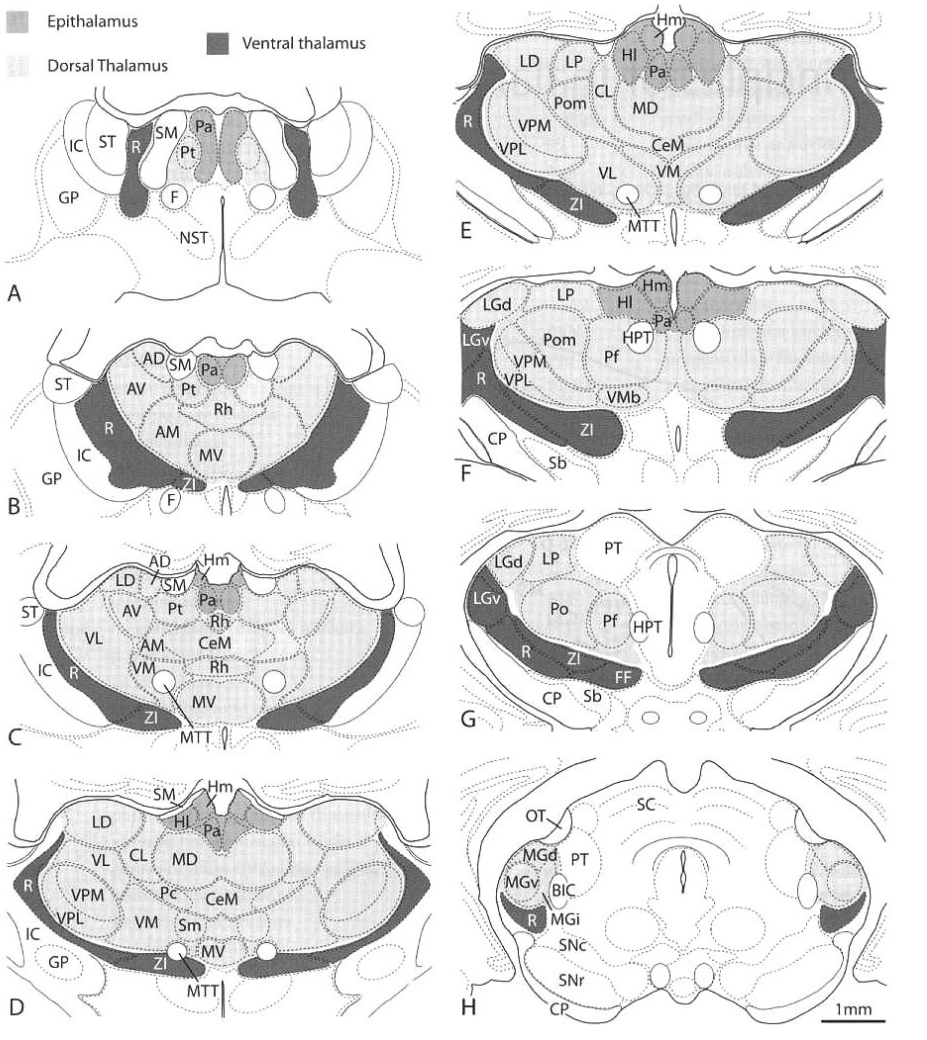

Figure 1-3. Schematic view of eight sections through the thalamus of a mouse. The major thalamic nuclei based on frontal sections in anterior (A) to posterior (H) order in three divisions of thalamus are shown: (I) Epithalamus: Hl, lateral habenular nucleus; Hm, medial habenular nucleus; Pa, paraventricular nucleus; Pf, parafascicular nucleus ;PoM, posterior medial nucleus. (II) Dorsal thalamus: AD, anterodorsal nucleus; AM, anteromedial nucleus; AV, anteroventral nucleus; CL, central lateral nucleus; CeM, central medial nucleus; LD, lateral dorsal nucleus; LGd, dorsal lateral geniculate nucleus; LGv, ventral lateral geniculate nucleus; LP, lateral posterior nucleus; MD, mediodorsal nucleus; MG, medial geniculate nucleus; Pf, parafascicular nucleus. (III) Ventral thalamus: R, reticular nucleus; ZI, zona incerta (Jones, 2007).

1.2.1.2 Ventral thalamus

The ventral thalamus occupies a relatively narrow zone of the diencephalon intercalated between the dorsal thalamus and hypothalamus. One important difference between the ventral and the dorsal thalamus is that the ventral thalamus sends no axons to the cortex. The ventral thalamus includes the reticular nucleus, zona incerta, perigeniculate nucleus and corpus subthalamicum or subthalamic nucleus (Jones, 2007). The main portion of the ventral thalamus is comprised of the thalamic reticular nucleus, which is known as the primary outflow into the dorsal thalamus. Reticular nucleus surrounds the lateral surface of the dorsal thalamus and composed of GABAergic neurons that project inhibitory fibers to the thalamic nuclei from which it receives input. The cortical and thalamic afferents to the reticular nucleus are predominantly excitatory, and the axons that go back from the reticular nucleus to the thalamus are inhibitory (Steriade et al., 1997; Jones, 2007). In this manner, reticular nuclei can play a crucial role in modulation of passing information through the thalamic relay to the cerebral cortex. However, unlike the reticular nuclei, the zona incerta and ventral lateral geniculate contain both GABAergic and non-GABAergic neurons (Steriade et al., 1997).

1.2.1.3 Epithalamus

Another major subdivision of the diencephalon is named Epithalamus, because of its topographical situation `above' (`epi') the thalamus. The epithalamus is constituted by the habenular nuclei (stria medullaris thalami and habenulointerpeduncular tract) and pineal complex. The ephithalamus is connected either directly with the hypothalamus or via the interpeduncular nuclei (Steriade et al., 1997). The pineal body is responsible for the secretion of melatonin, which is important in the sleep/wakefulness cycle (Arendt and Skene, 2005), and the habenula nucleus that projects to the midbrain and is thought to be important for emotions and behavior (Hikosaka, 2007).

1.2.2 Major neurons in the thalamus

1.2.2.1 Relay Neurons

Neurons with cortical projection are named Thalamocortical (TC) neurons. All TC neurons are glutamatergic and therefore excitatory. We will discuss the morphological and electrophysiological properties of TC neurons in the next section.

1.2.2.2 Reticular neurons

Reticular neurons are GABAergic inhibitory cells. These neurons are located in RE nucleus. Reticular neurons have long dendrites with vesicle-containing appendages on the secondary and tertiary branches that form synapses on dendrites of neurons on the same nucleus (Deschenes et al., 1985). It has been shown that RE neurons are electrically coupled and form an interconnected network (Venance et al., 2000; Landisman et al., 2002; Jones, 2007; Steriade and Paré, 2007). As a result, RE neurons show spikelet response in their electrophysiological response, that might account for generation of synchronized rhythms in the isolated RE nucleus (Fuentealba et al., 2004; Long et al., 2004).

1.2.2.1 Interneurons or local-circuit neurons

Interneurons are GABAergic inhibitory cells, which their axonal connections stay in the thalamus. Generally, the interneuron populations in mammalian are about 3-4 times less than relay cell, except for the mouse and rat (Arcelli et al., 1997). Local interneurons are characterized by their small soma and complex dendritic arborization, and their axon terminals form inhibitory synapses on soma and dendrites of TC neurons. In addition, the local interneurons have presynaptic vesicles on their dendritic appendages (named as F2 terminal), which form a specific inhibitory synapse on the dendrites of TC neurons (Montero, 1986; Steriade and Paré, 2007).

1.3 Thalamic relay neuron

The term “relay” indicates the main function of relay neurons, which is the transferring of sensory information from ascending afferent pathways to the cerebral cortex. Among various nuclei in the thalamus, only neurons in the dorsal thalamus send fibers to the cerebral cortex and serve as a vital pathway to relay information from the periphery to the cortex.

Relay neurons can be found among all thalamic nuclei (LG; visual lateral geniculate, MG; auditory medial geniculate, and VP; somatosensory ventroposterior). However, the relay of incoming inputs is not their only function. The presence of the local inhibitory circuit and their interaction with reticular neurons account for their complex integrative process on synaptic inputs, mainly consisting of response selectivity higher than that recorded at prethalamic levels (Steriade and Paré, 2007).

Relay neurons usually are divided in two categories. On one hand, they can be classified on base of morphological properties such as the cell body, axon diameter, pattern of dendritic arborization or position in particular nucleus and even Ca^{2+} binding proteins (Steriade et al., 1997; Jones, 2007). On the other hand, the relay neurons can be categorized into the first or higher order relay neuron based on cortical connections (Steriade et al., 1997; Sherman and Guillery, 2006; Jones, 2007).

Relay neurons can be classified based on:

(a) Morphological properties: such as the cell body, axon diameter, pattern of dendritic arborization or position in particular nucleus and even Ca^{2+} binding proteins. It has been shown that large neurons (i.e., soma size) projecting to middle and deep cortical layers, whereas small neurons project preferentially to superficial layers (Steriade et al., 1997; Jones, 2007).

(b) Afferent connections: from the periphery or the cerebral cortex

(I) The first order nuclei receive a major part of their afferent connections from ascending pathways that bring information from the environment (i.e., visual, auditory, somatosensory or taste). These types of inputs can be considered as driving inputs to the thalamic nuclei. Other inputs to first order nuclei are regarded as modulatory or inhibitory afferents that come from the brain stem, the thalamic reticular nucleus, the hypothalamus, and from the cerebral cortex itself.

(II) The higher order thalamic nuclei receive most or all of their inputs (i.e. driving and modulatory) from the cerebral cortex (Sherman and Guillery, 1996; Sherman and Guillery, 2006). The driver inputs can be defined as the transmitter of receptive field properties, while the modulatory inputs alter the probability of certain aspects of that transmission. The drivers represent the main information to be relayed, and the modulators modify the thalamocortical relay. One such modification is the burst/tonic firing mode (Llinas and Jahnsen, 1982; Deschenes et al., 1984; Steriade and Deschenes, 1984). It has been shown(Guillery, 1995) that the corticothalamic afferents arising in cortical layer 5 are likely to be drivers, whereas those arising in layer 6 are likely to be modulators (see Figure 1-4). In addition to the origin of the inputs, the drivers and modulators differ in structure of terminals and the nature of the synaptic transfer to thalamic cells. However, it is not clear yet that this classification and variability related to nature of massage that is being passed through the thalamus or the nature of thalamic function (gating, modulation) on transmitted information (Sherman and Guillery, 1996, 1998).

Generally, the neuron's firing properties and the way a neuron integrates synaptic inputs depends on several factors including intrinsic membrane properties, type and properties of inputs, pattern of synaptic connectivity and morphological characteristics of a neuron as well as the state of the network. Therefore, investigation of how thalamic neurons influence the relay of information to the cortex is a challenging puzzle that was greatly increased in

recent years by the discovery of diverse transmitters, voltage- and ligand-gated ion channels, and receptors that contribute to the synaptic organization in the thalamic relay (Steriade et al., 1997; Sherman and Guillery, 2006; Jones, 2007).

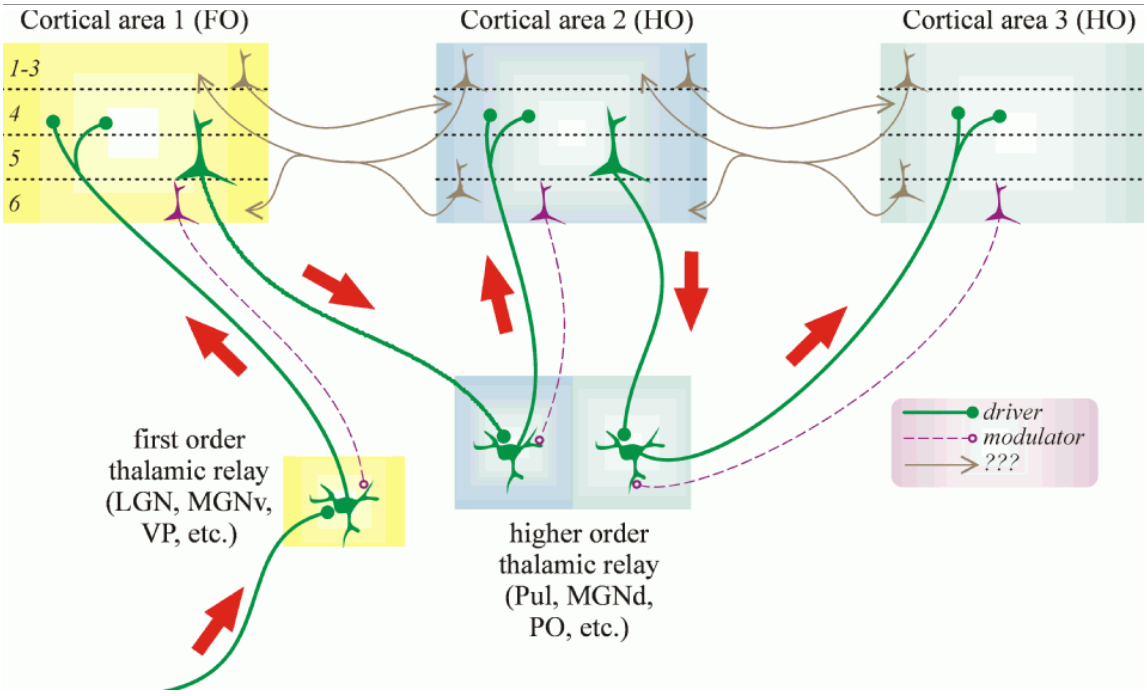

Figure 1-4. Schematic illustration of cortical and thalamic pathways. A first order (FO) relay receives its driver inputs on proximal dendrites from subcortical sources via ascending pathways whereas a higher order (HO) relay receives its driver inputs from cells in cortical layer 5. The first order relay sends a driver input to layer 4 of cortical area A, and that same cortical area sends a modulator input onto distal dendrites cell from layer 6 back to the same first order thalamic nucleus. Cortical area A in turn sends a driver input from layer 5 to the higher order thalamic relay. This higher order relay sends its thalamocortical axons to cortical area B and receives a modulator input back from layer 6 of cortical area B. Abbreviations: LGN, lateral geniculate nucleus; MGNd and MGNv, dorsal and ventral portions of the medial geniculate nucleus; PO, posterior nucleus; Pul, pulvinar; TRN, thalamic reticular nucleus; VP, ventral posterior nucleus (Sherman, 2006).

1.3.1 Membrane properties

Linear summation of synaptic inputs is the first step to understand how a neuron carries out the input-output functions. Even, with the linear integrative assumption, the way a synaptic event may affect somatic membrane potential (or axon hillock) depends on complex dendritic morphology and passive electrical properties of the dendritic sections.

Besides the hypothesis of the cable model, estimation of passive electrical properties such as membrane capacitance, cytoplasmic and membrane resistance has its limitation. These parameters are typically assumed to be uniform spatially and temporally throughout the somatic and dendritic membrane.

Several methods proposed to estimate not only passive but also voltage-dependent electrical properties of a neuron (Maltenfort and Hamm, 2004; Keren et al., 2005; Achard and De Schutter, 2006; Huys et al., 2006; Gold et al., 2007; Badel et al., 2008). Generally, these methods are based on fitting the response of the modeled neuron to the experimental data. Therefore, validity of estimated electrical properties depends on the quality of the experimental data and the precision of the modeled neuron. Usually, once a set of parameters is obtained for a neuron, it applies for other neurons as well within the same class, requiring only a small tuning in a reasonable physiological range.

Two sets of experimental data were used to estimate the cable properties of the thalamocortical cell: in vitro slice (Destexhe et al., 1998) or in vivo preparation (Bloomfield et al., 1987). However, estimating electrical parameters from the in vitro data include errors from non-complete dendritic arborization and much less (or diminished) spontaneous activity in vitro slice preparations. Although in vivo recordings provide more reliable data than those made in vitro, the reproducibility of the experimental data is strongly depended on the quality of the modeled. Errors in morphological reconstruction and the assumption of uniform or non-uniform electrical properties leads to a different set of parameters that only represent a specific feature of the electrophysiological response of the neuron (Achard and De Schutter, 2006).

After revealing the presence of voltage-dependent electrical properties (i.e. active properties) and, thus, nonlinear membrane properties, the estimation of the membrane parameters becomes a challenging problem (Prinz et al., 2003; Jolivet et al., 2008; Van Geit et al., 2008; Huys and Paninski, 2009). In addition, propagation of synaptic inputs toward the soma or axon hillock is not only affected by dendritic morphology (e.g. Rall's power law) and passive properties (e.g. low-pass filtering effect), but it is also strongly controlled by active properties of the neuronal membrane (e.g. voltage dependent conductance).

In addition to activity-dependent fluctuations of the intercellular ionic concentration (e.g. Ca^{2+}), synaptic inputs alter ionic conductance, and therefore lead to a change in membrane or postsynaptic potential and intrinsic responses (Steriade and Timofeev, 1997). Thus, exploring the type, kinetics and distribution of voltage dependant ionic conductances is an essential step toward understanding the input-output function of a neuron.

A thalamic relay cell is one of the richest types of neuron throughout the brain in terms of variety of ionic conductance in their membrane (Steriade et al., 1997; Sherman and Guillery, 2006; Jones, 2007; Stuart et al., 2007). In the next section, we will review its electrophysiological behavior and underlying ionic currents.

1.3.2 Electrophysiological response of TC neuron

In vivo and in vitro experimental data illustrated two firing modes in thalamic neurons, tonic firing at relatively depolarized membrane potentials (more positive than -60 mV) and burst discharges at more hyperpolarized levels (more negative than -65 mV) (Llinas and Jahnsen, 1982; Deschenes et al., 1984; Jahnsen and Llinas, 1984b, a). Figure 1-5 shows the response of TC neuron to a constant DC pulse at different level of membrane potential: (A) Tonic firing mode; at relatively depolarized membrane potential. (B) Passive response; the injected current is not sufficient to depolarize membrane potential up threshold value to generate action potential. (C) Burst firing mode; when the cell is relatively hyperpolarized,

low threshold Ca^{2+} channels are deinactivated, and the current pulse could open activation gate and generate an low threshold Ca^{2+} spike (LTS) with four action potentials riding its crest.

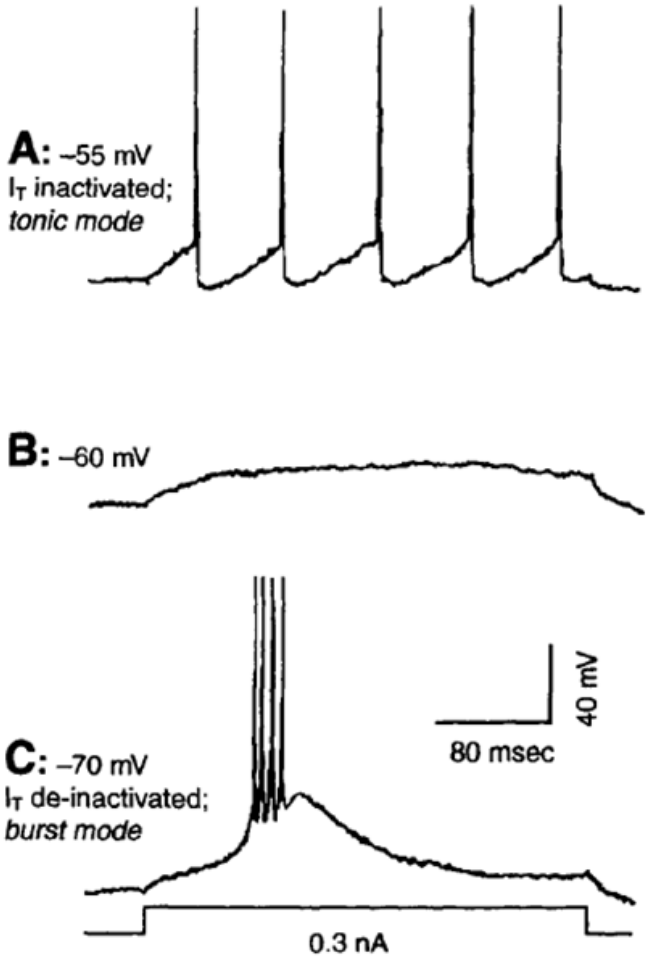

Figure 1-5. Firing mode of a relay cell. The graph shows the response of a lateral geniculate nucleus of cat from an in vitro intracellular recording. (A) At relatively depolarized membrane potential, the constant injected current creates an initially passive membrane depolarization sufficient to evoke a stream of conventional action potentials. This is tonic mode of firing. (B) When the membrane potential is not hyperpolarized enough to activate T-channel and the injected current is not sufficient to depolarize membrane potential up threshold value to generate action potential, the response of the cell will be purely passive, resistive-capacitance, response. (C) When the cell is relatively hyperpolarized (b), IT is de-inactivated and the current pulse activates an LTS with four action potentials riding its crest. This is the burst mode of firing (Llinas and Jahnsen, 1982)

It has been shown that only tonic firing occurs during normal, waking behavior and bursting is limited to drowsiness, slow-wave sleep or certain pathological conditions (Steriade et al., 1993b; Llinas and Steriade, 2006). However, some other data, mostly arising from studies on the lateral geniculate nucleus, found burst firing mode during waking behavior. Although, this burst mode is arrhythmic and the extent of bursting in during wakefulness is relatively low; about 10% of the time in monkeys and with a probability of 0.09 in any 1s period in awake cat (Guido and Weyand, 1995; Ramcharan et al., 2000).

In the next section, we will discuss the different types of the ionic currents and their functional role on forming the electrophysiological response of the TC neurons.

1.3.3 Ionic membrane conductances

The intrinsic electrophysiological properties of TC neurons recorded from different dorsal thalamic nuclei are similar (Steriade et al., 1997; Jones, 2007; Steriade and Paré, 2007). They consist mainly of (a) a transient Ca^{2+} current (I_T); (b) high-voltage Ca^{2+} currents (I_L); (c) a hyperpolarization-activated cation current (I_h); (d) a persistent Na^+ current ($I_{Na(p)}$) and (e) different types of K^+ currents. These intrinsic properties are important in the generation and synchronization of thalamic oscillations. Table 1-1 shows all intrinsic ionic currents in relay neurons and a brief description of their functional role.

Current	Description	Function
I_T	Low-threshold Ca^{2+} current	Generation of burst of action potential
I_{Na}	Transitent Na^+ current	Generation of action potential
$I_{Na(p)}$	Persistent Na^+ current	Promotes depolarization
$I_{K[Ca]}$	Ca^{2+} - dependent K^+ current	Repolarization of action potential
I_h	Hyperpolarization activated cation current	Generation rhythmic oscillation by interacting with I_T
I_A	Fast inactivation, transient K^+ current	Affects timing of action potential and low-threshold Ca^{2+} spike
I_{KL}	Leak K^+ current	Hyperpolarization during changes of state
I_L, I_N	High-threshold Ca^{2+} current	Activation of $I_{K[Ca]}$ during action potential
I_{K2},I_{AS},I_{KM}, I_{Ks}	Slow inactivation, transient K^+ current	Influence duration of low-threshold Ca^{2+} spike and reduce response to depolarization
I_{KG}	G-protein-activated K^+ current	Mediate inhibitory effects of acetycholine, GABA and certain modulators

Table 1-1. Intrinsic ionic currents in thalamic relay neurons (Jones, 2007).

1.3.3.1 Voltage- independent Leakage conductance

The ionic conductance underlying the leak current is independent of voltage. Indeed, this leakage is results of partial impermeability of the neuronal membrane and ionic pumps. The leak current keeps the membrane potential close to the equilibrium of an ionic concentration gradient across the membrane, which generates the resting membrane potential. The major ions participating in the leakage current are K^+, Na^+ and Cl^-. However, the passive leakage is greater for K^+, therefore, it is also called potassium-leak current.

1.3.3.2 Voltage- dependent conductances

1.3.3.2.1 Na+/ K+ conductances underlying action potential

The presence of Na^+/K^+ currents on soma and axon hillock mediates the generation of action potential in all type of neurons (Hodgkin and Huxley, 1952b, a). However, experimental data illustrated the presence of Na^+/K^+ conductances on the dendrites of a relay neuron (Williams and Stuart, 2000). This may affect the transmission of post synaptic potential toward the soma, and play an important role in the synaptic integration and backpropagation of action potential (Stuart et al., 1997).

1.3.3.2.2 Low- threshold Ca^{2+} conductance

Apart from Na^+/K^+ currents underlying the action potential, this is the most important voltage dependent conductance in relay cells in all dorsal thalamic nuclei of all mammals, which is responsible for the characteristic firing pattern of TC neurons (Huguenard, 1996; Sherman and Guillery, 2006; Jones, 2007). This channel and the resulting current are known as T- channel and T- current ("T" for transient), respectively, because when this channel is open, Ca^{2+} ions enter the neuron, and the resulting inward current generates a transient depolarization of the cell.

Low- threshold Ca^{2+} conductance underlying the generation of a spike-like depolarization of about 20-30 mV and lasts for about 50 msec, which crowned by high frequency bursts of fast Na^{+} action potentials (Jahnsen and Llinas, 1984b; Steriade and Deschenes, 1984; Huguenard, 1996). This spike-like depolarization is called the Low-threshold Ca^{2+} spike (LTS). In- vitro and in- vivo experimental evidence showed that the refractory period of LTS in most TC neurons with few exceptions (i.e., rostral intralaminar nuclei) is quite long, that is, 150-200 ms (Llinas and Jahnsen, 1982; Deschenes et al., 1984; Steriade et al., 1993a). It has been shown that TC neurons cannot follow frequencies above 6 Hz, and therefore, spike-bursts would not be able to follow rapidly recurring signals during wakefulness (McCormick and Feeser, 1990; Steriade and McCarley, 2005).

Figure 1-6 shows the response of TC neurons to afferent stimulation at different level of membrane potential; (top) at the depolarized level (with action potentials), (middle) at the resting level (with EPSPs), and (bottom) under hyperpolarized level (with LTS in isolation or crowned by spike-burst).

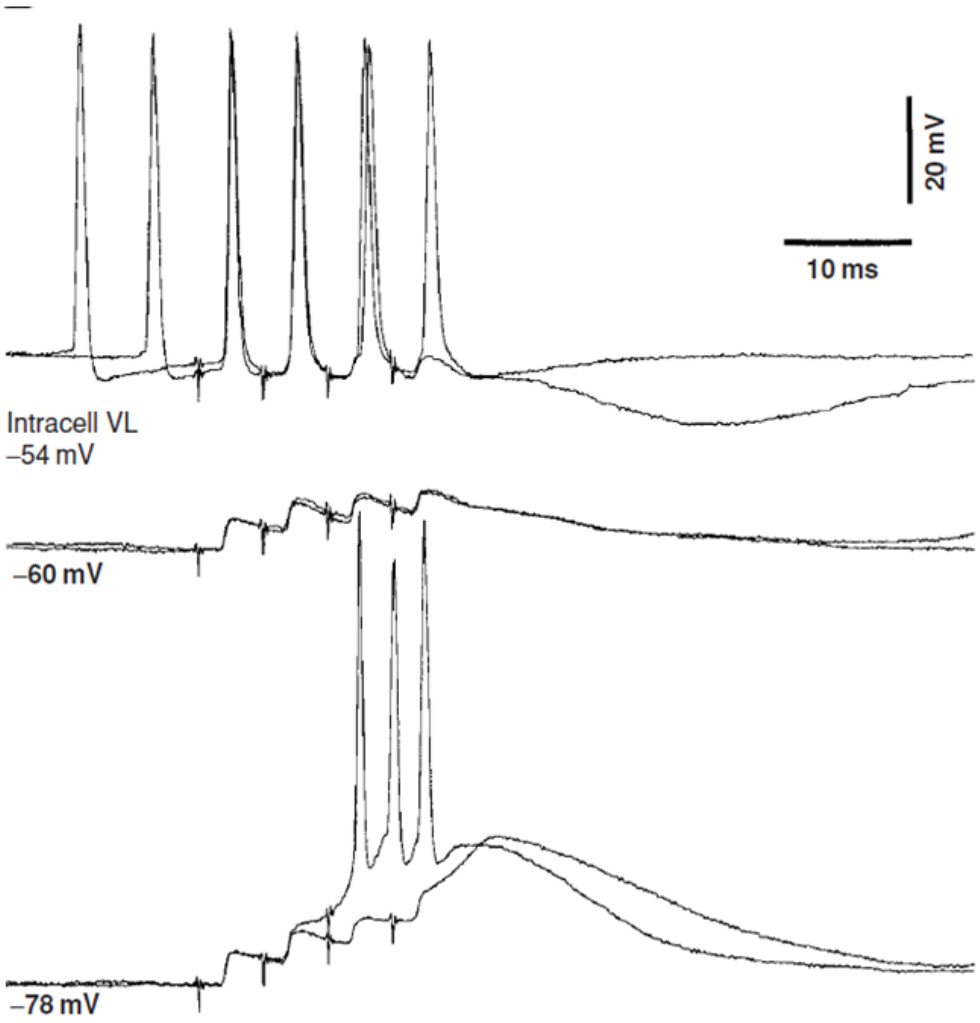

Figure 1-6. Intracellular recording of TC (VL) neuron under ketamine—xylazine anaesthesia. Four Stimulation of the brachium conjunctivum at 200 Hz: (Up) evoked monosynaptic EPSPs and action potentials under slight steady depolarizing current (−54 mV). (Middle) EPSPs at rest (−60 mV). (Bottom) During hyperpolarizing current (−78 mV) the cell responded with EPSPs, leading to LTS in isolation or crowned by a high-frequency burst of action potentials (Steriade and Paré, 2007).

1.3.3.2.2.1 Voltage and time- dependency of I_T

Although, the behavior of T-channel is very similar to Na^+ channel underlying action potential, and it has the same three state of channel: inactivation, de-inactivation and activation states, the voltage dependency and kinetics are quite different. Figure 1-7 illustrated the quantitative description of voltage dependency of T-channel for different relay cells from VP nucleus of the rat (Huguenard and McCormick, 1992). The inactivation curve (dashed lines) obtained from clamping the cell at the different hyperpolarized levels (in order to partially de-inactivate), which suddenly jumped to a depolarized level (in order to active channel). In the same way, the activation curve (solid lines) obtained from clamping membrane at a hyperpolarized level (sufficient for completely de-inactivate T-channel) with sudden changes to various depolarized levels. The low-threshold Ca^{2+} current is activated at a membrane potential positive to approximately -65 mV, and inactivated at a membrane potential positive to approximately -90 mV.

In addition, the T-current not only shows a membrane potential dependency but also the state of channel depends on time. Activation, inactivation, and de-inactivation occur with variable time constants. Although, the activation time constant is faster than other states, full inactivation (following depolarization) or full de-inactivation (following hyperpolarization) usually takes on the order of 100 msec. This hyperpolarization might happen either through intrinsic membrane properties or through the inhibitory synaptic potential, such as during the generation of spindle wave oscillations (Steriade et al., 1997).

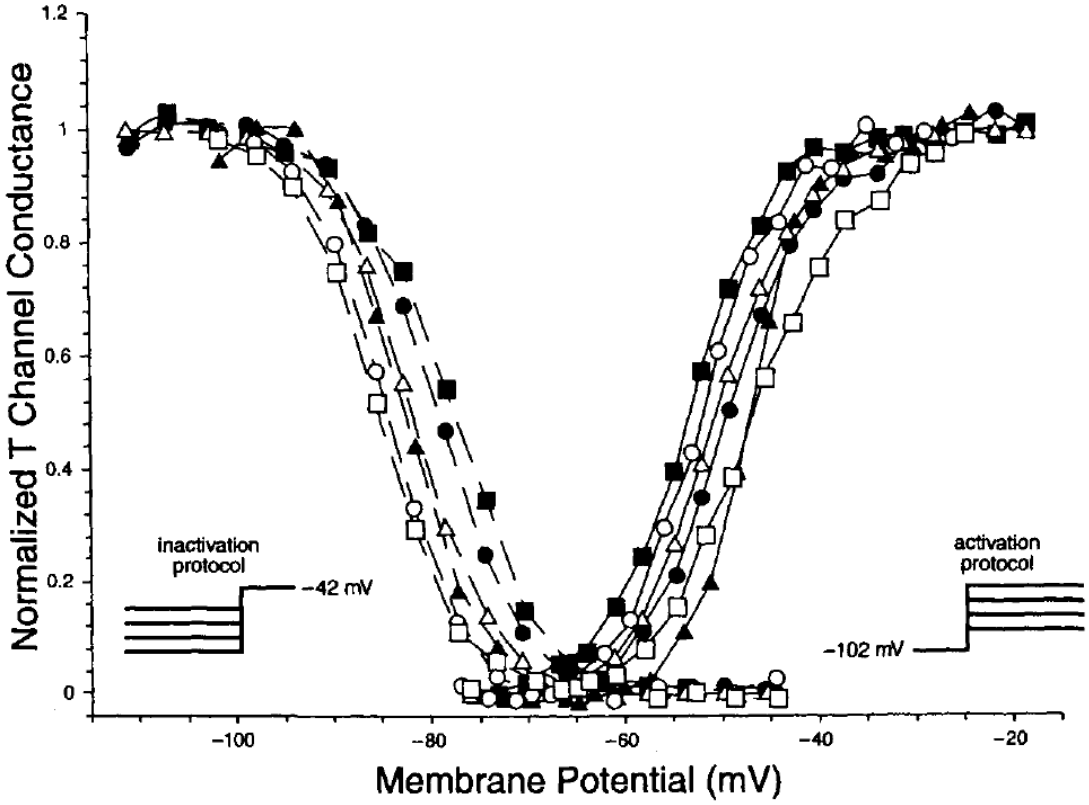

Figure 1-7. Voltage-dependent activation and inactivation of I_T. Graphs show the result of voltage-clamp experiments on acutely isolated rat relay neurons (6 neurons) from VP nucleus. The activation curve (dash lines) obtained by first holding the membrane at various hyperpolarized levels (which are plotted on the abscissa) for 1 sec and then stepping up to -42 mV. The voltage protocol for this is shown in the inset at left. The more hyperpolarization produces more T-current, because more initial hyperpolarization produces more de-inactivation of T-channels. The activation curves (solid lines) obtained by first holding at -102 mV, which would completely de-inactivate I_T, and then stepping up to the various membrane voltages plotted on the abscissa. The voltage protocol for this is shown in the inset at right. The larger depolarizing steps activate more T-channel and produce more T-current (Huguenard and McCormick, 1992).

1.3.3.2.2.2 Voltage-clamp problem

Extracting the kinetics of T-channel from voltage clamp data is based on two assumptions. First, because the presence of T-channel in dendritic arbor (Destexhe et al., 1998; Williams and Stuart, 2000), keeping the membrane potential at a constant level is not a feasible task. Therefore, most experimental data were obtained from a dissociated cell in which most parts of the dendrites are absent. Second, by measuring the kinetics of T-channel in soma, it is presumed that T-channel has identical kinetic in all part of the dendritic arbors. However, recent evidence indicated the variation between kinetics of T-type channels with different subunits (Joksovic et al., 2005) and non-uniform distribution of different T-type subunit along dendritic trees (Kovacs et al., 2010).

1.3.3.2.2.3 Window I_T

Figure 2.5 shows a little overlap between the activation and de-inactivation curve, which indicates T-channel maybe partially active and de-inactive. In this voltage window, T-current is constantly present. This may lead to bistability and spontaneous rhythmic discharge if the membrane potential lies within this window (Toth et al., 1998; Crunelli et al., 2005). However, experimental data indicates that under normal physiological conditions, there is neither significant window current, rhythmogenic nor bistability properties for these neurons (Toth et al., 1998; Gutierrez et al., 2001).

1.3.3.2.2.4 Functional role of I_T

T-channel conductance controls the bursting response of thalamic relay cells. When T-channels are inactivated, the relay neuron generates tonic firing pattern in response to depolarizing current. When the low threshold Ca^{2+} conductance is de-inactivated and thus able to be activated, the response of a relay neuron to a depolarizing input consists of high frequency (250-400Hz) bursts of two to eight action potentials separated by silent periods about 150-200 ms (Deschenes et al., 1984; Jahnsen and Llinas, 1984b; Roy et al., 1984; Huguenard, 1996; Destexhe et al., 1998).

Experimental evidence in cats (Gutierrez et al., 2001) indicated that only when the rate of depolarization from a hyperpolarized level exceeded a minimum value (5-12 mV/sec), the relay neuron can produce low-threshold Ca^{2+} spikes. A lower depolarization rate by synaptic inputs (i.e., via metabotropic receptors) may inactivate T-current without ever activating it, which may reduce or eliminate the LTS and switch the response to tonic firing (McCormick and von Krosigk, 1992; Godwin et al., 1996).

These two response modes of the relay neuron strongly affect input-output relationships (see Figure 1-8) and the way it transfers information to the cortex (Zhan et al., 1999; Zhan et al., 2000). First, in the tonic mode the input-output relationship (i.e., the current steps v.s. the firing frequency) is more linear, while in the burst mode the relay neuron shows a discontinuity between input current and output firing frequency. In tonic mode, larger depolarized (or EPSPs) current elicits higher firing rate and in burst mode do not. Second, during tonic firing, the response lasts as long as the injected current, but during burst firing, the response does not faithfully represent the duration of the injected current (Sherman and Guillery, 2002).

While the tonic and burst firing response of geniculate nucleus to a visual stimuli transmit approximately equal levels of information (Reinagel et al., 1999), but response in tonic mode has lower signal-to-noise than during burst firing mode (Mukherjee and Kaplan, 1995; Smith et al., 2000; Sherman and Guillery, 2002).

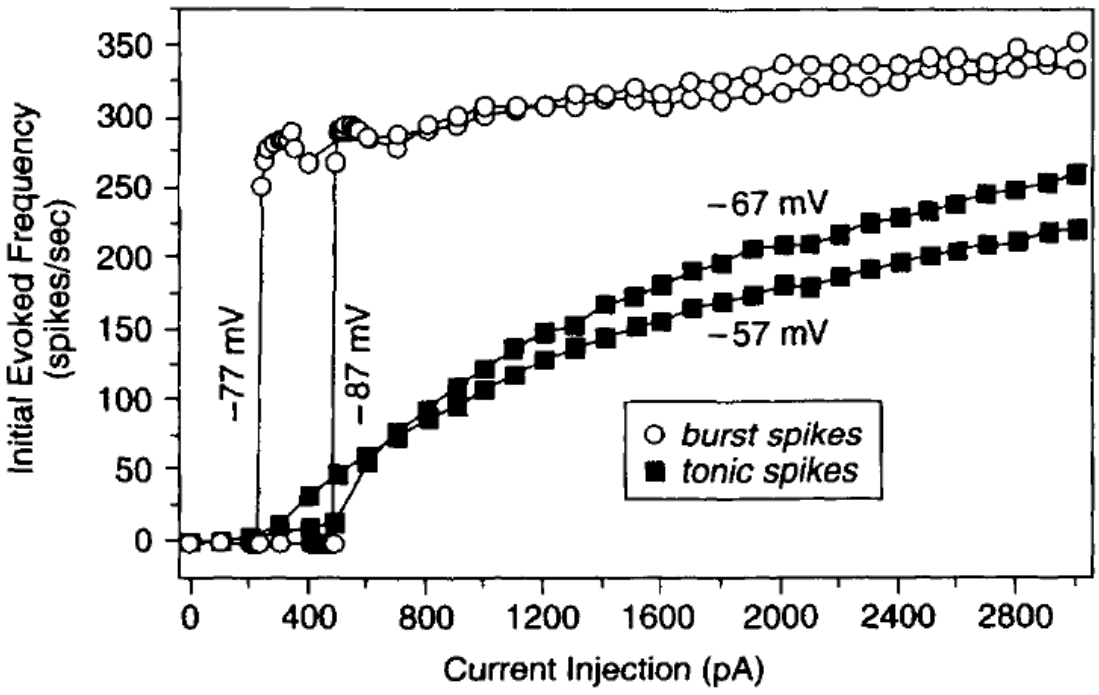

Figure 1-8. Frequency response of a relay neuron to various levels of current injection from different initial membrane potentials. Graphs show the initial frequency of firing mode for a relay neuron from cat's lateral geniculate nucleus. Initial firing frequency was calculated from the first six action potentials evoked. By holding potentials of —77 mV or —87 mV (at levels that de-inactivate I_T), burst firing was evoked, and the relationship between current injection and firing frequency shows a sudden, nonlinear jump. At levels that inactivate I_T and produce tonic firing (-47 mV and -59 mV), the relationship between current injection and firing frequency is much more linear (Zhan et al., 1999).

1.3.3.2.3 Hyperpolarization-activated cation conductance

In general, two different types of hyperpolarization-activated inward currents (I_h current) have been reported (Halliwell and Adams, 1982; Rudy, 1988; Pape, 1996). One is carried by K^+ ions, with fast activation kinetics, and its activation range depends on the difference between membrane potential and potassium equilibrium potential. Another type is permeable for both Na^+ and K^+ ions with comparatively slow activation kinetics. Experimental data illustrated that the inward rectifier current of thalamic relay neurons resembles those with slow activation kinetics, which strongly depends on voltage (McCormick and Pape, 1990b).

1.3.3.2.3 .1 Voltage and time- dependency of I_h

A brief hyperpolarization, due to a hyperpolarizing current pulse or an inhibitory postsynaptic potential, leads to activation of the hyperpolarization-activated cation channels, which moves the membrane potential back towards the initially more depolarized level. Voltage clamp data from TC relay neurons revealed that the hyperpolarization-activated cation channels have no inactivation gates and its activation is relatively slow with a time constant more than 200 msec. Figure 1-9 illustrated the quantitative description of voltage dependency of the hyperpolarization-activated cation conductance from 6 different guinea pig geniculate relay neurons (Huguenard and McCormick, 1992). The kinetics of activation and deactivation of I_h, were described by a continuous and bell-shaped function of membrane potential, with the slowest rate of activation (time constant of - 1 s at 35°C) occurring at -80 mV, which is near the membrane potential for half activation (-75 mV). In addition, experimental data indicated that maximum conductance of this channel is in the range of 15-30 nS, and reversal potential is about to -43 mV (McCormick and Pape, 1990b).

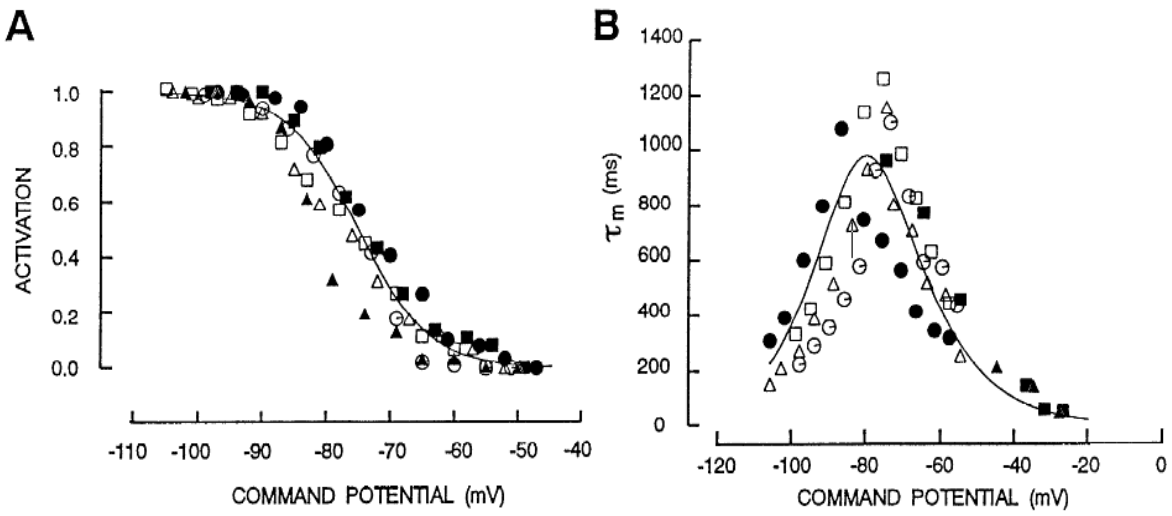

Figure 1-9. Voltage dependency of the hyperpolarization-activated cation current, I_h, in relay neuron. (A) The activation curve for I_h of 6 lateral geniculate neuron from guinea pig and (B) kinetics of activation and deactivation of I_h. The slowest rate of activation (time constant of - 1 s at 35°C) occurring at -80 mV, which is near the membrane potential for half activation (-75 mV) (McCormick and Pape, 1990b).

1.3.3.2.3 .2 Functional role of I_h

First functional property of I_h appears in controlling the rest membrane potential. The activation range of the Ih lies within the range of the rest membrane potential of a TC neuron between -65 and -75 mV. Experimental data illustrated that blocking the hyperpolarization-activated cation conductance by Cs^+ leads to a hyperpolarization of 5-10 mV (McCormick and Pape, 1990b, a). This hyperpolarization of the membrane from the rest not only may change the firing response of the neuron to the burst, but also blocks the slow after-hyperpolarization that appears upon termination of depolarizing membrane responses (McCormick and Pape, 1990b).

Second, I_h current contributes substantially to rhythmic burst firing of relay neurons. The rhythmic burst firing, during sleep or inattentiveness, is the prominent electrophysiological feature of individual thalamocortical relay neuron (Steriade and Deschenes, 1984; McCormick and Pape, 1990b; Steriade et al., 1993b). In vivo (Steriade et al., 1991; Dossi et al., 1992; Nunez et al., 1992) and in vitro (McCormick and Prince, 1988; Leresche et al., 1990; McCormick and Pape, 1990b, a) studies demonstrated an intrinsic delta oscillation of thalamocortical relay neurons. The generation of this slow oscillation (0.5-4 Hz), proposed to be due to the interaction of two currents: the low-threshold Ca^{2+} current (l_T) and the hyperpolarization-activated cation current (I_h) (McCormick and Pape, 1990b).

It has to be noted that only this slow rhythmic burst firing (05-4 Hz) is an intrinsic property of thalamic relay neurons and other type of burst firing are mediated via interaction with GABAergic neurons of the reticular nuclei, spindle waves (7-12 Hz), or within thalamocortical loops, absence seizures (~3 Hz),(Steriade et al., 1997).

Figure 1-10 shows the occurrence of delta frequency rhythmic burst firing of thalamic relay neuron (i.e., LGNd neuron) in vitro (McCormick and Pape, 1990b). The cycle of delta oscillation starts with a large enough hyperpolarization of membrane to de-inactivate T-channels. This hyperpolarization will later activate I_h current, which depolarize membrane potential and activate I_T current. Activation of I_T leads to the generation low-threshold Ca^{2+} spikes and subsequently a burst of fast Na^+-K^+- mediated action potentials. However, until

the cell has been hyperpolarized for some time (—100 msec for I_T and —200 msec for I_h), I_T is inactivated and I_h is de-activated. The prolonged hyperpolarization will eventually activate I_h, but this activation is so slow that, before it begins I_T becomes fully de-inactivated, and the cycle begins again. This leads to the rhythmic activation of low-threshold Ca^{2+} spikes and bursts of action potentials. The Ca^{2+} spiking can occur at a variety of frequencies, and the actual value depends on other parameters, including the presence of local feedback inhibitory circuits that may become involved during rhythmic bursting (Steriade et al., 1997). This bursting can be switched to tonic mode only by a sufficiently strong and prolonged depolarization to inactivate I_T and prevent I_h from activation.

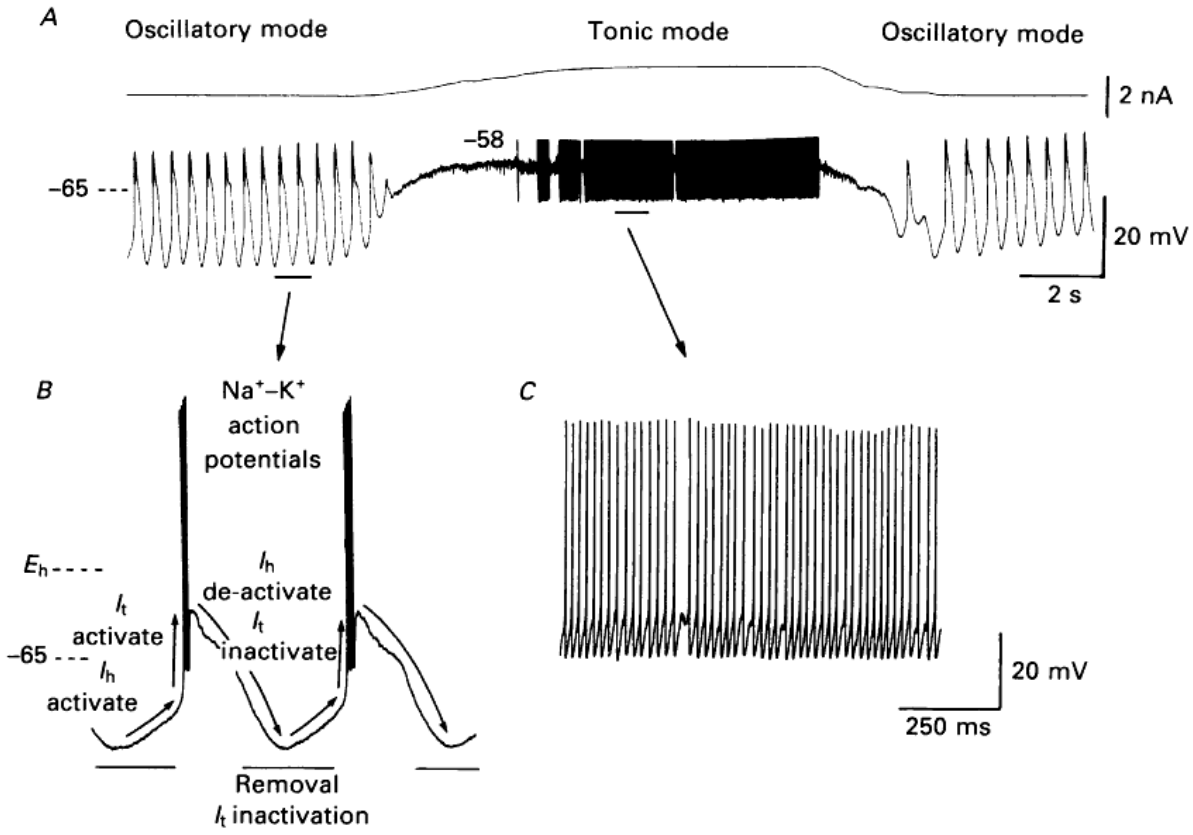

Figure 1-10. Tonic and rhythmic burst firing of thalamic relay neurons and the proposed ionic current interactions. (A) Rhythmic burst firing of the relay neuron from cat's lateral geniculate nucleus can switched to the tonic, or single-spike, mode of action potential generation, by depolarizing cell to -58mV. The neuron backs to the oscillatory activity by removing depolarization. (B) expanded trace of oscillatory activity and the proposed ionic currents which mediate this response (McCormick and Pape, 1990b).

1.3.3.2.4 High-threshold Ca^{2+} conductances

In addition to the transient and low threshold $Ca^{2+,}$ current, experimental data revealed the presence of sustained and high threshold calcium conductances in thalamic relay neurons (Jahnsen and Llinas, 1984b; Roy et al., 1984; Coulter et al., 1989; Huguenard and McCormick, 1992; Pedroarena and Llinas, 1997; Steriade and Timofeev, 1997; Zhou et al., 1997; Budde et al., 1998; Wu et al., 1998).

The high-threshold currents contained both non-inactivating and slowly inactivating components, which based on their specific subunits and kinetics named as L, N, R, P/Q type channel. These channels activated at membrane potential positive to -50 to -10 mV. However, inactivation of these channels is Ca^{2+} dependent (Budde et al., 2002; Meuth et al., 2002). Among these channels, L-type channel ("L" for "Long-lasting") has relatively major contribution to the total high threshold Ca^{2+} current. While the average ratio of maximum transient to the maximum sustained current is greater than 2 (Coulter et al., 1989), electrophysiological recording on thalamic neurons revealed a 40% contribution of L-type channels to the total high-voltage-activated calcium current (Budde et al., 1998).
Experimental data indicated the presence of the high-threshold Ca^{2+} channels in the dendrites and synaptic terminals (Coulter et al., 1989; Pedroarena and Llinas, 1997; Zhou et al., 1997; Pedroarena and Llinás, 2001; Jones, 2007). specifically, analysis of L-type channel in thalamic neurons (i.e., thalamocortical relay , local interneurons and reticular thalamic neurons) showed that the channel density was highest in the soma and decreased significantly in the dendritic region (Budde et al., 1998).

Since high threshold conductances are activated at a relatively depolarized membrane potential, they might actively influence the back propagation of the action potentials through dendritic arbors or may represent the fast prepotentials (FPPs) in thalamic cells (Maekawa and Purpura, 1967; Deschenes et al., 1984; Steriade and Timofeev, 1997; Jones, 2007).

In thalamic neurons, L- type channels might predominately influence Ca^{2+} dependent process in the cell body and proximal dendrites rather than in distal dendrites (Budde et al.,

1998). The possible function of L-type channel in thalamic neurons could be (i) the modulation of excitatory synaptic inputs in proximal dendrites (Mooney et al., 1993; Guyon and Leresche, 1995). (ii) Promotion of transition from the rhythmic burst to tonic mode activity (Hirsch et al., 1983; Steriade et al., 1993b; McCormick and Bal, 1997). (iii) Enhancement the induction of calcium release from intracellular stores (Chavis et al., 1996), and (IV) Augmentation of responses in TC neurons (Steriade and Timofeev, 1997). In addition, in synaptic terminals, these channels provide the required Ca^{2+} for transmitter release (Jones and Elmslie, 1997).

1.3.3.2.5 Voltage-dependent K+ conductance

Thalamocrtical neurons possess at least five different K^+ currents (Steriade et al., 1997). The identified voltage-dependent potassium current in thalamic relay neuron can be divided into fast and slow transient currents (Jahnsen and Llinas, 1984b, a; Budde et al., 1992; Huguenard and McCormick, 1992; McCormick and Huguenard, 1992).

1.3.3.2.5.1 Fast transient potassium current (I_A)

The fast transient potassium current (I_A) has similar voltage dependency as T-type Ca^{2+} current. A-current is activated by a depolarization from a hyperpolarized membrane potential and inactivated at depolarized membrane potentials. However, experiments on relay thalamic neurons indicated that the activation and inactivation curve of I_A channel occurs at more depolarized potential and it has much faster time constant than I_T (see Figure 1-11). A-type potassium channels are activated at around - 70 mV, and they quickly increase in amplitude with the slowest time constant of 2.5 ms at -60 mV and 23°C. The inactivation time of A-channel is independent of voltage in the range of -60 to 40 mV (i.e., τ=21 ms), but recovery from inactivation in the range of -80 to -140 mV is highly voltage dependent and varied between 10 and 60 ms (Budde et al., 1992; Huguenard and McCormick, 1992; Pape et al., 1994).

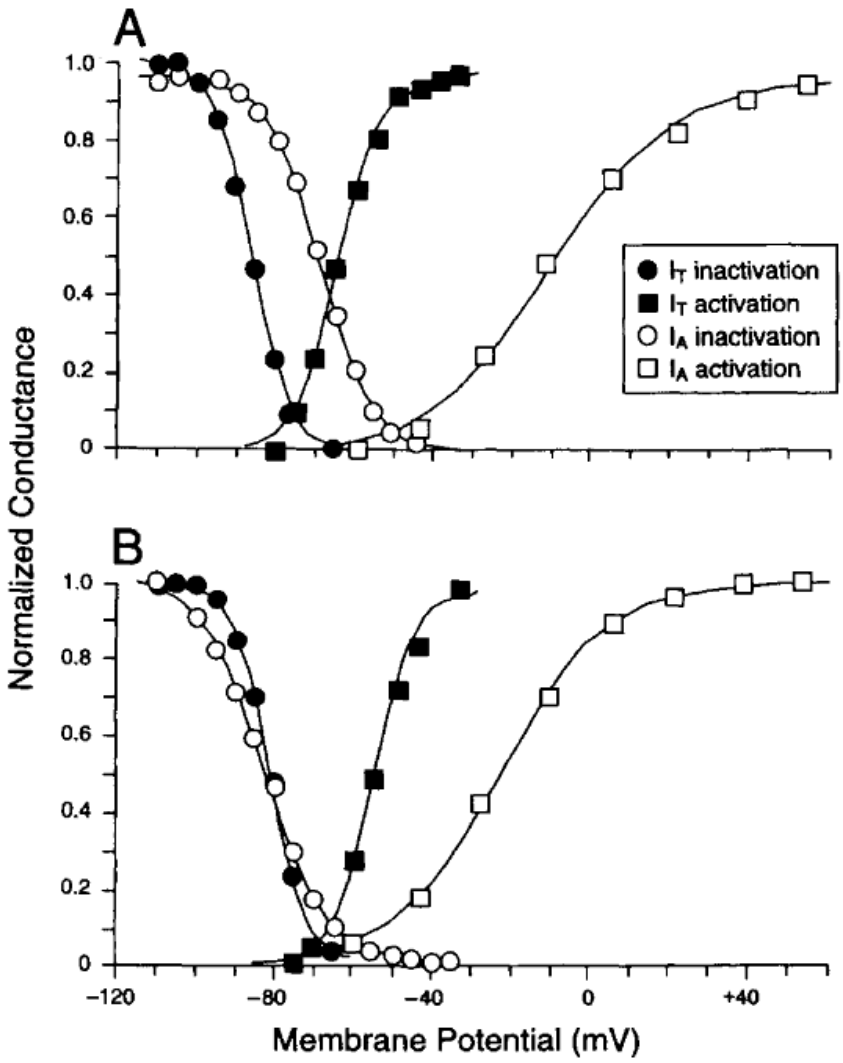

Figure 1-11. Activation and inactivation curves for both I_T and I_A in cells of the rat's lateral geniculate nucleus. (A) Comparison between IT and IA kinetics for a relay cell. Note that the curves for IT are shifted in a hyperpolarized direction with respect to those for I_A. (B) Comparison between I_T and I_A kinetics for an interneuron. Note that the inactivation curves for I_T and I_A are largely overlapped (Sherman and Guillery, 2006).

2.3.3.2.5.1.1 Functional role of I_A

Partly overlapping the voltage dependency and kinetics of fast transient K^+ current, I_A, with the T-type Ca^{2+} current suggests that these currents may interact, specifically, in shaping the low-threshold Ca^{2+} response. However, I_T current depolarizes the cell while I_A hyperpolarizes, thus, they might tend to offset one another if both were activated.

In relay neurons, I_T is activated at more hyperpolarized membrane potential than needed to activate I_A (see Figure 1-12). Thus, a strong depolarization could generate the low-threshold Ca^{2+} spikes before I_A has a chance to affect it. I_A would be activated with longer latency, which would probably affect the raising phase and reduce the size of the low-threshold Ca^{2+} spike. On another hand, A-channels inactivate rapidly, and probably do not contribute to regulating rhythmic LTS activity (Huguenard and Prince, 1991; Huguenard and McCormick, 1992; Pape et al., 1994). However, the activation of I_A may contribute to the control of repetitive firing (Connor and Stevens, 1971), and if the thalamic relay cell responds in tonic mode, I_A may delay and reduce the frequency of action potentials.

In the local interneurons, the ranges of steady-state inactivation and activation of I_T and I_A were largely overlapping, in this way the activation of A-channels may compensate the effect of T-channels in terms of net membrane current and prevent a regenerative Ca^{2+} response (Pape et al., 1994).

It has been suggested that I_A might extent the dynamic range of input/output relationships for neurons (Connor and Stevens, 1971; Zhang et al., 2009). Upon activation of A-channel, it will slow down the buildup of the EPSP, which will reduce the level of overall depolarization and enhance the range of EPSPs that evoke firing before response saturation. For relay cells, such a proposed function only makes sense for tonic mode because the response of low-threshold spikes in burst mode already has a limited dynamic range, and the low-threshold spike will be evoked before I_A can influence it much (Sherman and Guillery, 2006).

Experimental data demonstrated that dendritic trees of TC neurons contain a non-uniform distribution of Na^+ channel and T-channel but K^+ channels have roughly a uniform distribution (Williams and Stuart, 2000). This might prevent backpropagating action potential from reaching distal dendrites and thus, it would have less effect on corticothalamic EPSPs than upon EPSPs generated by more proximal located subcortical afferent terminals (Jones, 2007).

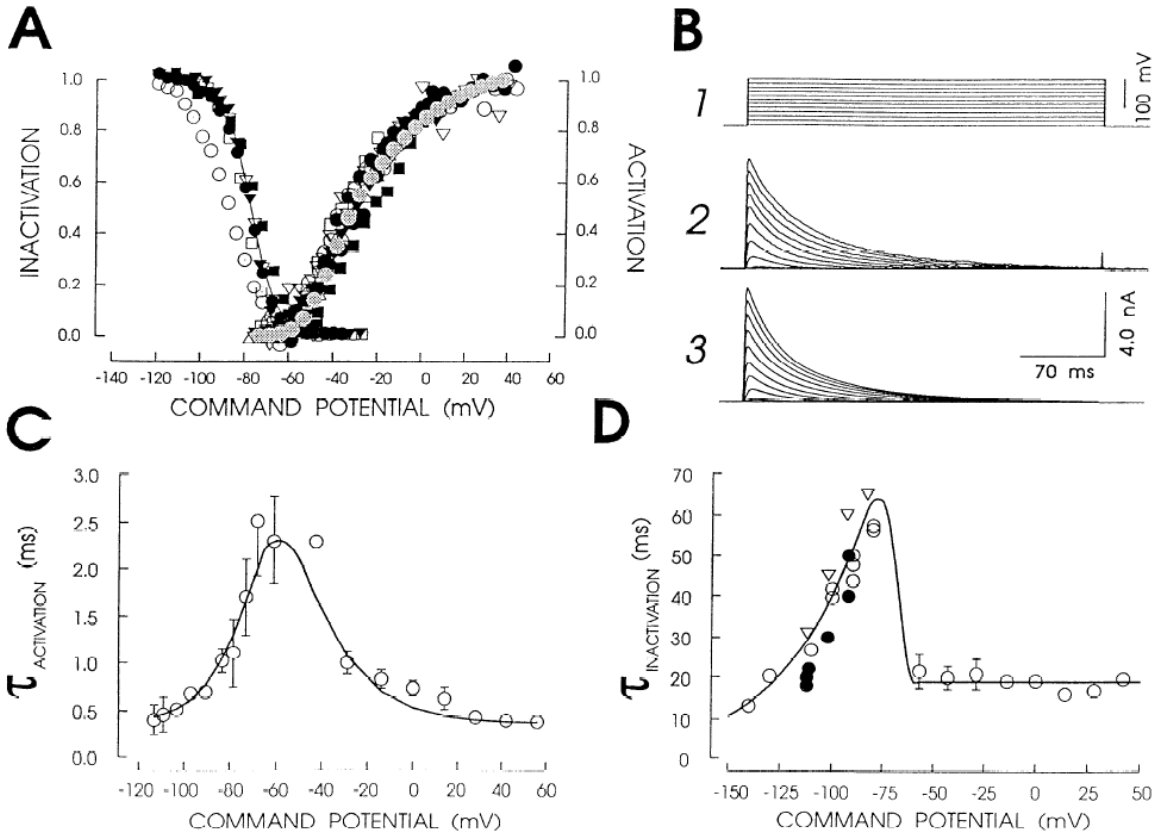

Figure 1-12. Voltage– dependent gating of fast transient potassium current (I_A). (A) steady state activation and inactivation curves of the fast transient potassium current (B) normal vs. simulated I_A. 1: voltage protocol, in which 300-ms depolarizations to membrane potentials between -96 and +58 mV from a holding potential of - 100 mV. 2: example I_A activation in a relay neuron. 3: simulation results. C: activation kinetics and model fit for I_A. D: inactivation kinetics and model fit for I_A. Inactivation measured as whole cell current decay was voltage independent in the range of -60 to +40 mV. On the other hand, de-inactivation as measured by the time course of recovery from inactivation at potentials between -80 and - 140 mV was highly voltage dependent (Huguenard et al., 1991).

1.3.3.2.5.2 Slow transient potassium currents

In vitro studies of relay neurons from rat LGN nucleus revealed three components of slow-transient K^+ current: I_{km}, I_{ks} and calcium- dependent potassium current, $I_{k[ca]}$ (Jahnsen and Llinas, 1984b; Budde et al., 1992).

The component I_{km}, is activated at around - 55 mV (τ = 20 ms at 23^{o}C), and recovers with τ = 128 ms from inactivation. I_{ks} is activated at a similar threshold, and recovers from inactivation occurred relatively fast with τ = 116 ms (Budde et al., 1992) .

The prominent component of slow-transient K^+ currents is Ca^{2+}-dependent potassium current, which is voltage and Ca^{2+} sensitive. $I_{K[Ca]}$ is activated at depolarizations positive to -40 mV with a slow time course (time to peak, from 263± 97 to 107± 31 ms in the voltage range - 15 to +45 mV) and which slowly declined (time constant >2 s) at depolarizations more positive than + 15 mV (Budde et al., 1992). Increasing intercellular Ca^{2+} concentration in the micromolar range will enhance the activation of $I_{K[Ca]}$ (Rudy, 1988; Steriade et al., 1997). However, in vitro intracellular recordings from TC relay neurons reveal that the Ca^{2+}- dependent potassium current is sensitive to increases in Ca^{2+} concentration resulting from high threshold Ca^{2+} current, but not those from low threshold Ca^{2+} current (Jahnsen and Llinas, 1984b; McCormick and Huguenard, 1992).

Slow inactivating K^+ current mainly contributes to the membrane repolarization during fast Na^+-dependent action potential or Ca^{2+} spike. While the fast transient potassium current modulates the initial component and peak amplitude of low threshold Ca^{2+} spikes, the slow inactivation potassium currents may affect more the later portions of Ca^{2+} spikes (Huguenard et al., 1991; Huguenard and Prince, 1991; McCormick and Huguenard, 1992). Intracellular recording from TC relay cells in vivo and in vitro suggested that different outward potassium currents in these neurons control the temporal characteristics of repetitive firing, and generate an apparent rectification of the neuron at resting membrane potentials (Budde et al., 1992; McCormick and Huguenard, 1992; Smith et al., 2000).

In addition to the functional role of K^+ current in the control of the neuronal responsiveness, it has to be noticed that inactivation of potassium current at hyperpolarized membrane potential of thalamic relay neurons depolarized level leads to more responsiveness to hyperpolarizing than depolarizing inputs. In this way, TC neuron may be specifically tuned to response to IPSPs with low-threshold Ca^{2+} spikes (Steriade et al., 1997).

1.3.3.2.6 Persistent Na^+ Conductance ($I_{Na(p)}$)

In vitro study from thalamic relay neuron showed that membrane depolarization positive to -55 mV generated a sudden sustained depolarizing plateau potential, which support repetitive firing and control the recovery of the neuron from after-hyperpolarization. This depolarization is the result of rapid activation of a persistent (non-inactivating) inward current ($I_{Na(p)}$) carried by Na^+ (Jahnsen and Llinas, 1984b, a).

Although the spatial distribution of this current in single TC neuron is not known, it is likely that $I_{Na(p)}$ may: (a) adjust the tonic firing mode of thalamic neuron (Parri and Crunelli, 1998; Tennigkeit et al., 1998, 1999). (b) contribute to functional state where the thalamic neuron displayed rhythmic oscillation (Jahnsen and Llinas, 1984a; Mulle et al., 1985; Jones, 2007). (c) control the electroresponsivness of thalamocortical dendrites, which may facilitate the transmission of distal synaptic potentials (Steriade et al., 1997).

1.3.4 Synaptic organization

Relay cells throughout the dorsal thalamus of all species show similar synaptic organization, with majority of synaptic inputs from the cerebral cortex (Steriade et al., 1997; Jones, 2007). Electron microscopic reconstruction of relay cells in VP (Liu et al., 1995), and Y cell in dLGN (Wilson et al., 1984) showed that these relay neurons receive about 5000-8000 synaptic inputs over whole cell and these synaptic inputs consisted of (see Figure. 1-13):

(I) the corticothalamic fibers, which forms about 44% of the synaptic connection. These synapses are localized on secondary, and particularly on tertiary, dendrites.

(II) sensory and motor pathway to the thalamus such as the medial lemniscal or optic tract fibres, which forms about 16% of synaptic inputs. These synaptic connections are localized on proximal dendrites, ending with multiple release sites

(III) the remaining 40% of synapses were derived from reticular neurons (≈35%) and interneurons (≈5%). These inhibitory synapses are tended to be concentrated on the soma, proximal and secondary dendrites.

TC neurons send their glutamatergic axons to the cerebral cortex and the reticular thalamic nucleus (RTN). The axons of specific TC neurons terminate in layers III, IV and VI, while TC projections from non-specific nuclei terminate in layers I and III (Steriade et al., 1997; Thomson and Bannister, 2003; Jones, 2007).

Corticothalamic inputs originating from layer VI have dual effects on relay neurons (Steriade et al., 1997; Jones, 2002b; Sherman, 2006; Jones, 2007). They could generate: (a) Excitatory postsynaptic currents through NMDA-, AMPA- and metabotropic glutamate receptors, (b) Indirect inhibitory effect via the collateral input from the same corticothalamic fibers to the GABAergic cells of the RTN. However, the influence of cortocothalamic stimulation on relay neurons, excitatory or inhibitory, depends on the functional state of these cells. When thalamic relay cells are relatively hyperpolarized, as occurs naturally during sleep and drowsiness, or under experimental conditions, the inhibition mediated by the RTN is commonly sufficient to overcome a weak direct excitatory effect of corticothalamic stimulation (Steriade, 2000, 2001; Jones, 2002b).

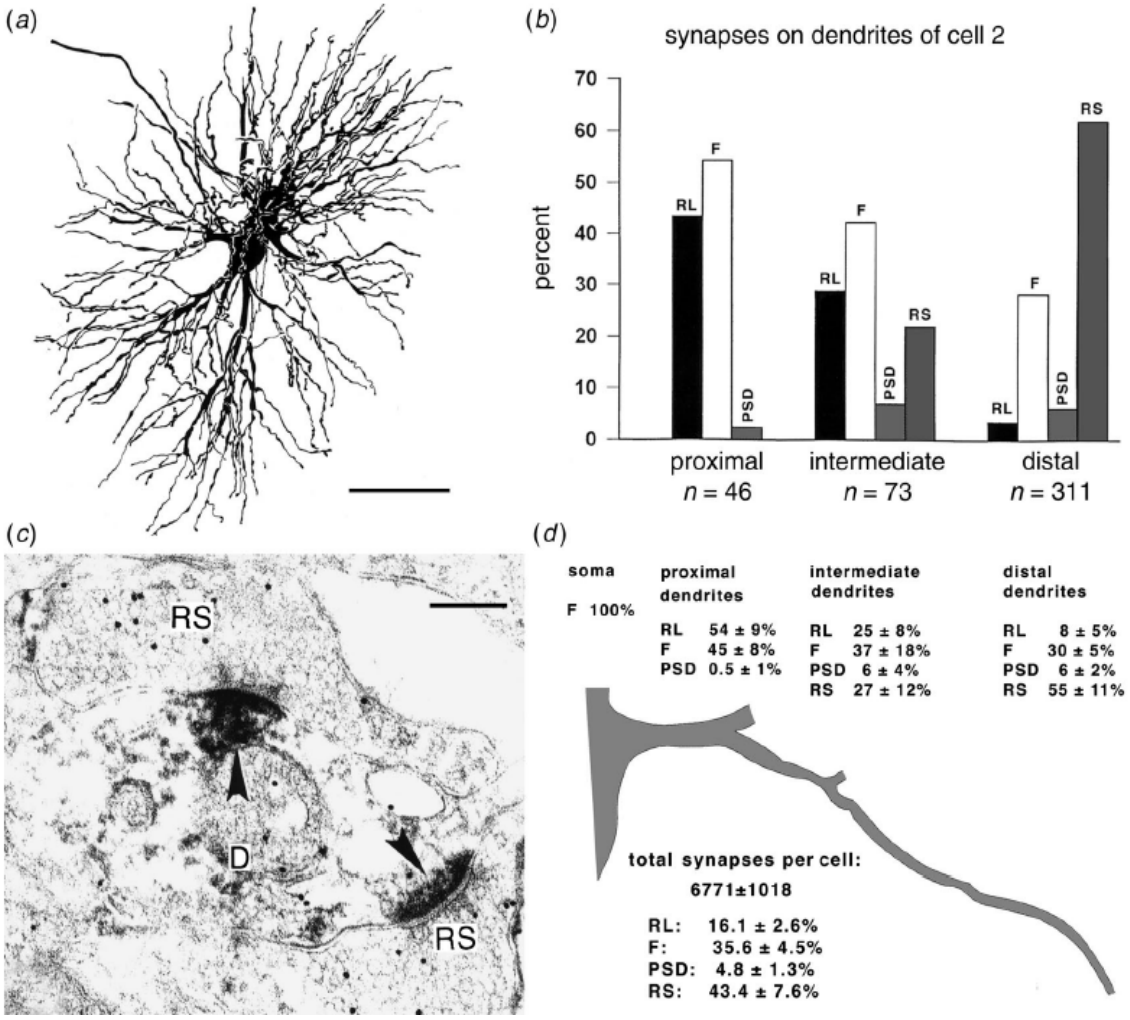

Figure 1-13. Synaptic distribution on a thalamic relay cell. (a) Reconstructed really neuron from the VPN of a cat. Scale bar=50μm. (b) Graph shows the distribution of synaptic inputs on the dendritic trees of a relay neuron from VPN of a cat. Abbreviations indicate medial lemniscal (RL), GABAergic (F), corticothalamic (RS) and presynaptic dendrites (PSD) of interneurons. (C) Electromicrograph of cortocothalmamic terminals (RS) in a rat, labeled for glutamate by immunogold particles, ending on a dendrite. Scale bar=1μm. (d) Estimated total number of synapses and relative proportions of the major types on a relay cell in the cat VPN (Jones, 2002b).

1.3.4.1 Synaptic properties

As mentioned in section 1.3 the synaptic inputs to the thalamus can be classified as driver and modulator inputs. The drivers are represented by ascending afferents to first order relays and by corticothalamic afferents from layer 5 to higher order relays. The modulators are corticothalamic afferents from layer 6 and other components arising from subcortical sources. Morphological analysis illustrated that axons with round vesicles and large terminals are drivers, whereas axons with round vesicles and small terminals are modulators (Guillery, 1995; Steriade et al., 1997; Jones, 2007).

The axon terminals on the thalamic relay neurons release different type of neurotransmitters, which can activate two different kinds of postsynaptic receptors found on relay neurons: lonotropic and metabotropic receptors (McCormick, 1992a, b; Jones, 2007).

The evoked postsynaptic potentials produced by activation of ionotropic receptors are fast, meaning they have a short latency and a fast rise to peak (i.g., $\tau \approx 10$ ms). On the other hand, postsynaptic potentials produced by activation of metabotropic receptors are very slow, meaning they have a long latency, usually >10 msec, very slow rise to peak (i.e., tens of msec), and they remain present for a long time, typically hundreds of milliseconds to several seconds or even longer. Single action potentials or a few closely spaced in time that invades the presynaptic terminal are generally able to activate ionotropic receptors. However, activation of metabotropic receptors typically requires long trains or high frequency of action potentials (McCormick, 1992a).

It has to be mentioned that according to the cable theory the attenuation along a dendritic pathway is frequency dependent. Thus, the faster events (i.e., faster postsynaptic potentials) will attenuate more during propagation toward to the soma, whereas the slower event will be minimally attenuated by these membrane properties (Spruston et al., 1994; Rall et al., 1995). Therefore, the postsynaptic potential evoked via ionotropic receptors activation will face more attenuation than slow postsynaptic potential produced by metabotropic receptors.

Figure 1-14 shows typical synaptic inputs to relay neuron from the lateral geniculate nucleus (Sherman and Guillery, 2006). This figure illustrates the type of receptors and their location on dendritic trees on the relay neuron as well as their effects on the postsynaptic neuron. The sign of the evoked postsynaptic potential (i.e., excitatory or inhibitory) will depend on the delivered neurotransmitter. In addition, it has to be noticed that most transmitters can activate several types of receptor within each of the ionotropic or metabotropic categories. Table 1-2 shows inputs that are common to many thalamic nuclei, receptor and neurotransmitter types.

The axon terminals on the thalamic relay neurons release different type of neurotransmitters such as glutamate, GABA, and neuromodulatory transmitter such as acetylcholine, noradrenalin, serotonin and histamine, that bind to corresponding postsynaptic receptors and generate excitatory of inhibitory postsynaptic potential (McCormick, 1992b).
Excitatory postsynaptic potential in thalamic relay neurons mediated via activation of NMDA, non-NMDA and metabotropic glutamate receptors. Activation of metabotropic glutamate receptors cause a depolarization in the membrane potential of relay neurons by reducing the K^+ "leak" conductance. This depolarization has long duration (seconds to minutes) and takes seconds to reach its peak. This slow depolarization can shift the rhythmic burst firing mode of TC neurons into the single spike activity (McCormick, 1992b). Activation of the non-NMDA receptors produces a fast EPSP caused by entry of Na^+ and perhaps other cations, while activation of NMDA receptors need more depolarization to remove Mg^+ block and involves significant Ca^{2+} influx. Although the generated EPSP via NMDA receptors has longer latency and duration than the non-NMDA ionotropic receptors, it is much faster than EPSP produced by activation of metabotropic glutamate receptors.

Inhibitory postsynaptic potential in TC neurons produced by activation of $GABA_A$ and $GABA_B$ receptors, which are iontropic and metabotropic receptors, respectively. Activation of $GABA_A$ receptors opens Cl^- channels, which tends to shift the membrane potential of TC neurons toward reversal potential of Cl^- around -70 to -75 mV. Activation of $GABA_B$ receptors increase conductance of potassium leak current, which cause more

strongly hyperpolarization toward reversal potential of K^+ close to -100 mV. Inhibitory PSP of $GABA_A$ last roughly about 50 msec and IPSP $GABA_B$ receptors has prolonged duration around 200-300 msec (Castro-Alamancos and Connors, 1997).

Neuromodulators in TC neurons, affect the response of the cell via metabotropic receptors: (a) In vivo extracellular recording from LGNd relay neurons of cat indicated that application of acetylcholine (ACh), which mainly release from axonal terminal arise from brainstem, leads to altering the firing mode from the rhythmic burst to single spike mode (McCormick, 1992a). (b) Applying of histamine presumably arising from the tuberomammillary nucleus of the hypothalamus, causes a slow depolarization and, like Ach, can completely switch the firing mode of cat LGNd relay neurons (McCormick and Williamson, 1991). (c) Retrograde labeling studies showed that noradergenic innervations of thalamus arise from locus coeruleus. Noradrenalin via its two receptors, α_1 and β , cause a slow depolarization mediated by decrees in potassium conductance and enhancement of I_h current (McCormick, 1992a). (d) The main part of serotoninergic fibers arises from the dorsal raphe. The application of serotonin to LGNd relay neurons leads to a small depolarization associated with an increase of I_h (McCormick, 1992a).

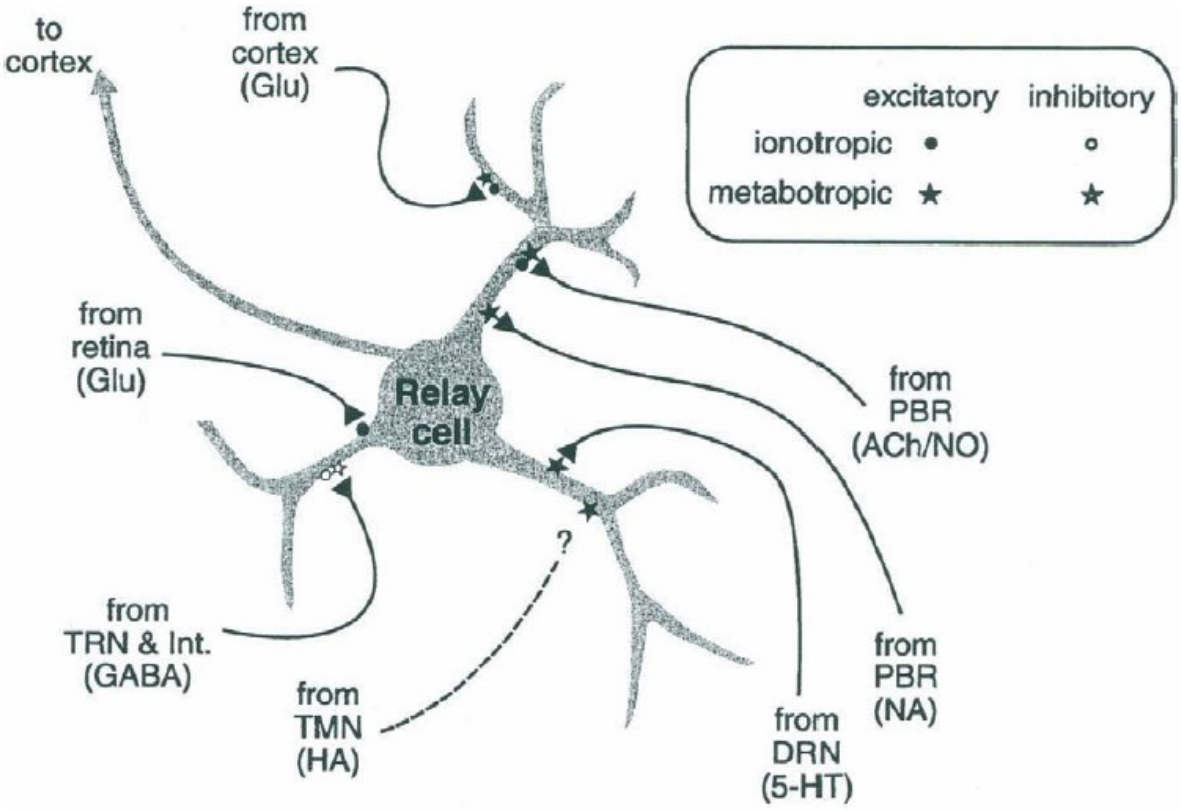

Figure 1-14. The neurotransmitters and postsynaptic receptors for the relay cell of the lateral geniculate nucleus. 5-HT, serotonin; ACh, acetylcholine; DRN, dorsal raphe nucleus; Glu, glutamate; HA, histamine; Int., interneuron; NO, nitric oxide; NA, noradrenaline; PBR, parabrachial region; TMN, tuberomamillary nucleus; TRN, thalamic reticular nucleus (Sherman and Guillery, 2006).

Source	Transmitter	Receptor type
Retina	Glutamate	Ionotropic
Cortex (layer 6)	Glutamate	Ionotropic and metabotropic
Parabrachial region	Acetyldioline	Ionotropic and metabotropic
Parabrachial region	Noradrenaline	metabotropic
Dorsal raphi nucleus	Serotonin	metabotropic
Tuberomamillary nucleus	Histamine	metabotropic
Thalamic reticular nucleus	GABA	Ionotropic and metabotropic

Table 1-2. Input to relay neurons of lateral geniculate and ventral posterior nucleus. (Sherman and Guillery, 2006)

1.4 NEURON simulation environment

NEURON is a simulation environment for modeling a single neuron or neuronal networks. It is mainly relevant to model cells with complex morphological and biophysical properties. It provides tools for conveniently building (i.e., designing artificial cells or imported morphological data), managing (i.e., passive properties, ionic conductance with different kinetics, and etc.) and running models in a computationally efficient way (i.e., number of compartments and integration time step). The programming Language are C, C++ and Python. Users can develop their code to define specific mechanism and properties with NMODL language of NEURON simulation environment (Hines and Carnevale, 1997).

1.5 Objectives of the thesis

Transferring nearly all sensory information through the thalamus strongly depends on the intrinsic properties of thalamocortical neurons. The rich variety of voltage-dependent ionic channels and the distinct dendritic arborization of thalamic relay neurons provide a strong computational power for integrating and processing synaptic inputs. Therefore, investigating the fine details of morphological parameters as well as exploring active properties of dendritic trees will provide us a better understanding of input-output function of thalamocortical neurons. We hypothesized that the biophysical properties and the complex dendritic arborization of thalamocortical neurons are optimized for generating the firing patterns and synaptic integration. In order to test this hypothesis, our study aimed to:

(i) extract precise data of thalamocortical morphology based on 3D reconstruction,
(ii) explore morphological parameters, to verify or modify the previous data and reveal new properties,
(iii) examine the intrinsic electrophysiological properties of TC neurons with a multi-compartmental model based on Hodgkin-Huxley type of equations in order to

find the consequence of non-uniform distribution of T-channels and relation between morphological properties and the efficacy of electrical signal propagation within dendritic trees.

Complete 3D reconstruction of Thalamocortical neurons will give us an opportunity to inspect morphological properties and develop multi-compartmental models. Among morphological parameters, we specially focus on the geometrical ratio value at branching points, which has a high impact on propagation of electrical signals and owned inconsistent values from different studies.

By applying the hypothesis of "minimizing metabolic cost", we try to find the optimized distribution of T-channel for generating the LTS response. Furthermore, multi-compartment models can be used to investigate how morphological parameters of each dendritic tree control the forward propagation of an excitatory postsynaptic potential toward the soma and adjust the extent of back propagating action potential.

2 Analysis of Morphological Features of Thalamocortical neurons from Ventro Postero Lateral Nucleus of the Cat

Reza Zomorrodi, Alex S. Ferecskó, Krisztina Kovács, Helmut Kröger, Igor Timofeev

J Comp Neurol. 2010 Sep 1; 518:3541-3556. Epub 20 MAY 2010

2.1 Résumé

Les caractéristiques morphologiques de l'arborisation dendritique peuvent affecter les réponses neuronales et donc la fonction d'entrée-sortie d'un neurone particulier. Dans cette étude, les données morphologiques de huit neurones thalamocorticaux (TC) entièrement reconstruits du noyau ventro postéro latérale (VPL) de chats adultes ont été analysés. Nous avons examiné plusieurs paramètres géométriques et topologiques qui ont préalablement démontrés avoir une forte incidence sur le patron de décharge neuronale et la propagation des signaux dans l'arborescence dendritique. En plus des paramètres morphologiques déjà connus tels que le nombre d'arbres dendritiques (8.3±1.5) et le nombre de points de branchements (80-120), nous avons étudié la distribution de la surface membranaire dendritique, les points de ramification , le ratio géométrique, l'indice d'asymétrie et la longueur du parcours moyen pour toutes les branches dendritiques des neurones TC. Nous démontrons qu'en raison de la vaste ramification des sections dendritiques proximales et du milieu, la valeur maximale de la distribution de la surface dendritique est atteinte à 120-160 μm de soma. Notre analyse révèle que les neurones TC sont des cellules très ramifiées et leur patron de ramification dendritique ne suit pas la règle de Rall du 3/2 de puissance et les valeurs moyennes des sections dendritiques proximales vs distales étaient différentes. Nous avons également constaté que le patron de ramification dendritique de chaque sous-arbre de la cellule a un large éventail d'index de symétrie, tandis que la longueur du parcours moyen n'a pas montré une grande variation selon les ramifications dendritiques.

2.2 Abstract

Morphological features of the dendritic arborization can affect neuronal responses and thus the input-output function of a particular neuron. In this study, morphological data of eight fully reconstructed thalamocortical (TC) neurons from the ventro postero lateral (VPL) nucleus of adult cats have been analyzed. We examined several geometrical and topological parameters, which have been previously shown to have a high impact on the neuron firing pattern and propagation of signals in the dendritic tree. In addition to well known morphological parameters such as number of dendritic trees (8.3±1.5), number of branching points *(*80-120*),* we investigated the distribution of dendritic membrane area, branching points, geometrical ratio, asymmetry index and mean path length for all sub-trees of the TC neurons. We demonstrate that due to extensive branching in proximal and middle dendritic sections, the maximum value of the dendritic area distribution is reached at 120-160 μm from soma. *O*ur analysis reveals that TC neurons are highly branched cells and their dendritic branching pattern does not follow Rall's 3/2 power rule and average values at proximal vs. distal dendritic sections were different. *W*e also found that the dendritic branching pattern of each sub-tree of the cell had a wide range in symmetry index, while the mean path length did not show a large variation through the dendritic arborizations.

2.3 Introduction

The thalamus is the main gateway of peripheral information ascending towards the cerebral cortex (Steriade and Pare, 2007). The principal neurons of the thalamus are thalamocortical (TC) cells. The basic morphological features of TC neurons are well known. These neurons have a round cell body and bushy dendrites, extending 200-250 μm from the cell body (Jones, 2007; Steriade et al., 1997).

The thalamus participates in the generation of a variety of TC oscillations (Castelo-Branco et al., 1998; Hughes et al., 2002; Steriade and Deschênes, 1984; Steriade et al., 1993; Timofeev and Steriade, 1997). Such ability of the TC system to generate a variety of oscillations triggered a large number of modeling studies involving TC neurons (Bazhenov et al., 1998; 2002; Destexhe et al., 1998; Destexhe and Sejnowski, 2001; Hill and Tononi, 2004; Rhodes and Llinás, 2005; Traub et al., 2005; Zomorrodi et al., 2008). In the majority of these models the electrophysiological properties of the neurons were simulated based on known conductances. Indeed, the basic electrophysiological properties of a neuron can be easily modeled with active conductances using a single structural compartment (Huguenard and McCormick, 1992; McCormick and Huguenard, 1992). In two or three compartment models, the previous studies were able to reproduce a large variety of electrographic activities of different neurons (Destexhe et al., 1996; Destexhe et al., 1998; Mainen and Sejnowski, 1996; Rulkov et al., 2004).

Recent studies demonstrated however, that the morphology of the neuron plays a critical role in the cell responsiveness (Turner et al., 1997). It has been shown that with the same active and passive properties of the dendritic tree, the geometrical (e.g. area) and topological (e.g. partition symmetry) properties strongly influence the neuronal firing patterns and modify the efficacy of back propagating action potentials or the forward propagation of postsynaptic potentials (Chklovskii, 2004; Duijnhouwer et al., 2001; Gulledge et al., 2005; Katz et al., 2009; Komendantov and Ascoli, 2009; Sterratt and van Ooyen, 2002; Timofeeva et al., 2008; van Pelt and Schierwagen, 2004; Weaver and Wearne, 2008).

The detailed characterization of the dendritic tree of TC neurons is still incomplete or controversial. A vast majority of data involving cell reconstructions was obtained from air dried sections mounted on gelatin-coated slides. Water evaporation from a section does not affect parameters such as the number of dendrites, branching pattern or total dendritic length, but it does strongly affect parameters such as the dendritic diameter, morphology of branching points or 3-dimensional dendritic structure. Sometimes this leads to contradictory findings. For example, an earlier study has shown that at the dendritic branching points TC neurons faithfully follow Ralls' power rule (Bloomfield et al., 1987). However, a later investigation demonstrated multiple exceptions from this law in TC neurons (Ohara et al., 1995).

The motivation for this study was to provide a detailed description of the morphology of TC neurons from the ventro postero lateral (VPL) nucleus of thalamus using three-dimensional reconstructions with the goal to obtain a deeper understanding of how morphological features affect neuronal integration in the thalamus.

2.4 Materials and Methods

2.4.1 Neuronal labeling and three-dimensional reconstruction

The understanding of thalamic gating during sleep oscillations is a crucial step in determining the functional role of sleep. During sleep oscillations, the highly specialized whisker system of rodents transmits sensory information towards the cerebral cortex with little alterations at the level of the thalamus (Hasenstaub e.t at., 2007). This is not the case in cats, in which ascending EPSPs arriving at TC neurons during silent states of slow oscillation do not reach the firing threshold, while they fire action potentials during active states (Rosanova and Timofeev, 2005). Therefore, four cats were used for neuronal staining and reconstruction in the experiments described below. In one out of four animals, a neuron from VPL nucleus was intracellularly injected with neurobiotin (Vector Laboratories, ON, Canada; Fig. 2-1 and 2- 5). In this experiment, the cat was deeply anesthetized with sodium pentobarbital (30 mg/kg). The intracellular pipette was lowered stereotaxically to the VPL nucleus. Under barbiturate anesthesia, TC neurons show typical spindle activity (Fig. 2-1D). To identify a TC neuron as VPL neuron during the experiment, we applied electrical stimuli to the medial lemniscus and obtained stable short latency EPSPs (Fig. 2-1C). The other details of experimental manipulations with animal were identical to those previously described (Rosanova and Timofeev, 2005). In the other 3 cats, retrograde tracer tetramethylrhodamine-labeled dextran (fluoro-ruby, Invitrogen Canada Inc., ON, Canada) was iontophoretically applied in the white matter (2.5-3 mm from cortical surface) underneath the somatosensory cortex. The injections were made underneath the area where the largest somatosensory field potential responses was obtained to the electrical stimuli of *nucleus cuneatus* (1.5 mm posterior to obex and 1.5 mm lateral to midline, Fig. 2-2A), the area that receives inputs from forelimb receptive fields. The injections were completed via borosilicate glass micropipettes pulled on a horizontal puller. The tips of the micropipettes were broken against a glass slide to 20-25 μm in diameter and were filled with 5% fluoro-ruby dissolved in 0.1 M phosphate buffer saline (PBS), pH=7.4. Iontophoretic injections were carried out using positive 5-8 μA current pulses (2-4 sec ON/2 sec OFF duty cycle)

for 20-30 minutes. To reduce injury during the chronic surgery the dura mater was left intact, only a tiny slit was made in order to position the micropipettes onto the cortical surface. After the extracellular injections, the animals were allowed to recover. In order to achieve a sufficient retrograde labeling of somata and dendritic trees of TC cells in the VPL, the survival time was 10-14 days. Thereafter, the animals were deeply anesthetized with ketamine-xylazine (10–15 mg/kg) in accordance with the guideline of the Canadian Council on Animal Care and approved by the Laval University Committee on Ethics and Animal Research. All animals in this study were perfused transcardially with Tyrode's solution (pH 7.2-7.6; 8g NaCl (137 mM); 0,2g KCl (236 mM); 1ml $CaCl_2$ X $2H_2O$ (26%); 1 ml NaH_2PO_4 X $2H_2O$ (5%); 1g glucose (5,56 mM); 1g $NaHCO_3$ (11,6 mM) for 3 minutes followed by a fixative (4% Paraformaldehyde, 0.1-0.5 % glutaraldehyde, in 0.1 M phosphate buffer (PB, pH 7.4) for 40 minutes or 2 liters of fixative. Tissue blocks containing the injection sites were dissected from the area of interest and submersed into sucrose solution (10%, 20% and 30% sucrose dissolved in 0.1 M PB) for cryoprotection. The blocks were mounted on a metal plate and 80 µm thick consecutive sections were cut using freezing microtome.

The sections were collected in 0.1M PB, transferred to Tris-buffered saline (TBS, pH 7.6) to which 0.01-0.02% Triton X-100 was added (TBS-T) and rinsed 3 times for 20 minutes. Then the sections were incubated in 5% normal goat serum (NGS) and TBS for 45 minutes. Fluoro-ruby was developed using primary (anti-tetramethylrhodamine rabbit IgG, 1:5000, Invitrogen Canada Inc., ON, Canada) and secondary (biotinylated goat anti-rabbit IgG, 1:500, Vector Laboratories, ON, Canada) antibodies. The incubation was performed under continuous, gentle agitation in 2% NGS and TBS overnight at 4°C. On the next day, the sections were further incubated in avidin-biotin complex (ABC, 1:200; Vector Laboratories, ON, Canada) for 4 hr. After several washes in TBS and Tris, the immunoperoxidase reaction was revealed by 3'3-diaminobensidine tetrahydrochloride (DAB; Sigma-Aldrich; 0.05% in Tris) and 0.005% $CoCl_2$ as a chromogen and 0.01% H_2O_2 as oxidant. In order to reduce the shrinkage of the sections for further 3-dimensional reconstruction and morphometrical measurements, they were treated with osmium-tetroxide (0.5-1% OsO_4) dissolved in 0.1 M PB for 10-20 minutes, washed again in 0.1 M PB and

dehydrated in an ascending series of ethanol and propylene-oxide (Somogyi and Freund, 1989). After dehydration, the sections were embedded in epoxy resin (Durcupan, Fluka, Buchs, Switzerland), mounted on microscope slides, covered with glass cover-slips and cured at 56°C for 24 hours.

Following the histological procedures, somata and dendritic arbor of one intracellulary and seven fully retrogradely labeled TC cells were chosen for further three-dimensional reconstruction. The reconstructed cells were located in dorsal middle and anterior part of the VPL nucleus (Fig. 2-2B). We did not select for reconstruction: (a) faintly stained neurons, (b) fully stained neurons that had another stained neuron in the vicinity to avoid errors in matching dendrites on consecutive sections. The sections were examined at 1000X magnification (using x100 objective lens) under the light microscope attached to the Neurolucida reconstruction system and fitted with a computer controlled motorized stage. Morphologically identified somata and dendritic fields of TC cells in the VPL nucleus were recovered systematically from each section. The reconstruction of labelled neurons, were stored and analyzed as a series of 3D coordinates. The anatomical reconstruction was corrected for virtual shrinkage in the Z-axis caused by the optical density of the embedding medium, the epoxy resin, and the microscope immersion oil. The microscopically measured Z-values were multiplied by the correction factor, $f = n_{resin}/n_{oil}$, where $n_{resin} = 1.549$ and $n_{oil} = 1.5180$ were the experimentally determined index of refraction for the epoxy resin and the index of refraction for the immersion oil (Buzas et al., 1998).

2.4.2 Morphological parameters

The complexity and morphological variability of the dendritic tree arborizations were classified by topological and geometrical features. Parameters like length, diameter or membrane area are considered as geometrical or metric properties and the parameters that show the connectivity between dendritic segments are defined as the topological property of a neuron.

Recently, several analytical and computational models have been developed to examine the complexity of the dendritic morphology in details (Samsonovich and Ascoli, 2005; Scorcioni et al., 2008). Here, we focused on the morphological features that have a strong correlation with the neuronal responsiveness. These parameters include: dendritic membrane area, branching density, Rall's geometrical ratio at branching points, mean path length, and partition asymmetry of a dendritic tree. These parameters not only influence the firing patterns of a neuron, but also strongly control the propagation of spikes along the dendritic tree (van Pelt and Schierwagen, 2004; Vetter et al., 2001; Weaver and Wearne, 2008). We used Matlab (version 6.5, MathWorks) and NEURON (Hines and Carnevale, 1997) to analyze the morphological data of the reconstructed TC neurons.

In order to determine the dendritic membrane area (A), we divided the dendrites in segments of 1 μm in length (dx=1 μm) where each dendritic segment was considered as a cylinder. The surface area of a dendritic segment was represented by the surface area of the corresponding cylinder segment. Such approximation was applied for each dendritic segment.

Another geometrical feature of the dendrite that has a functional link to the propagation of potentials is the ratio of the input impedance of the dendritic sections before and after the branching points. It determines the transient change in the amplitude of a potential when approaching the branching point from the parent to the daughter (Goldstein and Rall, 1974; Lüscher and Shiner, 1991). It has been shown for branches of constant diameter that such ratio of the input impedance can be expressed by Rall's geometrical ratio (GR), as follows

$$GR = \frac{\sum_{d} D_d^{3/2}}{D_p^{3/2}} \qquad (2\text{-}1)$$

where D_d and D_p are the diameter of daughter and parent branches at the branching point, respectively. Branching points with GR > 1 cause a transient decrease in the amplitude, while those with GR<1 cause a transient increase in the amplitude of the propagating

potential. For transients with GR=1, the amplitude is unchanged (Goldstein and Rall, 1974). The case of GR=1 is denoted as Rall's 3/2 power rule. To calculate the GR values we used the diameter of the last point before bifurcation as parent diameter and the diameters of first points after bifurcation as daughter diameters (L-measure, Scorcioni et al., 2008).

The connectivity pattern of the dendritic segments is another morphological factor, which affects the neuronal responses. Here, we analyzed the partition symmetry and the mean path length of the dendritic tree. Those have been shown to have strong correlations to neuronal responsiveness (Duijnhouwer et al., 2001; van Pelt and Schierwagen, 2004). A measure for the topological asymmetry of a tree is the tree asymmetry index (Van Pelt et al., 1992). For a given tree α^n with n terminal segments, the tree asymmetry index A_t is defined by

$$A_t(\alpha^n) = \frac{1}{n-1}\sum_{j=1}^{n-1} A_p(r_j, s_j) \tag{2-2}$$

where n-1 is the number of bifurcation points, $A_p(r_j, s_j)$ is the partition asymmetry at the j^{th} bifurcation point, and r_j and s_j are numbers of the terminal segments in the two subtrees emanating from the j^{th} bifurcation point. At each of the n-1 bifurcation points, partition asymmetry indicates the relative difference in the number of bifurcation points, r_j-1 and s_j-1, in the two subtrees:

$$A_p(r_j, s_j) = \frac{|r_j - s_j|}{r_j + s_j - 2} \tag{2-3}$$

for $r_j + s_j > 2$. By definition, $A_p(1, 1) = 0$. The tree asymmetry index is zero for a fully symmetrical tree and goes to 1 (for $n \to \infty$) for a maximally asymmetric tree. The tree

asymmetry index has been shown to be a good measure of topological structure (Van Pelt et al., 1992).

The mean path length is the sum of all dendritic path lengths measured from the soma to the tip of the dendrite divided by the number of the terminal segments. Thus, for a given tree α^n with n terminal segments, the mean path length P is

$$P(\alpha^n) = \frac{1}{n}\sum_{j=1}^{n} P_j \qquad (2\text{-}4)$$

where P_j is the length of the dendritic path between the tip of the j^{th} terminal segment and the soma.

2.5 Results

Three-dimensional reconstruction of eight TC neurons has been performed using Neurolucida (Fig. 2-1, Fig. 2-2), and the data have been imported to NEURON for morphological analysis. Reconstructed TC neurons had a typical bushy shape, with a radially symmetrical dendritic tree composed of average 8.37±1.5 dendrites that spread out in a spherical zone of 200-250 µm in radius (Deschênes et al., 1984). Each neuron had both thin and thick dendrites (Table2-1). The average surface of soma was 2956.24 ±918.89 μm^2. These and other standard data for individual neurons are given in Table2-1. Our results are in line with previously findings (Reviewed in Jones, 2007; Steriade et al., 1997). From 3D reconstructions, we calculated the total dendritic area. The mean total dendritic area was found to be 44160.08 ±14297.16 μm^2 (see Table 2-1), which is 15.01± 2.17 times larger than the total somatic area.

The distribution of the dendritic membrane area versus the path distance from the soma had approximately the same distribution in all reconstructed dendrites (e.g.: cell 6 in Fig. 2-3A)

and in all reconstructed neurons (Fig. 2-3B). For each TC neuron, we estimated the membrane area of the dendritic sections using 1 μm step bins and summed up all with the same path distance from the soma. Despite small tapering, at the dendritic bifurcations, the sum of the daughter branches leads to an overall increase in the dendritic membrane area. When a dendritic branch terminates, the total dendritic area decreases. Because dendritic trees have more sections in the middle part of their arborization, the membrane area attain its maximum in the middle part of the dendritic tree (120-160 μm from soma).

TC neurons have highly ramifying dendrites with 121±17 branching points on average. The maximal number of branching points is located at 80±15 μm from the soma (Fig. 2-4). A high ratio (90%) of bifurcations at the branching points was previously reported (Havton and Ohara, 1993). There is no criterion to distinguish between multi-furcation and several close consecutive bifurcation points. Using 0.5 mm steps, we estimated that multi-furcation (trifurcation) occurred only 18 times (2% of the cases, Fig. 2-5B). In all the other cases, the branching points gave rise to bifurcations (Table 2-1). The number of end segments in each neuron varied between 96 and 154 with a mean value of 130.37±19.97 (Table 2-1).

We investigated another geometrical feature of the dendritic tree, i.e. the diameter of dendritic sections at the branching points. We determined the value of the exponent number (n) in Rall's power rule and of the geometrical ratio (GR) at each branching point. Figure 2-5A, shows a light macroscopic picture of a TC soma, several dendritic sections and one reconstructed subtree. A comparison of the reconstructed tree at branching points and their corresponding microscopic image is illustrated at higher magnification in the bottom panels of figure 2- 5A. When the diameter of parent branch is smaller or equal to the diameter of one daughter branch at the branching point (Fig. 2-5A, 1), then the exponent (n) in Rall's power rule is not defined (can take only imaginary value that cannot be calculated). Further examples and averaged data of the value of exponent (n) in Rall's power rule and geometrical ratio (GR) at different branching point of the reconstructed sub-trees are shown in Figure 2-6A and B. The mean values of GR from 8 reconstructed neurons were usually found to lie above 1. The average GR value in proximal (<60 μm), middle (60-120 μm) and distal (>120 μm) dendrites was 1.30 ± 0.45, 1.54 ± 0.58 and *1.45 ± 0.41* respectively (Fig.

2-6B). The overall GR for 969 branching points was 1.43±0.12. These results predict a strong attenuation of the back propagating action potentials to distal dendrites in the majority of branching points. However, during normal brain operations, synaptic potentials arriving to the distal dendrites propagate towards the neuronal soma. Therefore, depending on direction of the signal propagation, the parameter GR will have a different value. Under these conditions, distal dendrites become parents for the more proximal dendrites. We calculated mean values of GR for signals propagating from distal to proximal parts of the dendrites toward the soma. The average GR value was 4.47 ± 3.15, 3.08 ± 1.39 and 3.10 ± 1.20 for proximal (<60 μm), middle (60-120 μm) and distal (>120 μm) dendrites (Fig. 2-6C), suggesting a very strong attenuation of the distal synaptic potentials propagating towards the soma.

Besides the particular geometrical properties, TC neurons show diversity in dendritic tree topology. Here, we analyzed the asymmetry index according to Eq. 2-2. Our morphological analysis revealed that TC neurons could have a fully symmetric sub-tree with only one bifurcation point or complex dendritic arborizations with a large value of asymmetry index. Figure 2-7 illustrates two dendritic trees from each of 8 reconstructed TC neurons with an extreme value of asymmetry index. In some cases, even though two sub-trees look quite similar in their arborization (see cell 2, 5 and 8), their asymmetry indices differ considerably (Fig. 2-7). We determined the value of the asymmetry index for each sub-tree of a TC neuron (Fig. 2-8A and Table 2-2). The average value of asymmetry index for all TC neurons was 0.41±0.02, which shows a trend towards a more symmetrical shape.

In contrast to the asymmetry index, the mean path length of the dendritic arborizations did not show a large variation throughout the sub-trees of TC neurons. The difference between minimum and maximum of the mean path length lies in the range of 100-200 μm (Fig. 2-8B), and the average mean path length is equal to 186.84 ± 27.87 μm.

2.6 Discussion

This study provides a quantitative description of eight reconstructed neurons from the VPL nucleus of adult cats. Analyses of their morphometrical parameters show the following: (i) TC neurons are highly branched cells and the majority (98 %) of branching points is dichotomous, with the highest density of branching points located at 80±15 μm from the soma. (ii) The maximum of the dendritic membrane area is located at 116±21 μm from the soma. (iii) In contrast to previous results, our reconstructions revealed different values of geometrical ratio at the branching points. The average GR value was mostly above 1 with higher values at middle and distal dendrites. Violation from Rall's power rule means that these neurons cannot be modeled by the cylinder model (Rall, 1959) and back propagating potentials would strongly attenuate at the branching points (see below). The GR values calculated for the signals propagating from distal dendrites towards soma were mostly found at GR>3. This finding indicates that, based on the passive properties only (excluding intrinsic currents), the amplitude of synaptic potentials propagating towards soma will be strongly attenuated due to such dendritic morphology of the TC neurons. (iv) The connectivity pattern of the dendritic segments on each subtree of TC cells, forms both, partially symmetric and asymmetric dendritic arborizations, with an overall relatively symmetric branching pattern. (v) The average value of the mean path length did not vary significantly through dendritic trees in spite of different number of branches found in path distance and asymmetry index.

The gross morphological features of thalamocortical cells such as diameter of the soma, number of dendrites, branching point distribution etc. observed in this and previous studies (Jones, 2007; Ohara and Havton, 1994; Ohara et al., 1995; Spreafico et al., 1983; Turner et al., 1997; Yen et al., 1985) were generally similar. However, we report some differences. A *p*revious study by Yen et al., 1985 reported the presence of two morphological types of TC neurons from ventral posterior nucleus of cats. Type 1 has larger somatic area, smooth primary dendrites that give rise to tufts of multiple secondary dendrites, which branch once or twice dichotomously; they possess a few appendages on distal dendrites. Type 2 has a smaller soma, thinner primary dendrites, which branch dichotomously instead of tufts; some of them have dendritic appendages at the primary branching points. The occurrence of type 2 neurons in ventral portion of the nucleus was higher in Yen et al., 1985 study. Our

neurons were labelled in the area responsible for the transfer of information from the forelimb. These neurons were preferentially located in the more anterior part of the nucleus and were virtually absent in the ventral part of the nucleus (Fig. 2-2B). The neurons reconstructed in this study cannot be classified as type 1 and type 2. Each neuron has both thick and thin dendrites (Table 2-1; see also some examples in Fig. 2-7). The same neuron has both proximal dichotomous branching and tuft branching patterns (see examples in Fig. 2-7, cell 1, cell 3). We also investigated the distribution of the appendages (not shown). We found appendages on every neuron, manly on thick proximal dendrites. Therefore, none of the neurons reconstructed in our study allow us to classify them as type 1 or type 2. *F*ine details such as dendritic surface, asymmetry index or morphology of branching points either represents new findings or was found to differ from previous results (Bloomfield et al., 1987; Ohara and Havton, 1994). The differences are likely due to the fact that in most of the previous studies, after fixation the tissue was sectioned and the sections were air dried on gelatinized slides, imposing major vertical shrinkage and to some extent also horizontal shrinkage. In the current study the sections, instead of being air dried, were treated with OsO_4 and embedded in resin, therefore leading to a better conservation of the fine cell morphology. There are at least two limitations of our study. (1) In our results some minor alternations in the cell morphology could arise from the cryoprotection, tissue fixation and dehydration. (2) We assume that sectional profiles of dendrites are cylinders. However, multiple electron microscopy (EM) images show a large variability of profiles from circular, through oval and elongated to irregular profiles (see review book by Jones, 2007). Cross section profiles of the dendrites in EM pictures depend on many factors. (1) The volume of the extracellular space in the brain occupies 20% (Sykova and Nicholson, 2008). This is not the case in EM images that are affected by embedding procedures. Quantum dot measurements of the extracellular space show that intermembrane space in vivo in the brain is 38-64 nm (Thorne and Nicholson, 2006) that is much larger than estimations from EM images (10-20 nm). (2) The appearance of dendrites on EM images is highly influenced by the cutting plane. Therefore, the EM approach cannot be used to provide information on exact shape of the dendrites and other structures.

The dendrites of TC neurons are contacted by terminals of ascending afferent fibers, descending corticothalamic axons, different types of inhibitory (GABAergic) terminals and afferent fiber systems arising mainly from the brainstem that transmit acetylcholinergic, noradrenergic serotoninergic inputs. Prethalamic afferent fibers mainly terminate on proximal dendrites, corticothalamic axons mainly establish synapses on distal dendrites, but all inputs converge in the middle part of the dendrites (Liu et al., 1995). We demonstrated here that the total dendritic area is the highest in the middle part of dendrites. Therefore, most of the interactions among synapses of different origin occur on the dendritic region providing the largest membrane surface.

Previous studies proposed a correlation between the morphology of TC neurons and their electrophysiological features (Turner et al., 1997; Yen et al., 1985). Our data of GR values suggest that in different dendrites attenuation of back propagating potentials takes place and that attenuation has different strength and range depending on the dendritic diameters. When GR is higher than 1 the back propagating potentials (back propagating action potentials or proximally generated synaptic potentials) will attenuate in amplitude and vice versa when the GR is lower than 1 the amplitude of back propagating potential will be enhanced. Our data indicate that in the majority of the cases the back propagating potentials will attenuate. Due to the high values of the GR, which are determined from distal to proximal dendrites, the individual synaptic potentials arriving from distal dendrites might have little or no impact at somatic level considering the cable theory. In order to reach the soma, distal inputs have to be either amplified by intrinsic currents or they have to be summated. In reticular thalamic neurons, the highest density of low-threshold Ca^{2+} channels (T channels) was observed on distal dendrites (Kovács et al., 2010), however physiological (Williams and Stuart, 2000), imaging (Zhou et al., 1997) and computational studies (Zomorrodi et al., 2008) have demonstrated that the highest density of T channels in TC neurons occurs at the proximal part of the dendritic tree. Therefore, it is unlikely that individual EPSPs arriving at the distal dendrites are amplified by the T current. Despite the fact that these synaptic potentials will not propagate to the soma, at a bifurcation point synaptic events from one dendritic branch may efficiently propagate into a neighboring

dendritic branch providing the basis for synaptic integration, hitherto not much investigated in TC neurons.

Experimental data and numerical simulations demonstrated that not only the distribution of ionic currents on the dendritic tree, but also dendritic arborizations strongly correlate with the neuronal responsiveness (Acker and White, 2007; Gollo et al., 2009; Gulledge et al., 2005; Komendantov and Ascoli, 2009; Saraga et al., 2003; Sjöström et al., 2008; Timofeeva et al., 2008). Our findings on the variability in the length of different dendrites of TC neurons and their asymmetry provide a basis for the assumption that distinct dendrites play different roles in neuronal computation.

We conclude that morphological features of TC neurons are likely to have a major influence on the synaptic and intrinsic responsiveness of these neurons. The presence of active conductances such as T and hyperpolarization-activated depolarizing (h) currents in TC neurons will play a major role in the modulation of dendritic inputs at different levels of the membrane potential.

2.7 Acknowledgements:

We thank Dr. Michael Hines for his technical advice on importing reconstructed neurons and analyzing morphological parameters in NEURON. We thank Sridevi Polavaram for his help in comparing the precision of our morphological analysis with L-measure.
Reza Zomorrodi contributed in reconstruction of neurons, performed all analysis and provides the first manuscript of the paper, Alex S Ferecskó performed 3D reconstruction of neurons, Krisztina Kovács contribute in staining procedure, Helmut Kroger contribute in analysis and correction the manuscript, Igor Timofeev designed the experiment, contribute in analysis and prepare the final version of the paper.

2.8 References

Acker CD, White JA. 2007. Roles of IA and morphology in action potential propagation in CA1 pyramidal cell dendrites. J Comput Neurosci 23(2):201-216.

Bazhenov M, Timofeev I, Steriade M, Sejnowski TJ. 1998. Cellular and network models for intrathalamic augmenting responses during 10-Hz stimulation. J Neurophysiol 79(5):2730-2748.

Bazhenov M, Timofeev I, Steriade M, Sejnowski TJ. 2002. Model of thalamocortical slow-wave sleep oscillations and transitions to activated states. J Neurosci 22(19):8691-8704.

Bloomfield SA, Hamos JE, Sherman SM. 1987. Passive cable properties and morphological correlates of neurones in the lateral geniculate nucleus of the cat. J Physiol 383:653-692.

Buzas P, Eysel UT, Kisvarday ZF. 1998. Functional topography of single cortical cells: an intracellular approach combined with optical imaging. Brain Res Brain Res Protoc 3:199-208.

Castelo-Branco M, Neuenschwander S, Singer W. 1998. Synchronization of visual responses between the cortex, lateral geniculate nucleus, and retina in the anesthetized cat. J Neurosci 18(16):6395-6410.

Chklovskii DB. 2004. Synaptic connectivity and neuronal morphology: two sides of the same coin. Neuron 43(5):609-617.

Deschênes M, Paradis M, Roy JP, Steriade M. 1984. Electrophysiology of neurons of lateral thalamic nuclei in cat: resting properties and burst discharges. J Neurophysiol 51(6):1196-1219.

Destexhe A, Contreras D, Steriade M, Sejnowski TJ, Huguenard JR. 1996. In vivo, in vitro, and computational analysis of dendritic calcium currents in thalamic reticular neurons. J Neurosci 16(1):169-185.

Destexhe A, Neubig M, Ulrich D, Huguenard J. 1998. Dendritic low-threshold calcium currents in thalamic relay cells. J Neurosci 18(10):3574-3588.

Destexhe A, Sejnowski T. 2001. Thalamocortical assemblies: How ion channels, single neurons and large-scale networks organize sleep oscillations. Lemon RN, editor. Oxford: Oxford University Press. 452 p.

Duijnhouwer J, Remme MWH, van Ooyen A, Van Pelt J. 2001. Infuence of dendritic topologyon firing patterns in model neurons. Neurocomput 38040:183-189.

Goldstein SS, Rall W. 1974. Changes of action potential shape and velocity for changing core conductor geometry. Biophys J 14(10):731-757.

Gollo LL, Kinouchi O, Copelli M. 2009. Active dendrites enhance neuronal dynamic range. PLoS Comput Biol 5(6): e1000402. doi:10.1371/journal.pcbi.1000402.

Gulledge AT, Kampa BM, Stuart GJ. 2005. Synaptic integration in dendritic trees. J Neurobiol 64(1):75-90.

Hasenstaub A, Sachdev RNS, McCormick DA. 2007. State changes rapidly modulate cortical neuronal responsiveness. J Neurosci 27:9607-9622.

Havton LA, Ohara PT. 1993. Quantitative analyses of intracellularly characterized and labeled thalamocortical projection neurons in the ventrobasal complex of primates. J Comp Neurol 336(1):135-150.

Hill SL, Tononi G. 2004. Modeling sleep and wakefulness in the thalamocortical system. J Neurophysiol 93:1671-1698.

Hines ML, Carnevale NT. 1997. The NEURON simulation environment. Neural Comput 9(6):1179-1209.

Hughes SW, Cope DW, Blethyn KL, Crunelli V. 2002. Cellular mechanisms of the slow (<1 Hz) oscillation in thalamocortical neurons in vitro. Neuron 33(6):947-958.

Huguenard JR, McCormick DA. 1992. Simulation of the currents involved in rhythmic oscillations in thalamic relay neurons. J Neurophysiol 68(4):1373-1383.

Jones EG. 2007. The Thalamus. New York: Cambridge University Press. 702 p.

Katz Y, Menon V, Nicholson DA, Geinisman Y, Kath WL, Spruston N. 2009. Synapse Distribution Suggests a Two-Stage Model of Dendritic Integration in CA1 Pyramidal Neurons. Neuron 63(2):171-177.

Komendantov AO, Ascoli GA. 2009. Dendritic excitability and neuronal morphology as determinants of synaptic efficacy. J Neurophysiol 101(4):1847-1866.

Kovács K, Sík A, Ricketts C, Timofeev I. 2010. Subcellular distribution of low-voltage activated T-type Ca2+ channel subunits (Cav3.1 and Cav3.3) in reticular thalamic neurons of the cat J Neurosci Res 88: 448-460.

Liu XB, Honda CN, Jones EG. 1995. Distribution of four types of synapse on physiologically identified relay neurons in the ventral posterior thalamic nucleus of the cat. J Comp Neurol 352(1):69-91.

Lüscher R, Shiner JS. 1991. Simulation of action potential propagation in terminal arborizations. Schweiz Arch Neurol Psychiatr 142(2):129-132.

Mainen ZF, Sejnowski TJ. 1996. Influence of dendritic structure on firing pattern in model neocortical neurons. Nature 382(6589):363-366.

McCormick DA, Huguenard JR. 1992. A model of the electrophysiological properties of thalamocortical relay neurons. J Neurophysiol 68(4):1384-1400.

Ohara PT, Havton LA. 1994. Dendritic architecture of rat somatosensory thalamocortical projection neurons. J Comp Neurol 341(2):159-171.

Ohara PT, Ralston HJ, 3rd, Havton LA. 1995. Architecture of individual dendrites from intracellularly labeled thalamocortical projection neurons in the ventral posterolateral and ventral posteromedial nuclei of cat. J Comp Neurol 358(4):563-572.

Rall W. 1959. Branching dendritic trees and motoneuron membrane resistivity. Exp Neurol 1:491-527.

Rhodes PA, Llinás R. 2005. A model of thalamocortical relay cells. J Physiol (Lond) 565(Pt 3):765-781.

Rosanova M, Timofeev I. 2005. Neuronal mechanisms mediating the variability of somatosensory evoked potentials during sleep oscillations in cats. J Physiol (Lond) 562.2:569-582.

Rulkov NF, Timofeev I, Bazhenov M. 2004. Oscillations in large-scale cortical networks: map-based model. J Comput Neurosci 17(2):203-223.

Samsonovich AV, Ascoli GA. 2005. Statistical determinants of dendritic morphology in hippocampal pyramidal neurons: A hidden Markov model. Hippocampus 15(2):166-183.

Saraga F, Wu CP, Zhang L, Skinner FK. 2003. Active dendrites and spike propagation in multi-compartment models of oriens-lacunosum/moleculare hippocampal interneurons. J Physiol (Lond) 552(Pt 3):673-689.

Scorcioni R, Polavaram S, Ascoli GA. 2008. L-Measure: a web-accessible tool for the analysis, comparison and search of digital reconstructions of neuronal morphologies. Nature Protocols 3(5):866-876.

Sjöström PJ, Rancz EA, Roth A, Häusser M. 2008. Dendritic excitability and synaptic plasticity. Physiol Rev 88(2):769-840.

Somogyi P, Freund TF. 1989. Immunocytochemistry and synaptic relationships of physiologically characterized HRP-filled neurons. In: Heimer L, Záborszky L, editors. Neuronal tract-tracing methods. New York: Plenum Publishing Corp.

Spreafico R, Schmechel DE, Ellis LC, Jr., Rustioni A. 1983. Cortical relay neurons and interneurons in the N. ventralis posterolateralis of cats: a horseradish peroxidase, electron-microscopic, Golgi and immunocytochemical study. Neurosci 9(3):491-509.

Steriade M, Deschênes M. 1984. The thalamus as a neuronal oscillator. Brain Res Rev 8:1-63.

Steriade M, Jones EG, McCormick DA. 1997. Thalamus: organization and function. Oxford: Elsevier Science Ltd. 959 p.

Steriade M, McCormick DA, Sejnowski TJ. 1993. Thalamocortical oscillations in the sleeping and aroused brain. Science, 262(5134):679-685.

Steriade M, Paré D. 2007. Gating in Cerebral Networks. New York: Cambridge University Press. 331 p.

Sterratt DC, van Ooyen A (2002) Does morphology influence temporal plasticity? In: Artificial neural networks — ICANN 2002 (Dorronsoro JR, ed.), pp 186-191. Berlin / Heidelberg: Springer

Sykova E, Nicholson C. 2008. Diffusion in brain extracellular space. Physiol Rev 88:1277-1340.

Thorne RG, Nicholson C. 2006. In vivo diffusion analysis with quantum dots and dextrans predicts the width of brain extracellular space. Proc Natl Acad Sci U S A 103:5567-5572.

Timofeev I, Steriade M. 1997. Fast (mainly 30—100 Hz) oscillations in the cat cerebellothalamic pathway and their synchronization with cortical potentials. J Physiol (Lond) 504(1):153-168.

Timofeeva Y, Cox SJ, Coombes S, Josic K. 2008. Democratization in a passive dendritic tree: an analytical investigation. J Comput Neurosci 25(2):228-244.

Traub RD, Contreras D, Cunningham MO, Murray H, LeBeau FEN, Roopun A, Bibbig A, Wilent WB, Higley MJ, Whittington MA. 2005. Single-column thalamocortical network model exhibiting gamma oscillations, sleep spindles, and epileptogenic bursts. J Neurophysiol 93(4):2194-2232.

Turner JP, Anderson CM, Williams SR, Crunelli V. 1997. Morphology and membrane properties of neurones in the cat ventrobasal thalamus in vitro. J Physiol (Lond) 505(3):707-726.

Van Pelt J, Schierwagen A. 2004. Morphological analysis and modeling of neuronal dendrites. Math Biosci 188:147-155.

Van Pelt J, Uylings HB, Verwer RW, Pentney RJ, Woldenberg MJ. 1992. Tree asymmetry--a sensitive and practical measure for binary topological trees. Bull Math Biol 54(5):759-784.

Vetter P, Roth A, Häusser M. 2001. Propagation of action potentials in dendrites depends on dendritic morphology. J Neurophysiol 85(2):926-937.

Weaver CM, Wearne SL. 2008. Neuronal firing sensitivity to morphologic and active membrane parameters. PLoS Comput Biol 4(1): e11. doi:10.1371/journal.pcbi.0040011

Williams SR, Stuart GJ. 2000. Action potential backpropagation and somato-dendritic distribution of ion channels in thalamocortical neurons. J Neurosci 20(4):1307-1317.

Yen CT, Conley M, Jones EG. 1985. Morphological and functional types of neurons in cat ventral posterior thalamic nucleus. J Neurosci 5(5):1316-1338.

Zhou Q, Godwin DW, O'Malley DM, Adams PR. 1997. Visualization of calcium influx through channels that shape the burst and tonic firing modes of thalamic relay cells. J Neurophysiol 77(5):2816-2825.

Zomorrodi R, Kröger H, Timofeev I. 2008. Modeling thalamocortical cell: impact of Ca^{2+} channel distribution and cell geometry on firing pattern. Front Comput Neurosci 2:5.

2.9 Figures

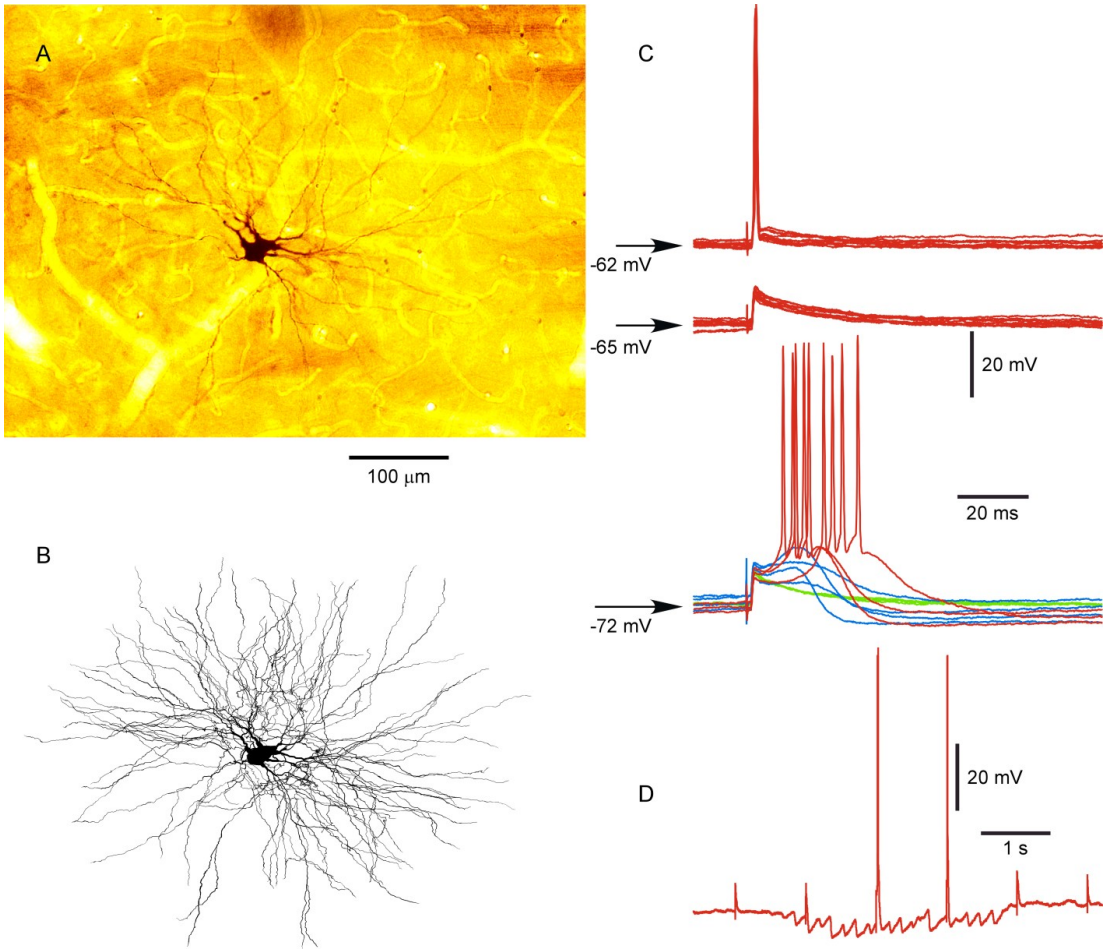

Figure 2-1. Morphological and electrophysiological features of TC neuron from the VPL nucleus. A, Light microscopic image of a TC neuron from the VPL nucleus. B, 3-D reconstruction of the same TC neuron. C, Synaptic responses of the same neuron to medial lemniscus stimuli delivered at different voltages. D, Spontaneous spindle oscillation of the same neuron.

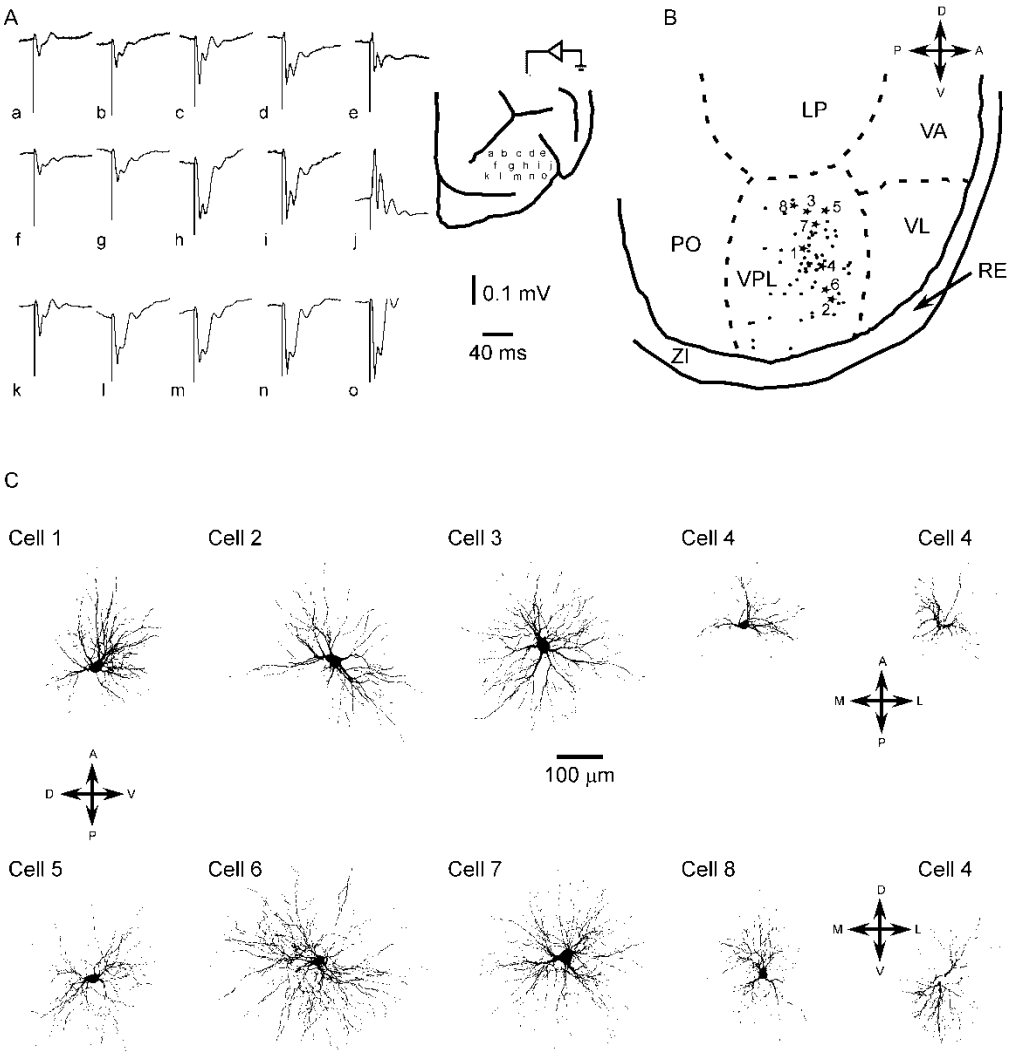

Figure 2-2. Location and three-dimensional reconstruction of TC neurons. A. Spatial distribution of local field potential responses in the somatosensory cortex to nucleus cuneatus stimuli, 1.5 mm posterior from obex, 1.5 mm lateral to midline. Figurine shows the approximate location of the recording points. The injection of tracer was made in the region where maximal evoked potential responses were obtained (tentatively indicated by pipette). B. Sagital view of the thalamus near the VPL nucleus and the location of the labelled neurons. Dots represent the locations of stained neurons; stars represent the locations of the reconstructed neurons. Numbers near stars correspond to cell numbers shown in panel C. C. 2D representation of 8 reconstructed TC neurons in Dorsal/Ventral - Posterior/Anterior (D/V-P/A) orientation. Last column shows Cell 4 in the indicated orientations. Cell 6 was intracellularly injected with neurobiotin, the other cells were retrogradely labelled by fluoro-ruby. (LP – lateral posterior nucleus, PO – posterior complex of thalamus, RE – reticular thalamic nucleus, VA – ventral anterior nucleus, VL – ventro lateral nucleus, VPL – ventro postero lateral nucleus, ZI – zona incerta).

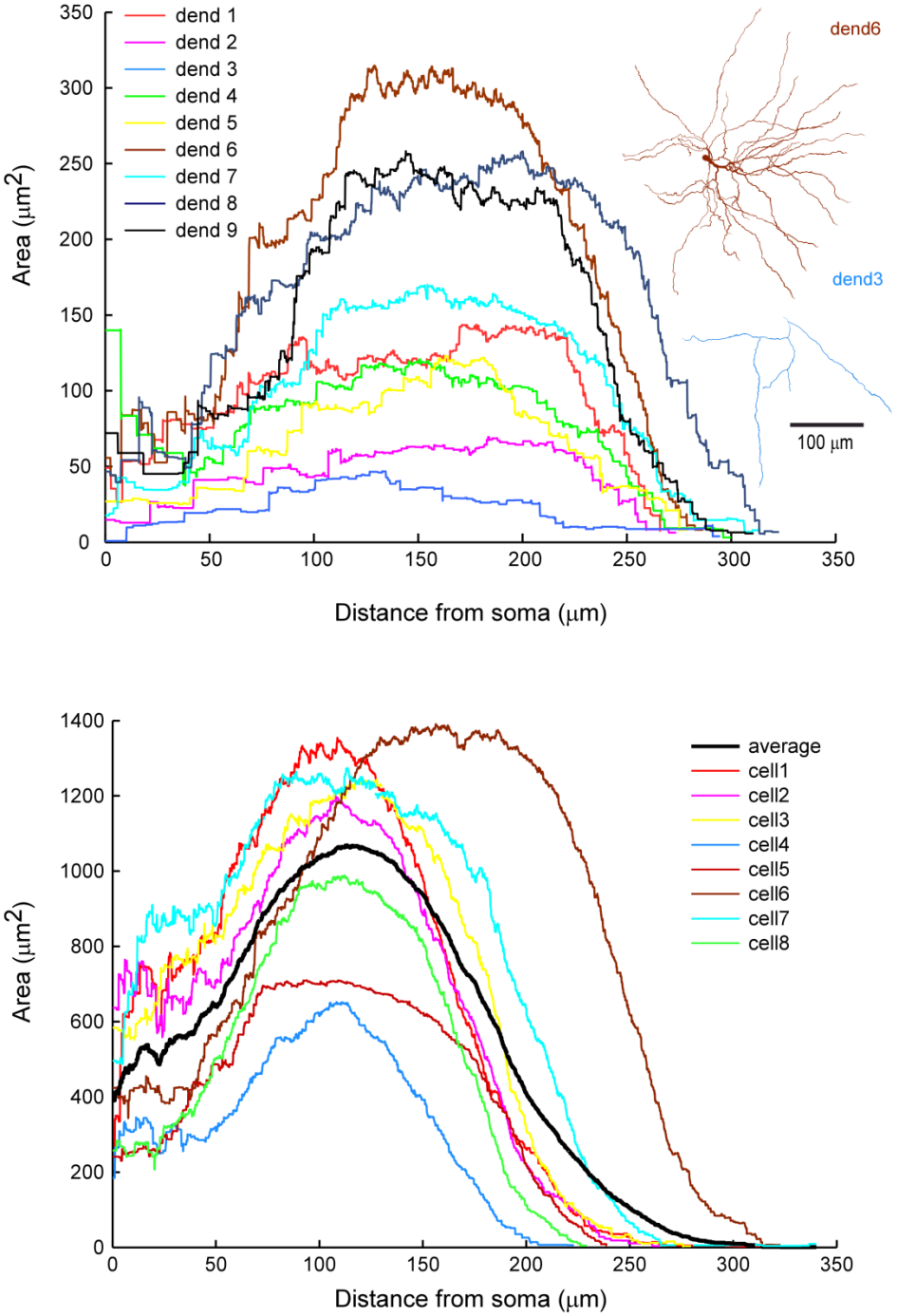

Figure 2-3. Relationship between dendritic membrane area and the distance from the soma. A. Distribution of the dendritic membrane area for each subtree of cell 6 using 5 μm step size. Two subtrees with maximal and minimal area are illustrated at right column. B. Total dendritic membrane area for each reconstructed neuron as a function of path distance from the soma calculated with 5 μm step size. The overall average of dendritic membrane area versus distance from soma is shown by the bold black curve.

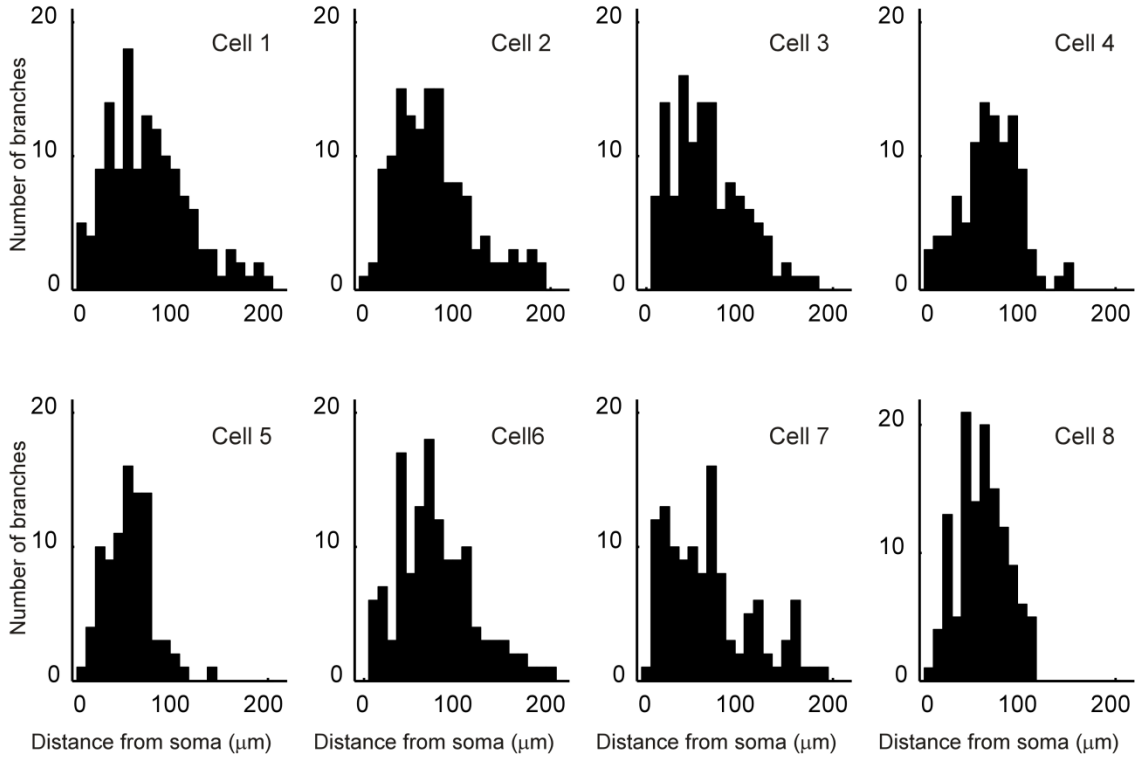

Figure 2-4. Distribution of branching points with respect to the distance from the soma. The histograms show the distribution of the branching points versus distance from the soma for the 8 individual cells. Branching points represent bi-furcation or multi-furcations.

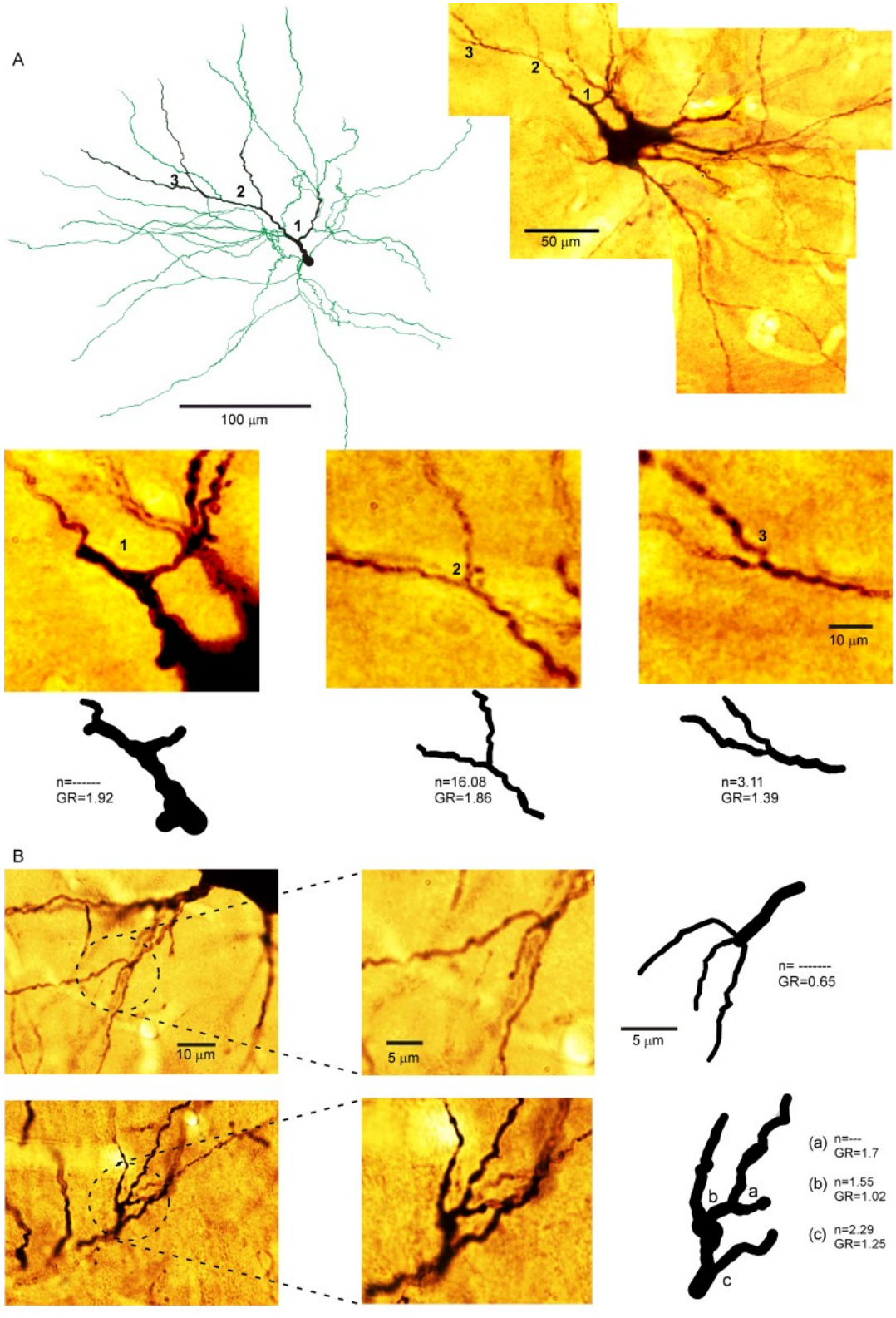
A
3
2
1
100 μm
50 μm
10 μm
n=------
GR=1.92
n=16.08
GR=1.86
n=3.11
GR=1.39
B
10 μm
5 μm
n= -------
GR=0.65
5 μm
(a) n=---
GR=1.7
(b) n=1.55
GR=1.02
(c) n=2.29
GR=1.25
a
b
c

Figure 2-5. High magnification light microscopic images of the dendritic trees and branching points. A**,** Light microscopic image of a thalamocortical neuron and a reconstruction of one dendritic tree. Black, a part of dendrite seen in the microscope photo. Green, another part of the same dendrite reconstructed from images lying out of focus in this section or being located on other sections. Numbers indicate the three bifurcation points. Lower part of the same panel shows these bifurcation points at high magnification and their reconstructions. For each branching point the geometrical ratio (GR) and the exponent (n) in Rall's power rule has been calculated. At some branching point, Rall's exponent does not have real value (see bifurcation point 1). B, An example of trifurcation point and two successive bifurcation points. In the morphological analysis two or more successive bifurcation points with distance less than 1 μm were considered as tri-(or multi-) furcation (upper panels). If the distance was longer than 1 μm we consider them to be successive bifurcation points (lower panel).

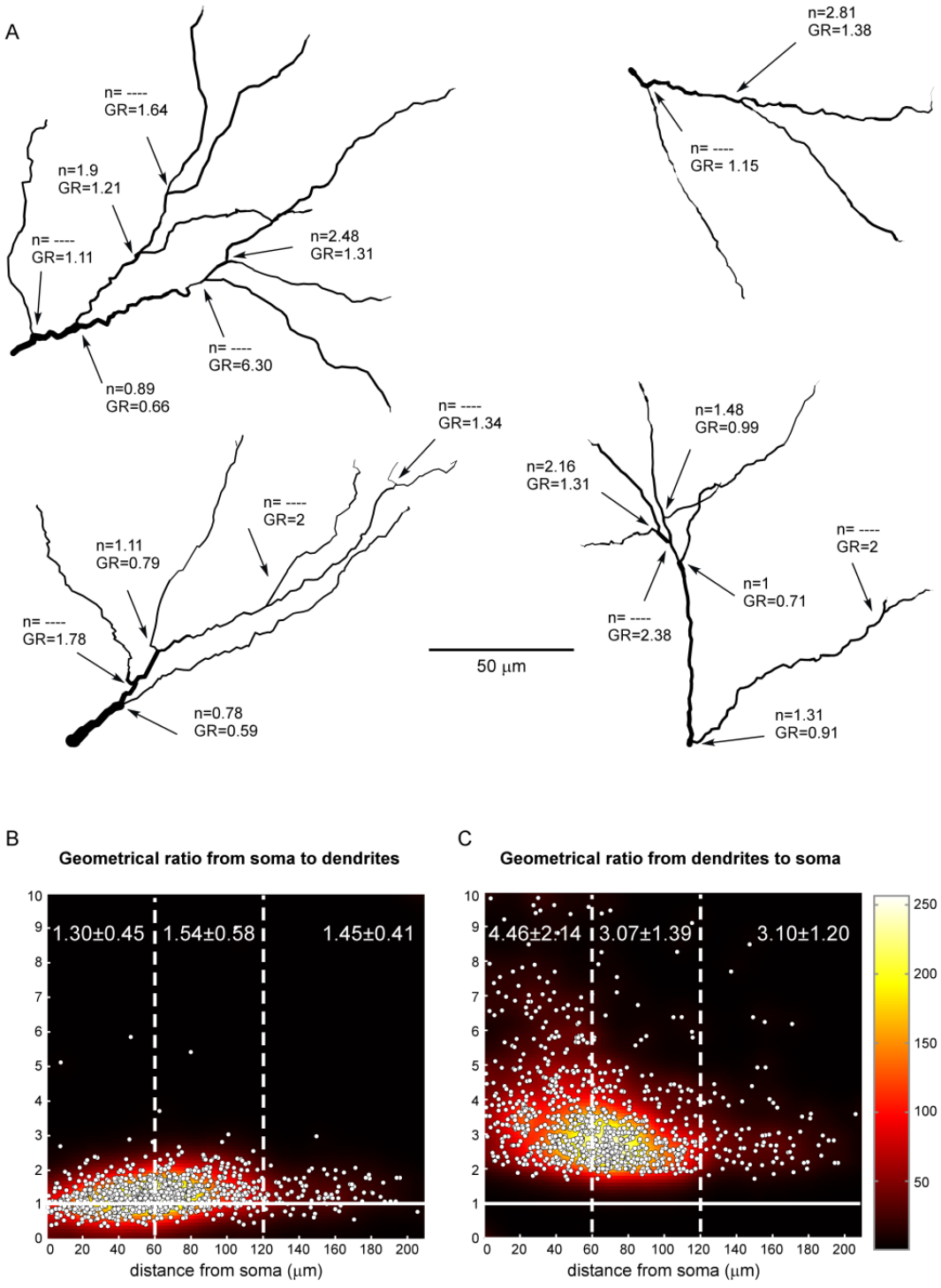

Figure 2-6. Geometrical ratio and Rall's exponent at dendritic branching points. Panel A shows several branching points on 4 different reconstructed dendritic trees from four different TC neurons. Geometrical ratio (***GR***) and exponent (***n***) in the Rall's power rule are indicated at each point. At some branching point, the diameter of one daughter is equal or larger than the diameter of parent, which means that no real value for ***n*** can be obtained (indicated by a dashed line). B, The plot shows the geometrical ratio at all

investigated branching points (n=969) when the proximal dendrite was considered as parent and distal dendrites were considered as daughters. Color map shows the relative density of branching points with given geometrical ratio as a function of distance from the soma. C, Similar plot calculated when distal dendrites were considered parents and proximal dendrites were considered daughters.

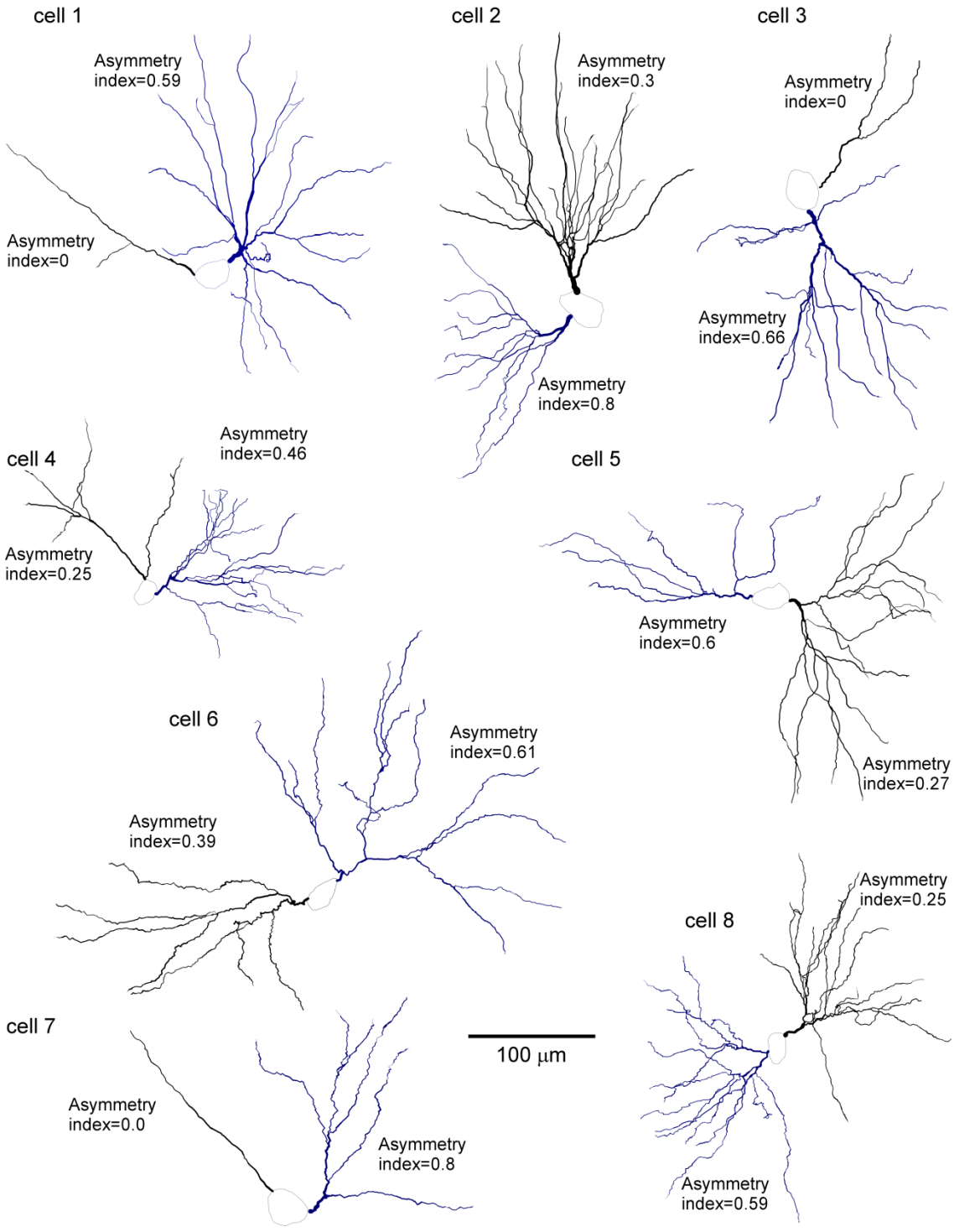

Figure 2-7. Three-dimensional reconstruction of two sub-trees for eight reconstructed TC neurons. For each neuron dendrites with highest and lowest value of asymmetry index are shown.

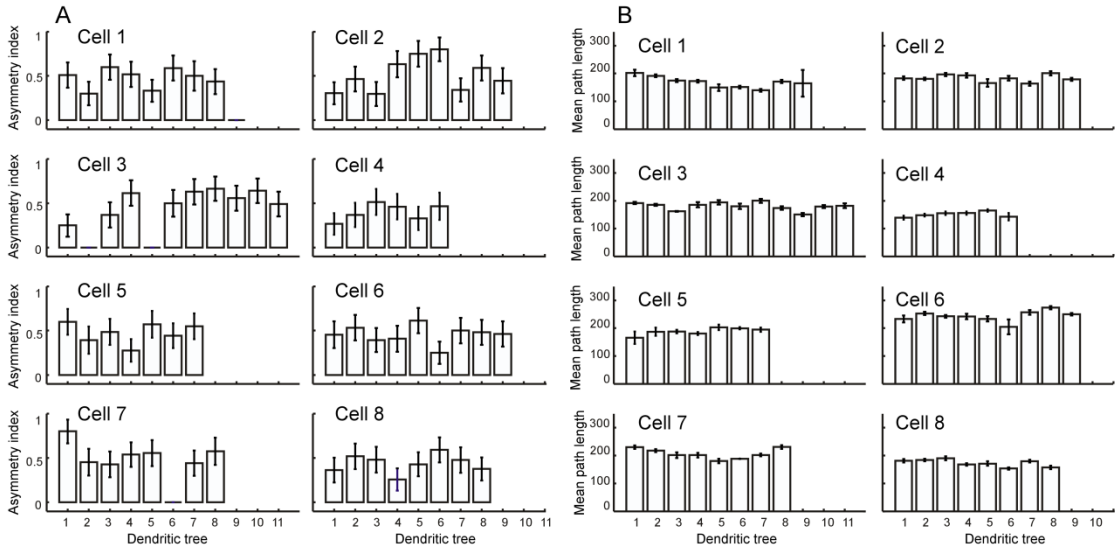

Figure 2-8. Asymmetry index and mean path length for each dendritic tree of the eight reconstructed TC neurons. A, The value of the asymmetry index. B, The value of the mean path length (μm). The number on the x-axis denotes the ordinal of the dendritic tree.

2.10 Tabels

Cell	Somatic surface	Dendritic area	Dendritic length	Branching points	Bifurcation points	Dendritic diameter at 10 µm			End segments	Sub tree
						mean	min	max		
1	3054.37	46851.12	16770.56	141	137	3.9	1.4	8.1	154	9
2	3911.35	45319.83	17111.41	136	134	4.3	1.2	5.7	147	9
3	3198.61	49233.81	16967.70	125	121	6.0	1.5	5.9	137	11
4	1701.59	22358.31	9811.16	101	101	3.4	2.2	6.2	107	6
5	2254.37	30994.35	13748.52	89	88	2.5	1.8	3.8	96	7
6	4263.91	68809.20	25212.75	132	130	3.5	0.2	5.6	143	9
7	3327.03	53203.54	18768.61	120	117	4.7	1.7	10.3	126	8
8	1947.67	36510.52	16023.27	125	123	2.5	1.9	3.1	133	8
Mean	2956.24	44160.08	168017.49	121.12	118.87	3.6	1.5	6.1	130.37	8.37
S.D.	918.89	14297.16	4367.64	17.73	16.81	0.8	0.6	2.3	19.97	1.50
Max.	4263.91	68809.20	25212.75	141	137	6.0	2.2	10.3	154	11
Min.	1701.59	22358.31	9811.16	89	88	2.5	0.2	3.1	96	6

Table 2-1. Metric properties of eight reconstructed thalamocortical neurons. The somatic membrane area (µm2), total dendritic area (µm2) and total dendritic length (µm) have been calculated for each TC neuron. Branching points were considered as separate bifurcation points, when the distance between two consecutive bifurcations was larger than 0.5 µm.

Cell / Tree	1	2	3	4	5	6	7	8
1	0.5	0.3	0.25	0.26	0.60	0.45	0.80	0.36
2	0.3	0.46	0.61	0.36	0.39	0.53	0.45	0.51
3	0.59	0.29	0.0	0.51	0.48	0.39	0.43	0.49
4	0.51	0.63	0.5	0.46	0.27	0.40	0.53	0.25
5	0.33	0.75	0.63	0.32	0.57	0.61	0.55	0.42
6	0.58	0.80	0.66	0.46	0.44	0.25	0.0	0.59
7	0.50	0.34	0.55		0.55	0.50	0.44	0.48
8	0.43	0.58	0.64			0.48	0.57	0.37
9	0.0	0.44	0.49			0.46		
10			0.0					
11			0.36					
Mean	0.41	0.51	0.42	0.39	0.47	0.45	0.47	0.43
S.D.	0.18	0.19	0.24	0.09	0.11	0.10	0.22	0.10
Max.	0.59	0.80	0.66	0.51	0.60	0.61	0.80	0.59
Min.	0.0	0.29	0.0	0.26	0.27	0.25	0.0	0.25

Table 2-2. Asymmetry index for eight reconstructed thalamocortical neurons. The partition asymmetry for each subtree of TC neuron has been calculated according to Eq.2-2. Each TC neuron has dendritic trees with low and high values of asymmetry index. The data show the presence of fully symmetric and partially asymmetric sub-trees in a single TC neuron. The overall average value is 0.44 ±0.03, which shows that sub-trees tend to be more symmetric in their arborizations.

Cell / Tree	1	2	3	4	5	6	7	8
1	202.30	182.99	192.08	139.44	165.54	233.07	230.05	181.12
2	191.42	180.57	185.46	148.46	187.11	253.05	217.97	184.04
3	172.58	196.39	162.32	155.36	188.15	242.85	201.35	190.10
4	172.54	193.49	185.67	156.00	181.04	242.30	201.57	168.28
5	149.37	165.98	194.21	165.06	202.84	233.46	180.37	171.29
6	151.05	182.69	180.46	142.82	199.70	205.11	188.52	153.27
7	139.55	163.47	200.13		194.80	256.68	202.02	179.55
8	171.31	200.74	174.44			273.75	230.72	157.45
9	164.58	178.83	150.88			250.21		
10			179.44					
11			182.35					
Mean	168.52	182.79	180.67	151.19	188.45	243.38	206.57	173.13
S.D.	20.16	12.73	14.16	9.47	12.62	19.07	18.32	12.98
Max.	202.30	200.74	200.13	165.06	202.84	273.75	230.72	190.10
Min.	139.55	163.47	150.88	139.44	165.54	205.10	180.37	153.27

Table 2-3. Mean path length for eight reconstructed thalamocortical neurons. The value of mean path length (MPL, μm) for each sub-tree of TC neuron has been calculated according to Eq. 2-4. The MPL shows a small variation throughout the sub-trees of a neuron.

3 Modeling Thalamocortical Cell: Impact of Ca^{2+} Channel Distribution and Cell Geometry on Firing Pattern

Reza Zomorrodi, Helmut Kröger, Igor Timofeev

Front Comput Neurosci. 2008;2:5. Epub 2008 Dec 12.

3.1 Résumé

L'influence de la distribution des canaux de calcium et de la géométrie de la cellule thalamocorticale sur la décharge de potentiels d'action en mode tonique et la génération de potentiel d'action calcique à seuil bas(low threshold spike, LTS) ont été étudiées dans un modèle à trois compartiments qui représente le soma et les dendrites proximales et distales ainsi que dans un modèle à compartiments multiples en utilisant la morphologie d'un neurone reconstruit. À partir d'une distribution uniforme des canaux Ca^{2+}, nous avons déterminé le nombre minimal de canaux de calcium à bas seuil voltage-dépendant et leur perméabilité requis pour l'apparition du LTS en réponse à un pulse de courant hyperpolarisant. Dans le modèle à trois compartiments, nous avons constaté que la distribution des canaux influence le mode de décharge seulement lorsque la valeur est 3 % inférieure à celle du seuil de la densité totale de canaux T. Dans le modèle multi-compartimental, le LTS peut être généré avec distribuant inégalement les canaux T et en utilisant seulement 64 % du nombre de canaux minimal requis lorsque les canaux T sont distribués également. Pour une densité de canaux et de courant injecté donnés, la fréquence de décharge tonique est inversement proportionnelle à la taille de la cellule. Toutefois, lorsque la densité de canaux Ca^{2+} était élevée au soma ou dans les dendrites proximales, l'amplitude des réponses LTS et les fréquences des bouffées de potentiels d'action ont été déterminées par le ratio du nombre total de canaux T à seuil bas dans la cellule pour une géométrie spécifique.

3.2 Abstract

The influence of calcium channel distribution and geometry of the thalamocortical cell upon its tonic firing and the low threshold spike (LTS) generation was studied in a 3-compartment model, which represents soma, proximal and distal dendrites as well as in multi-compartment model using the morphology of a real reconstructed neuron. Using an uniform distribution of Ca^{2+} channels, we determined the minimal number of low threshold voltage-activated calcium channels and their permeability required for the onset of LTS in response to a hyperpolarizing current pulse. In the 3-compartment model, we found that the channel distribution influences the firing pattern only in the range of 3% below the threshold value of total T-channel density. In the multi-compartmental model, the LTS could be generated by only 64% of unequally distributed T-channels compared to the minimal number of equally distributed T-channels. For a given channel density and injected current, the tonic firing frequency was found to be inversely proportional to the size of the cell. However, when the Ca^{2+} channel density was elevated in soma or proximal dendrites, then the amplitude of LTS response and burst spike frequencies were determined by the ratio of total to threshold number of T-channels in the cell for a specific geometry.

3.3 Introduction

Thalamocortical (TC) neurons at depolarized membrane potential fire in tonic mode, while when released from a hyperpolarizing state and crossing the potential between -65 and -70 mV they generate low-threshold spikes (LTS), accompanied by sodium spikes (Jahnsen and Llinás, 1984a). During slow-wave sleep, TC neurons are hyperpolarized and fire preferentially LTS accompanied by high-frequency spike-bursts, while during paradoxical sleep and likely other activated brain states they fire mainly in the tonic mode (Hirsch et al., 1983; Steriade et al., 1993). Spike-burst elicited during slow-wave sleep precedes and follows a period of at least 100 ms of silence, lasts 5-20 ms and usually consists of 3-5 action potentials (Domich et al., 1986). Extracellular unit recordings demonstrated also the presence of high frequency spike-trains during waking states (Sherman and Guillery, 2002; Bezdudnaya et al., 2006). Both high frequency spike-trains at depolarized potentials and low-threshold spike-bursts elicited by synaptic volleys can have similar shape despite different underlying mechanisms (Rosanova and Timofeev, 2005). The low-threshold calcium current (I_T) underlies burst generation in TC relay cells and plays a central role in the generation of synchronized sleep oscillations (Steriade and Deschénes, 1984; Steriade et al., 1993; Steriade et al., 1997; Destexhe and Sejnowski, 2001; Timofeev et al., 2001).

Ascending and descending inputs to thalamic relay cells arrive at different compartments of the dendritic tree (Jones, 1985) and their integration depends on a large set of intrinsic currents. In order to reproduce correctly synaptic integration, numerical simulations need to incorporate the electrically active properties of the dendritic tree. A multi-compartment model is required to consider the effects of dendritic currents. A first step in this regard was carried out by Destexhe and co-workers (Destexhe et al., 1998) who studied relay cell models with a dendritic tree, which incorporated dendritic T-current densities. In that work, a comparison of T-current density recorded from acutely dissociated and relatively intact cells suggested a higher T-current density in the dendrites compared to the soma. In addition, the high distal T-current density predicted in that model led to a number of speculations (Zhan et al., 2000) on relay cell responses to synaptic inputs arriving to distal

dendrites. Fluorescent imaging study (Zhou et al., 1997) and patch clamp recordings from soma and proximal dendrites (Williams and Stuart, 2000) suggested a higher density of T-channels on proximal dendrites. However, a high density of T-channels in distal dendrites was not required to reproduce low-threshold spikes in a model (Rhodes and Llinas, 2005). Previously, both, experimental and modeling studies were not efficient in detecting the presence and the amplitude (value) of T-current in distal dendrites. Thus, the distribution of T-channels in the membrane of TC neurons remains to be elucidated.

Since the active property of the dendrites affects synaptic integration and response of the neuron (De Schutter and Bower, 1994b, a; Mainen and Sejnowski, 1996; Koch, 1999; Goldberg et al., 2007), in the present study the pattern of T-channel distribution was investigated in computational experiments. Given the experimental fact that T-channels are distributed unevenly over the TC neuron membrane, we examined different forms of non-uniform distribution in the multi-compartment model in order to find possible effects of channel distribution on the cell response. We started with 3-compartment model and then we extended the model to 1267 compartments with a realistic morphology of the TC cell. We hypothesize that the low-threshold response of a TC neuron can be correctly reproduced in a multi-compartment model with an appropriate distribution of T-channel density. Moreover, we hypothesize that the specific form of channel distribution should have physiological benefits for the cell. Here we show that the number of T-channels in the cell has a prime influence on LTS bursting and that the shape of the distribution becomes important only in a specific range of the total number of T-channels. Since different types of TC cells have different geometrical parameters, we also investigated the influence of the cell geometry on the firing pattern.

3.4 Methods

3.4.1 Model

The electrophysiological response of a thalamocortical cell can be modeled by a set of coupled differential equations with an appropriate set of parameters (Rose and Hindmarsh, 1985; McMullen and Ly, 1988) based on experiments by Jahnsen and Llinás (Jahnsen and Llinás, 1984a, b). In our simulation, we also used the Hodgkin-Huxley model for the TC cell. In order to reproduce the low-threshold response of the TC neuron, the kinetics of the T-current was taken from voltage clamp experiments (McCormick and Huguenard, 1992).

The main feature of the electrophysiological response of a TC cell can be reproduced already from a single-compartment model involving Na^+, K^+ and T-currents in the framework of Hodgkin-Huxley equations. Figure 3-1 shows the tonic response and the burst spiking of the modeled TC neuron. Above we proposed the hypothesis that all features of rebound spike-burst behavior can be reproduced in a multi-compartment model, if one takes into account the channel distribution in dendrites. The 3- compartment model simulations of TC neuron responses shown in this article have been carried out using the NEURON simulating environment (Hines and Carnevale, 1997).

3.4.2 3-compartment model

The ultimate goal of our study is to understand how the T-channel distribution influences the electrophysiological response of real TC neurons. The first steps of the study, however, were carried out using the 3-compartment model, which allows to test parameters with high computational efficiency. Those compartments represent the somatic segment and the dendritic arbor composed of proximal and distal segments. According to a previous study (Destexhe et al., 1998), the 3-compartment model allows with good precision to reproduce major electrophysiological features of TC cells. In our simulations, the basic ("control") parameters of the three sections are the following: length (l) and diameters (d): l_s=38.41

μm, d_s=26 μm for soma, l_p=12.49 μm, d_p=10.28 μm for proximal section and l_d=84.67 μm, d_d=8.5 μm for distal section (Fig. 3-2). We have made the assumption that passive parameters of the cell (e.g. leak conductance, cytoplasmic resistance, and capacitance) are held constant in each compartment. The passive response of the model with a dendritic correction factor, C_d= 7.95 (see Eq. 3-1) is fitted to the passive response of the cell during voltage-clamp recording. The Hodgkin-Huxley equations for the 3-compartment model are given by

$$
\begin{aligned}
C_m \frac{dV_1}{dt} &= -g_L(V_1 - E_L) - \bar{g}_{Na}\, m^3 h (V_1 - E_{Na}) - \bar{g}_k n^4 (V_1 - E_k) \\
&\quad - \bar{P}_{Ca}\, r^2 s G(V_1, Ca_o, Ca_i) - g_2^1 \frac{(V_1 - V_2)}{A_1} + I_{inj}, \\
C_d C_m \frac{dV_2}{dt} &= -C_d g_L(V_2 - E_L) - C_d \bar{P}_{Ca}\, r^2 s G(V_2, Ca_o, Ca_i) - g_2^1 \frac{(V_2 - V_1)}{A_1} - g_3^2 \frac{(V_3 - V_2)}{A_2}, \\
C_d C_m \frac{dV_3}{dt} &= -C_d g_L(V_3 - E_L) - C_d \bar{P}_{Ca}\, r^2 s G(V_3, Ca_o, Ca_i) - g_3^2 \frac{(V_3 - V_2)}{A_3}.
\end{aligned}
$$

(3-1)

Here V_1, V_2, and V_3 represent the membrane potential of the soma, proximal and distal compartments, respectively. A_1, A_2, and A_3 denote the area of the compartments. In this model, the membrane capacitance, the leak conductance and the leak reversal potential were set to C_m =0.878 μF/cm^2, g_L=0.0379mS/cm^2, E_L=-69.85 mV, respectively. The axial conductance (g_j^i) between compartments depends on the geometry of the compartment and the cytoplasmic resistance (R_a) in the following way:

$$
\frac{1}{g_j^i} = r_j^i = \frac{2 R_a}{\pi} \left(\frac{l_i}{d_i^2} + \frac{l_j}{d_j^2} \right)
$$

(3-2)

Thus, the axial conductance in our model takes the following values: $g^1{}_2$=5.187 μS and $g^2{}_3$=0.703 μS. Voltage-dependent conductances were modeled using a Hodgkin–Huxley type of kinetic model. The kinetics of the Na^+ and K^+ currents responsible for fast action potentials, were taken from a model of hippocampal pyramidal cells (Traub and Miles, 1991), assuming a resting potential of V_T= -52 mV, maximal conductance $\bar{g}_{Na}$ =0.1 S/cm^2 and $\bar{g}_k$ =0.1 S/ cm^2, and reversal potentials of E_{Na} = 50 mV and $E_{K=}$-100 mV. This model has been shown to be adequate to model the repetitive firing within bursts of action potentials (Destexhe et al., 1996). Because of the nonlinear and far-from-equilibrium behavior of calcium ions to model Ca^{2+} current we used Goldman-Hodgkin-Katz (GHK) equation (Hille, 2001):

$$I_T = P_{Ca}\ m^2\ h\ G(V,[Ca]_o,[Ca]_i),$$

$$\frac{dm}{dt} = -\frac{1}{\tau_m(V)}(m - m_\infty(V))$$
$$\frac{dh}{dt} = -\frac{1}{\tau_h(V)}(h - h_\infty(V))$$

(3-3)

Here P_{ca} denotes the maximum permeability and *m, h*, denote the activation and inactivation variables, with τ_m and τ_h being the corresponding time constants. The kinetic functions are taken from Destexhe et al. (Destexhe et al., 1998). G (V, Ca_o, $Ca_{i)}$ is a nonlinear function of the potential and ion concentration;

$$G(V,[Ca]_o,[Ca]_i) = \frac{Z^2F^2V}{RT}\frac{[Ca]_i - [Ca]_o \exp[-ZFV/RT]}{1-\exp[-ZFV/RT]}$$

(3-4)

Here Z= 2 denotes the valence of calcium ions, F the Faraday constant, R the gas constant, and T the temperature measured in Kelvin. $[Ca]_i$ and $[Ca]_o$ represent the intracellular and extracellular Ca^{2+} concentrations expressed in units of millimolar. The fluctuation of

intracellular Ca^{2+} concentration is denoted by $[Ca]_i$. It is due to Ca^{2+} pumps and buffers (McCormick and Huguenard, 1992), and is taken into account by the following differential equation:

$$\frac{d[C]_i}{dt} = -\frac{i_{ca}}{2Fd} + \frac{([C]_\infty - [C]_i)}{\tau} \tag{3-5}$$

Here i_{ca} denotes the current density, $d = 0.1\mu m$ the depth of the shell below the membrane, $[C]_\infty = 240nM$ the equilibrium concentration and τ =5 msec the time constant of decay of $[Ca^{2+}]$, respectively. The parameters were taken from the 3-compartment model by Destexhe et al., (Destexhe et al., 1998).

The value of permeability P_{ca} in the low-threshold calcium current (Eq. 2.2.3) indicates the maximum permeability of the section expressed in units of cm/sec. This value represents the permeability of a patch of 1 cm^2 of membrane. Therefore, the total permeability of the section is obtained by integration over the entire surface. On the other hand, the total permeability of a section is the product of permeability of a single channel and total number of channels. Thus holds

$$N^{total} = \frac{1}{P_{ca}^{(1)}} \int P_{ca}(A)\, dA \tag{3-6}$$

Here N^{total}, $P_{ca}^{(1)}$ and A denote the total number of T-channels, the permeability of a single channel and surface of compartment, respectively. For a given section area, increasing the number of channels is equivalent to increasing the permeability of the section. In the following, we will refer to the permeability of channels in an area of 1 cm^2 of the membrane simply as channel permeability. In section 3.4.1., we consider the influence of the number of channels and its distribution on the burst response of TC cell. We also

consider in section 3.4.3 the influence of geometrical parameters (e.g. diameter, area) on the response of the cell.

In order to simplify calculations, we did not take into account the h-current in the model, because this current does not contribute directly to the generation of LTS.

3.4.3 Multi-compartment model

We developed a multi-compartment model of the TC cell in order to consider the effects of dendritic currents upon response of the cell with realistic morphology. The simulations were performed based on a TC cell reconstructed using the NeuroLucida digital system. In order to obtain precise morphological features of the TC neuron from the VPL nucleus of thalamus, a retrograde tracer (fluorogold) was iontophoretically applied to the somatosensory area (SI) in adult anesthetized cat in sterile conditions. After a survival period of two weeks the cat was deeply anesthetized with thiopental and intracardialy perfused. Stained neurons were revealed using a standard ABC kit. All experimental procedures used in this study were performed in accordance with the Canadian guidelines for animal care and were approved by the committee for animal care of Laval University. The reconstructed cell used for the model included 11 primary branches and 224 segments with a dendritic membrane area of 45000×10^{-6} m^2. Our model contains 1267 compartments, based on the d-lambda rule of NEURON. The simulation of the multi-compartment model took approximately 12 min on a Pentium(R) M with 2.00 GHz processor to run 800 ms of neuronal activity.

3.5 Results

3.5.1 Calcium channel distribution

In the following simulations, we determined the minimum value (threshold) of the number of T-channels (N^{thr}) and a corresponding value of permeability (P^{thr}) in each section, which

enables the generation of LTS in the TC cell. The threshold number of T-channels is defined here as the minimal number of T-channels required to produce LTS in the 3-compartment model. This threshold value corresponds to the onset of the first sodium spike generated by LTS in response to a depolarized current of I_{inj}=0.1 nA, while the cell is being hyperpolarized to V_m= -75 mV. However, if threshold LTS was obtained under different conditions (e.g., different level of V_m and/or different level of I_{inj}) it did not affect the results presented in this study.

3.5.2 Results of numerical simulations

In the first simulation, based on the 3-compartment model, the calcium channel density was kept equal in each compartment, which means equal permeability for Ca^{2+} ions in each compartment (Fig. 3-2 A). According to experimental data from dissociated cells (Destexhe et al., 1998), the permeability in each compartment was set to the value of P_{Ca}=1.7 x 10^{-5} cm/sec. Using this value in each compartment, the model gives a passive response to a depolarizing injected current (0.1 nA), at a hyperpolarized membrane potential (-75 mV). Parallel increase in permeability in the three compartments by the same amount induced first a sub-threshold response, which grew in amplitude as P_{Ca} increased (Fig. 3-2B, D). When the value of permeability at each compartment reached P_{Ca}=1.56 x 10^{-4} (cm/sec), the modeled cell reproduced the first LTS mediated action potential (Fig. 3-2E). This permeability was defined as the threshold permeability under conditions of V_m=-75mV and I_{inj}=0.1nA. The threshold permeability corresponds to the threshold number of Ca^{2+} channels (N^{thr}) in the cell necessary to generate the first rebound spike in the model. The total number of T-channels in the cell is proportional to the product of compartment area and permeability of Ca^{2+} channels in each compartment. The membrane potential fluctuates due to changes in channel permeability. Because the threshold value depends on the level of membrane potential, we used a steady holding current to keep the membrane potential at -75 mV when we changed P_{Ca}. In the case of an uniform T-channel distribution further increase in permeability produced LTS of larger amplitude leading to multiple spike generation with increasing intra-burst firing frequency (Fig. 3-2F-I). Because the experimental data suggest a non-uniform T-channel distribution in TC neurons (Zhou et al.,

1997; Williams and Stuart, 2000), we examined different shapes of non-uniform distribution of T-channels in the model leading to an LTS response.

The total number of T-channels was kept constant and equal to N^{thr}, which is the minimum number of T-channels necessary to generate an LTS response in a cell with uniform channel distribution. We explored a variety of T-channel distributions that produced a first LTS mediated action potential in the model. Some examples of permeability distribution and its corresponding channel number in each compartment leading to an action potential are shown in Figure 3-3. Both, uniform and non-uniform distributions of T-channels can produce an LTS response with sodium spike in the model cell. This suggests that when the total number of T-channels equals N^{thr} then the shape of channel distribution does not affect the LTS response of the cell (Fig. 3-4A). However, if the total number of channels was lowered the response of the cell depended on the shape of channel distribution. Far from the threshold value of the total number of T-channels, any form of distribution gave a passive response, but when the total number of T-channels was close to threshold value, the response of the cell depended on the form of channel distribution (Fig. 3-4B, C).

Using small changes in the channel number in the 3-compartment model with non-uniform channel distribution, we found a small window in the total number of channels located below the defined threshold of onset of LTS with spikes which was able to induce an LTS mediated action potential

$$N_{\min} = 0.97 N^{thr} \leq N^{total} < N_{\max} = N^{thr} \quad . \tag{3-7}$$

In such window, the spiking behavior was found to be variable: when the total number of channels was between N^{thr} and 0.97x N^{thr}, a uniform permeability distribution did not generated LTS with sodium spikes, while a non-uniform distribution could generate a full

LTS response (Fig. 3-3,3-4). We also tested extreme cases where the Ca^{2+} permeability took the value 0 in two out of three compartments, and N^{total} was still 0.97 x N^{thr}. These results led to the assumption that the modeled cell can generate a rebound burst response for an optimal number of T-channels, which were distributed in a specific non-uniform pattern. We hypothesize that the physiological reason for the existence of such window on one hand may be related to reduced metabolic energy consumption (see discussion), and on the other hand to the ability of the TC cell to generate a variable response pattern.

3.5.3 Effect of cell geometry on firing pattern

Firing patterns do not only depend on the channel density and type of current, but also on the geometry of the cell (length, diameter, area, etc.) (Mainen and Sejnowski, 1996) as well as on the cell topology (symmetry, mean path length, etc.) (van Ooyen et al., 2002). Here we examined the influence of the cell geometry on the firing pattern in the 3-compartment model of the TC neuron. For this purpose, we changed the diameter of each compartment, while holding constant the diameter of other sections, the channel densities, and the injected current. In addition, we set the total number of channel equal to 0.98 x N^{thr} where the spiking induced by the LTS response of the cell is sensitive to the shape of distribution of the T-channels. Like in previous simulations, the model includes the Na^+/K^+ current in soma and the T-current in soma, proximal and distal compartments. First, a non-uniform T-channel distribution has been considered obeying the following relation:

$$P_{ca}(distal\ \ dendrite) < P_{ca}(soma) < P_{ca}(proximal\ \ dendrite) \tag{3-8}$$

In a control situation, a hyperpolarizing current pulse induced an LTS response accompanied with action potentials and a depolarizing current pulse induced tonic firing with six spikes (Fig. 3-5A). We kept constant the channel density for different cell geometries. The variation of N^{total} and N^{thr} altered the response of the cell. With channel

density held constant, a decrease in the size of all compartments led to an increase in the input resistance, higher frequency of tonic firing and stronger LTS response (Fig. 3-5B, I and V). Increasing the size of the cell led to a decrease in input resistance of the cell, and as consequence to lower excitability, expressed as a reduced firing frequency and absence of tonic or LTS response (Fig. 3-5C, I and V).

We analyzed the effect of size of the section on the cell responses. A reduction in the size of an individual compartment (soma, proximal or distal denrites) led to an increase in input resistance and frequency of tonic response (Fig. 3-5 B, II-IV). However, the LTS response to a hyperpolarizing current injection was different. When the diameter of soma changed to 1/3 of its initial value, the total number of T-channels reduced to 69% of threshold value, which was far from the lower limit (97%) of total T-channels to generate a rebound burst response (Fig. 3-5, B VI). When the diameter of proximal or distal dendrite was decreased, then N^{total} decreased. Despite this, such number was higher than the threshold (minimal) number of T-channels required to generate an LTS response. During rebound, the neuron fired with large number of action potentials (Fig. 3-5 B VII-VIII). Increasing the size of the cell reduced input resistance resulting in passive responses in reaction to a depolarized or hyperpolarized current (Fig. 3-5, C I and V). Smaller soma or dendritic section reduced firing frequency and even prevented induction of action potentials during tonic or LTS response (Fig. 3-5, C; II-V, VII and VIII). Again, for a T-current distribution with higher density in proximal section, an LTS response for a bigger soma does not follow the expected pattern. Increasing the somatic area reduced tonic frequency but generated more sodium spikes during the rebound burst. In this case, the total number of T-channels was 150% of the threshold value. This means that the same hyperpolarized current can activate more T-channels, which leads to a larger LTS response with more action potentials (Fig. 3-5, C VI). These numerical simulations based on a 3-compartment model of TC cell for the case of a higher density of T-channel in proximal dendritic section show that smaller distal dendrites and bigger soma are favorable to generate rebound bursts in the TC neuron.

Further, we investigated the effect of cell size on rebound spike generation when the density of T-current was higher in soma (Fig. 3-6 A) or distal dendrite (Fig. 3-6 B). When a

higher density of T-channels was located in the somatic section, increasing/decreasing somatic diameter increased/reduced the input resistance of the cell. Hence, a higher/lower frequency in the response to a depolarizing current pulse was obtained (not shown). When the total number of T-channels exceeded the threshold value in a larger cell, having a lower input resistance, the injected hyperpolarizing current activated a sufficient number of T-channels to generate a rebound burst (Fig. 3-6A II and VI). Increasing size of both, the proximal and distal dendritic section, did not shift the ratio of the number of total and threshold T-channels to a specific range which generates a rebound burst response (Fig. 3-6A VII and VIII). Decreasing the diameter of dendritic sections provided a higher than threshold value for T-channels which led to more sodium spikes during LTS response (Fig. 3-6A III and IV). When a higher density of T-channels was located in distal dendrites (Fig. 3-6B), reducing the size of the cell increased input resistance and N^{total}, causing more sodium spikes during LTS (Fig. 3-6B I-IV). With increased cell size and constant channel density, the rebound burst was found absent (Fig. 3-6B V-VIII).

3.5.4 Multi-compartment model

In a multi-compartment model of the TC cell, reconstructed from fluorogold retrograde staining (Fig. 3-7, (Ferecskó et al., 2007)), we distributed non-uniformly the T-channels throughout the cell. We assumed a Gaussian distribution with specific mean value attributed to a high density of T-channels in the proximal, middle, and distal dendrites. In addition, the width of the Gaussian function, defined by parameter σ was changed to study the effect of local channel density on LTS generation (Fig. 3-8). Like in the 3-compartment model we defined the minimum number of T-channels in the uniform distribution, as the number sufficient to generate an LTS leading to a single spike in response to a depolarized current of 0.1 nA, at hyperpolarized level of Vm=-75 mV. The numerical simulation of an LTS response in which a non-uniform T-channel distribution was used shows that a smaller number of T-channels were sufficient to generate an LTS response. In all simulations with non-uniform channels distribution (σ between 0.5 and 2), the LTS with a single spike was generated when $N^{total} = 0.9 \times N^{thr}$, and it was $N^{total} = 0.8 \times N^{thr}$, independently on the

location of highest density of T-channels (Fig. 3-8). However, when the local T-channel density on proximal dendrites was high (σ=0.5), the LTS accompanied by action potential was generated with only $N^{total} = 0.64 \times N^{thr}$ (Fig. 3-8). Thus, our model predicts that a high local channel density on proximal dendrites favors LTS generation with a minimal number of channels.

3.6 Discussion

The prime objective of this study was to investigate how different patterns of T-channel distributions influence the LTS response of a TC cell in a 3-compartment and a multi-compartment model. We also investigated the influence of the cell size on the firing pattern. The major findings of this study are: (i) An increase in the value of permeability (number of channels) uniformly in three compartments changed the response of the TC cell from passive to LTS behavior being accompanied by an action potential. (ii) The onset of firing does not only depend on the total permeability of T-channels, but also on their distribution. (iii) In a 3-compartment model, with a channel number equal or above threshold the TC cell always responded by spiking. If a non-uniform distribution of channels was used, a number of channels smaller than threshold can lead to neuronal firing. (iv) In a multi-compartmental model a minimal number of channels required for the generation of LTS with spikes was found to be much lower than in the 3-compartment model. (v) For a high density of T-channels in the soma and proximal section, the frequency of tonic firing was inversely proportional to the diameter of the section, while the low threshold spiking frequency was directly proportional to the diameter of the section. (vi) The steepness of channel distribution (higher local density of channels) lowers the required minimal number of T-channels necessary for LTS generation.

Previous modeling studies on the subject compared results obtained in dissociated cells with cells recorded from 200 μm thick slices (Destexhe et al., 1998). Dissociated cells contained almost no dendrites, while cell recorded from slices contained several truncated dendrites. As we show here, the dendritic arbor of TC cells extends for more than 400 μm

(Fig. 3-7). The study by Destexhe et al. (1998) demonstrated the presence of significant T-currents in the dendrites. It also demonstrated that the most robust features of LTS can be reproduced in a reduced 3-compartment model. In our numerical simulations, we took a 3-compartment model and demonstrated that in such model the uniform vs. non-uniform channel distribution can influence LTS generation in the range 97-100% of channel number ratio (Fig. 3-4). However, when we used a morphologically intact cell as basis of our model (Fig. 3-7), the shape of channel distribution played a major role. If the highest density of T-channels was located on proximal dendrites, the minimal number of T-channels able to generate an LTS-spike response was only 64% of threshold value. Therefore, comparison of our data to the dissociated cells or cells recorded from slices (Destexhe et al., 1998) provided solid differences, because most of distal dendrites are absent in the cells from slices.

A general principle, which living organisms use to accomplish many functions, is the principle of minimal resources. The result of our study predicts that similar to sodium channels distribution (Crotty et al., 2006), the non-uniform distribution of T-channels, could be essential for the generation of LTS using minimal resources. Most of proteins, including T-channels are synthesized in the cell body and transported from there to its destination. Protein synthesis and transport requires energy. In addition, the metabolic energy consumption is proportional to the ionic currents generated in the neuron via ATPpase Na^+/K^+ or Ca^{2+}/Na^+ metabolic exchangers (Laughlin et al., 1998; Goldberg et al., 2003; Lennie, 2003; Dipolo and Beauge, 2006). Following LTS generation, the intracellular Ca^{2+} concentration increases, and reestablishing Ca^{2+} concentration takes additional energy. Thus, optimizing the number of channels would optimize metabolic energy consumption. The closest place for T-channels to be located in the plasma membrane is the cellular body. However, most of inhibitory synapses are formed in the body of TC neurons (Liu et al., 1995a; Liu et al., 1995b). Thus, the shunting created by inhibitory activities would prevent generation of LTS even with relatively high density of T-channels. The next closest place being energy efficient for T-channels would be the proximal portion of the dendritic tree. Indirect experimental measures (Zhou et al., 1997; Williams and Stuart, 2000), congruent with the current study suggested the presence of high density of T-channels on proximal

dendrites of TC cells. Our parallel electron microscopy study using immunogold staining of T-channel subunits in reticular thalamic nucleus demonstrated that in reticular nucleus cells, the T-channels are non-uniformly distributed (Kovács et al., 2007). The definite conclusion about the exact distribution of T-channels in the TC cytoplasmic membrane may be reached from high-resolution electron microscopy experiments. Optimization of metabolic energy consumption is a decisive factor for the ion channel distribution (Crotty et al., 2006). Our results from the three- and multi-compartment model predict the existence of such window.

Even if T-channels would be equally distributed over the cytoplasmic membrane, the T-channels could be either in the phosphorylated or de-phosphorylated state. Phosphorylation facilitates the generation of T-current at resting membrane potential (Leresche et al., 2004). Thus, state dependent changes of the membrane potential could create a non-uniform distribution of phosphorylated T-channels in different compartments of TC neurons and would facilitate the generation of LTS.

We conclude that although different factors could be responsible for a decrease in the availability of T-channels for LTS generation (physical number of channels or ratio of phosphoreleted/de-phosphorelated channels), all the factors inducing a non-uniform distribution of T-channels on LTS generation will favor generation of LTS. The effect of non-uniform distribution of T-channels on LTS generation in neurons with realistic (much more complex) dendritic tree was found to be stronger.

3.7 Acknowledgements

H.K has been supported by NSERC Canada. I.T has been supported by NSERC Canada, CIHR, and NIH. We are grateful to Alain Destexhe and Maxim Bazhenov for valuable advises that helped to develop our model and K Kovács for help with staining procedure.

3.8 References

Bezdudnaya T, Cano M, Bereshpolova Y, Stoelzel CR, Alonso JM, Swadlow HA (2006) Thalamic burst mode and inattention in the awake LGNd. Neuron 49:421-432.

Crotty P, Sangrey T, Levy WB (2006) Metabolic energy cost of action potential velocity. J Neurophysiol 96:1237-1246.

De Schutter E, Bower JM (1994a) An active membrane model of the cerebellar Purkinje cell II. Simulation of synaptic responses. J Neurophysiol 71:401-419.

De Schutter E, Bower JM (1994b) Simulated responses of cerebellar Purkinje cells are independent of the dendritic location of granule cell synaptic inputs. Proc Natl Acad Sci U S A 91:4736-4740.

Destexhe A, Sejnowski T (2001) Thalamocortical assemblies: How ion channels, single neurons and large-scale networks organize sleep oscillations. Oxford: Oxford University Press.

Destexhe A, Neubig M, Ulrich D, Huguenard J (1998) Dendritic low-threshold calcium currents in thalamic relay cells. J Neurosci 18:3574-3588.

Destexhe A, Contreras D, Steriade M, Sejnowski TJ, Huguenard JR (1996) In vivo, in vitro, and computational analysis of dendritic calcium currents in thalamic reticular neurons. J Neurosci 16:169-185.

Dipolo R, Beauge L (2006) Sodium/calcium exchanger: Influence of metabolic regulation on ion carrier interactions. Physiol Rev 86:155-203.

Domich L, Oakson G, Steriade M (1986) Thalamic burst patterns in the naturally sleeping cat: A comparison between cortically projecting and reticularis neurones. J Physiol 379:429-449.

Ferecskó A, Zomorrodi R, Kovács K, Timofeev I (2007) Morphometric analyses of dendritic arbourization of thalamocortical neurons in somatosensory and motor nuclei of the thalamus. Can J Neurol Sci 34:S73.

Goldberg DH, Sripati AP, Andreou AG (2003) Energy efficiency in a channel model for the spiking axon. Neurocomputing 52-54:39-44.

Goldberg JA, Deister CA, Wilson CJ (2007) Response properties and synchronization of rhythmically firing dendritic neurons. J Neurophysiol 97:208-219.

Hille B (2001) Ionic channels of excitable membranes, Third edition Edition. Sunderland, Massachusetts: Sinauer Associates INC.

Hines ML, Carnevale NT (1997) The NEURON simulation environment. Neural Comput 9:1179-1209.

Hirsch JC, Fourment A, Marc ME (1983) Sleep-related variations of membrane potential in the lateral geniculate body relay neurons of the cat. Brain Res 259:308-312.

Jahnsen H, Llinás R (1984a) Electrophysiological properties of guinea-pig thalamic neurones: an *in vitro* study. J Physiol 349:205-226.

Jahnsen H, Llinás R (1984b) Ionic basis for electroresponsiveness and oscillatory properties of guinea-pig thalamic neurones *in vitro*. J Physiol 349:227-247.

Jones EG (1985) The thalamus. New York: Plenum.

Koch C (1999) Biophysics of Computation: Information Processing in Single Neurons. New York: Oxford University Press.

Kovács K, Sik A, Timofeev I (2007) Localisation of low-voltage activated t-type Ca2+ channel subunits (Cav3.1 and Cav3.3) along the soma and dendrites of reticular and thalamocortical neurons in the cat. Can J Neurol Sci 34:S80.

Laughlin SB, de Ruyter van Steveninck RR, Anderson JC (1998) The metabolic cost of neural information. Nat Neurosci 1:36-41.

Lennie P (2003) The cost of cortical computation. Curr Biol 13:493-497.

Leresche N, Hering J, Lambert RC (2004) Paradoxical potentiation of neuronal T-type Ca2+ current by ATP at resting membrane potential. J Neurosci 24:5592-5602.

Liu XB, Honda CN, Jones EG (1995a) Distribution of four types of synapse on physiologically identified relay neurons in the ventral posterior thalamic nucleus of the cat. J Comp Neurol 352:69-91.

Liu XB, Warren RA, Jones EG (1995b) Synaptic distribution of afferents from reticular nucleus in ventroposterior nucleus of cat thalamus. J Comp Neurol 352:187-202.

Mainen ZF, Sejnowski TJ (1996) Influence of dendritic structure on firing pattern in model neocortical neurons. Nature 382:363-366.

McCormick DA, Huguenard JR (1992) A model of the electrophysiological properties of thalamocortical relay neurons. J Neurophysiol 68:1384-1400.

McMullen TA, Ly N (1988) Model of oscillatory activity in thalamic neurons: role of voltage- and calcium-dependent ionic conductances. Biol Cybern 58:243-259.

Rhodes PA, Llinas R (2005) A model of thalamocortical relay cells. J Physiol 565:765-781.

Rosanova M, Timofeev I (2005) Neuronal mechanisms mediating the variability of somatosensory evoked potentials during sleep oscillations in cats. J Physiol 562.2:569-582.

Rose RM, Hindmarsh JL (1985) A model of a thalamic neuron. Proc R Soc Lond B Biol Sci 225:161-193.

Sherman SM, Guillery RW (2002) The role of the thalamus in the flow of information to the cortex. Philos Trans R Soc Lond B Biol Sci 357:1695-1708.

Steriade M, Deschénes M (1984) The thalamus as a neuronal oscillator. Brain Res Revi 8:1-63.

Steriade M, McCormick DA, Sejnowski TJ (1993) Thalamocortical oscillations in the sleeping and aroused brain. Science 262:679-685.

Steriade M, Jones EG, McCormick DA (1997) Thalamus: organization and function. Oxford: Elsevier Science Ltd.

Timofeev I, Bazhenov M, Sejnowski T, Steriade M (2001) Contribution of intrinsic and synaptic factors in the desynchronization of thalamic oscillatory activity. Thalamus & Related Systems 1:53-69.

Traub RD, Miles R (1991) Neuronal network of the hippocampus.: Cambridge University Press (May 31, 1991).

Van Ooyen A, Duijnhouwer J, Remme MW, van Pelt J (2002) The effect of dendritic topology on firing patterns in model neurons. Network 13:311-325.

Williams SR, Stuart GJ (2000) Action potential backpropagation and somato-dendritic distribution of ion channels in thalamocortical neurons. J Neurosci 20:1307-1317.

Zhan XJ, Cox CL, Sherman SM (2000) Dendritic depolarization efficiently attenuates low-threshold calcium spikes in thalamic relay cells. J Neurosci 20:3909-3914.

Zhou Q, Godwin DW, O'Malley DM, Adams PR (1997) Visualization of calcium influx through channels that shape the burst and tonic firing modes of thalamic relay cells. J Neurophysiol 77:2816-2825.

3.9 Figures

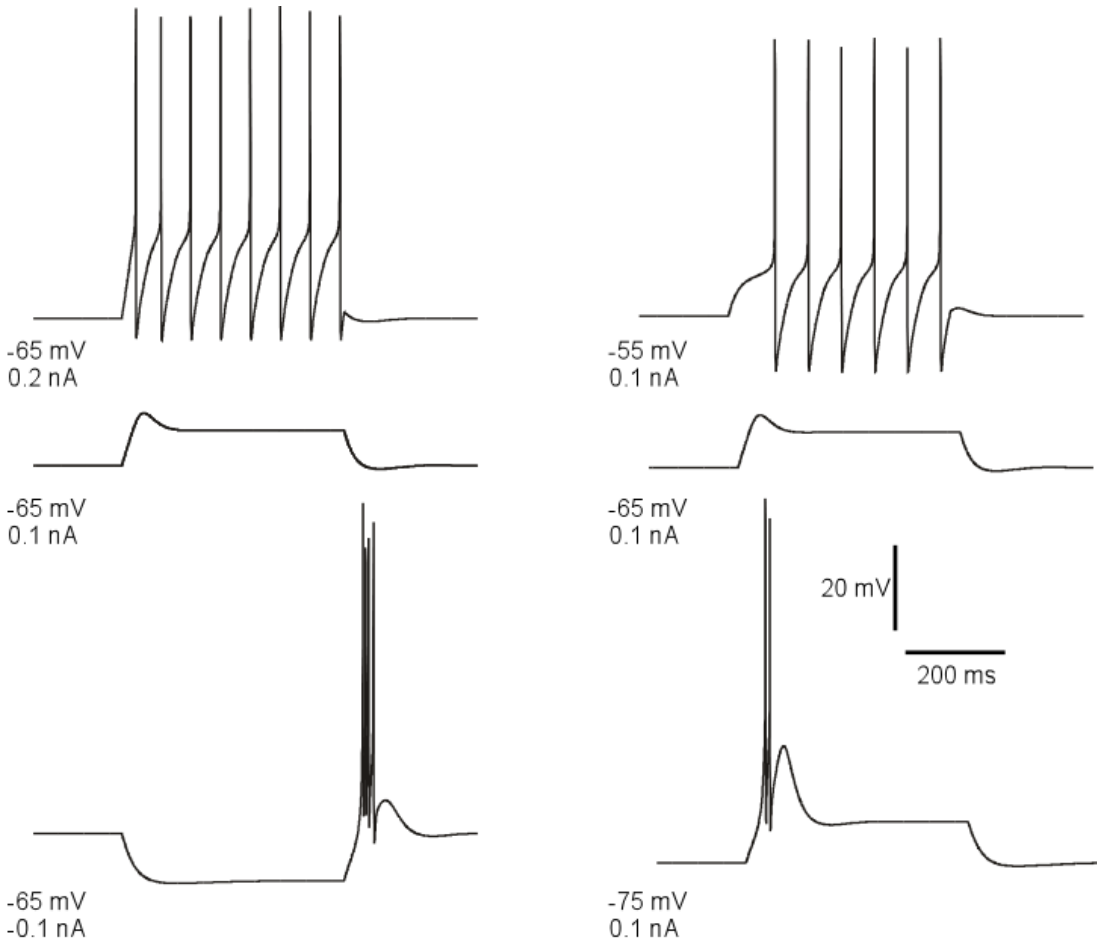

Figure 3-1. Simulated rebound burst in TC cell from a single-compartment model.
The model involves the leak current, fast Na^+/K^+ currents and the low-threshold Ca^{2+} current. Left panel: response of cell to different injection currents, at the same level of membrane potential: tonic firing for 0.2 nA (top), passive response for 0.1 nA (middle) and burst firing for -0.1 nA (bottom). Right panel: response of the cell to a depolarizing current (0.1 nA) at different levels of membrane potential: tonic firing for V_m=-55 mV, passive response for V_m=-65 mV and burst firing for V_m=-75 mV.

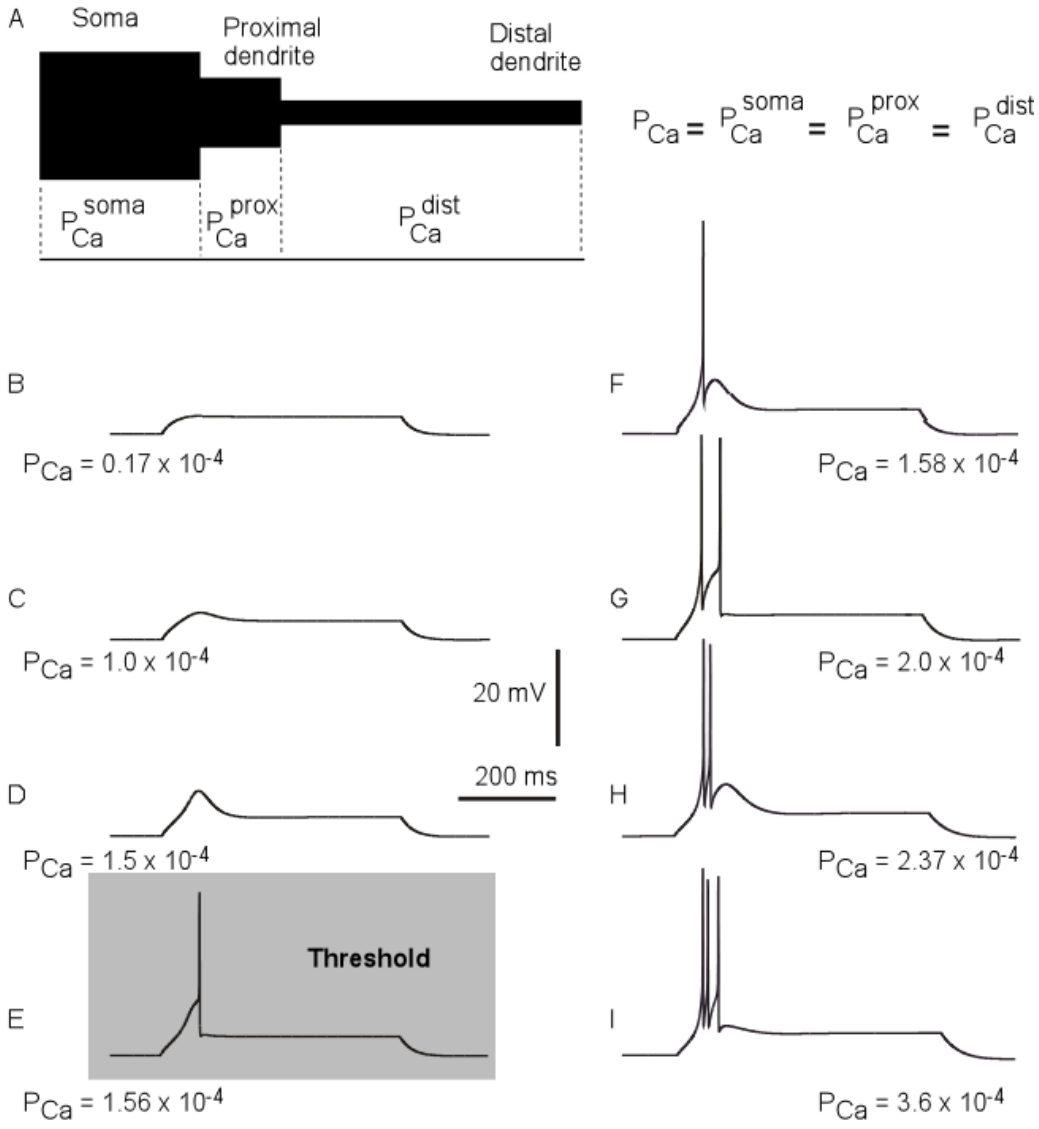

Figure 3-2. Effects of permeability from Ca^{2+} increase on generation of LTS response in a 3-compartment model with uniform channel distribution. Schematic representation of 3-compartment model with uniform channel distribution. (B-I) Response of modeled TC neuron (V_m=-75 mV) to depolarizing current pulse (0.1 nA). The permeability for Ca^{2+} in each compartment increases from B to I as indicated. With this morphology, channel distribution and membrane potential, the onset of LTS leading to an action potential required the permeability P_{ca}=1.56 x 10^{-4} (cm/sec).

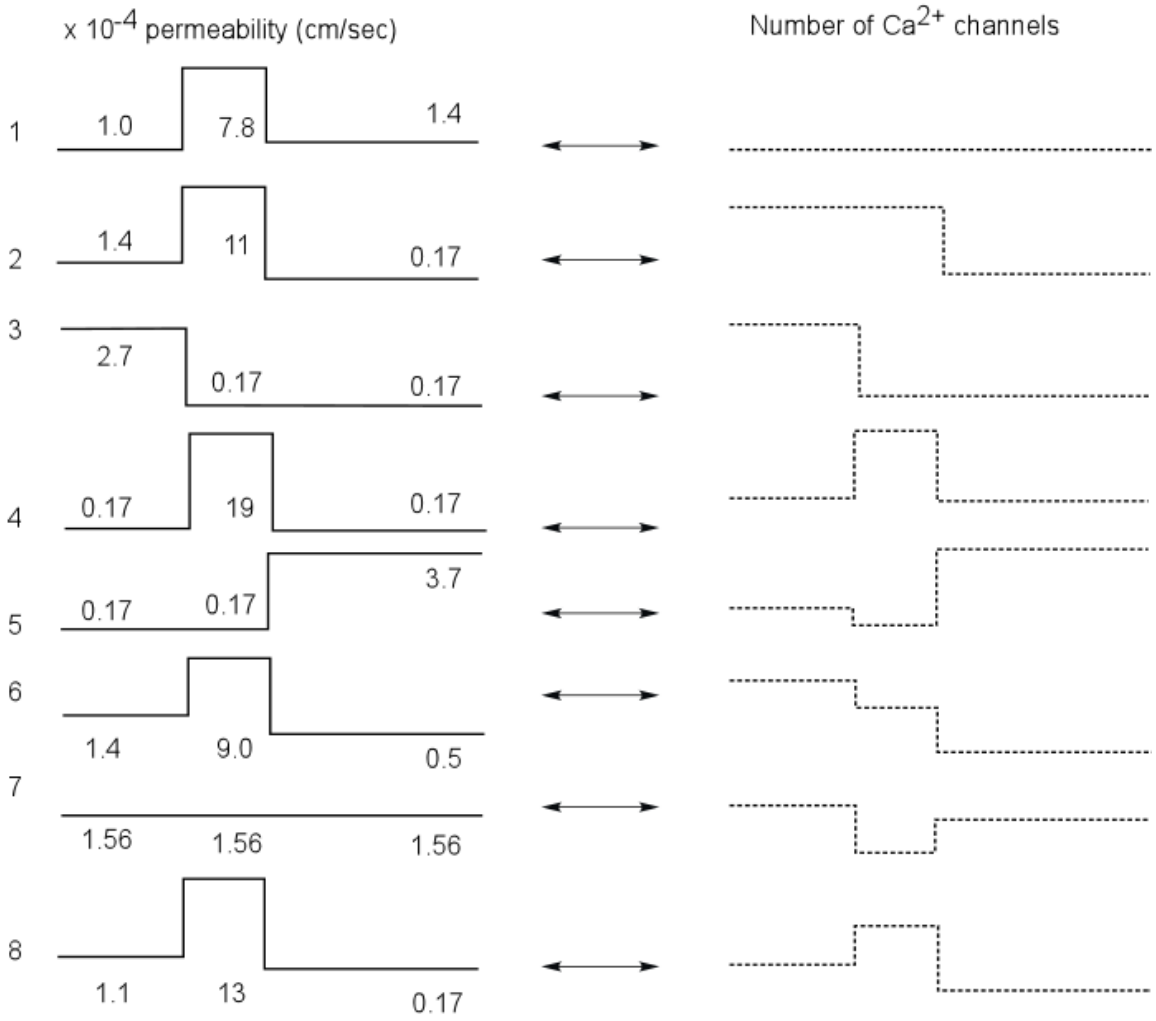

Figure 3-3. Different shapes of Ca^{2+} channel distribution can generate LTS spiking. Each line shows schematically the level of permeability in each compartment and its corresponding number of channels, which generate the threshold sodium spike similar to the response in Fig. 2 E. The channel number in each section is given by integration over the entire surface of the section. Both uniform and non-uniform distribution of T-channels can produce LTS response in the modeled cell.

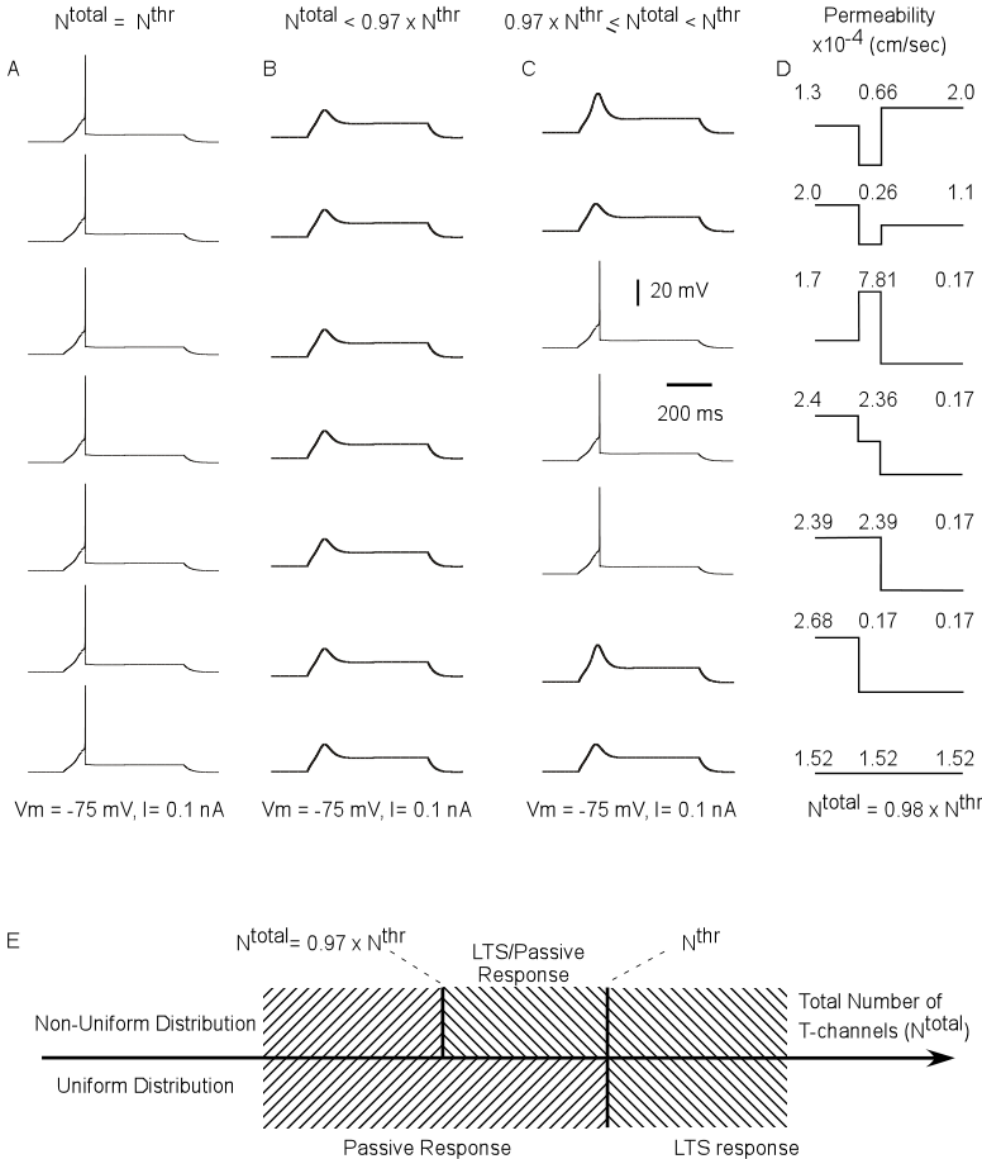

Figure 3-4. Total number of Ca^{2+} channels and its distribution determines whether LTS will lead or not to an action potential. (A) When the total number of T-channels was equal to threshold value (N^{thr}), the model neuron produced an LTS - action potential response with both, non-uniform and uniform channel distribution. (B) When the total number of channels was far from threshold value, the model gave LTS response not accompanied by action potentials. In this 3-compartment model, the response has no spikes as long as the total number of T-channels was below 0.97 x N^{thr}. (C) Between these two limits, the response of the neuron was sensitive to the shape of the T-channel distribution. To illustrate this feature, we set the total number of channels equal to 0.98 x N^{thr}. (D) Numbers show T-channel permeability in each compartment for different patterns of T-channel distribution, when the total number of T-channels was equal to 0. 98 x N^{thr}.

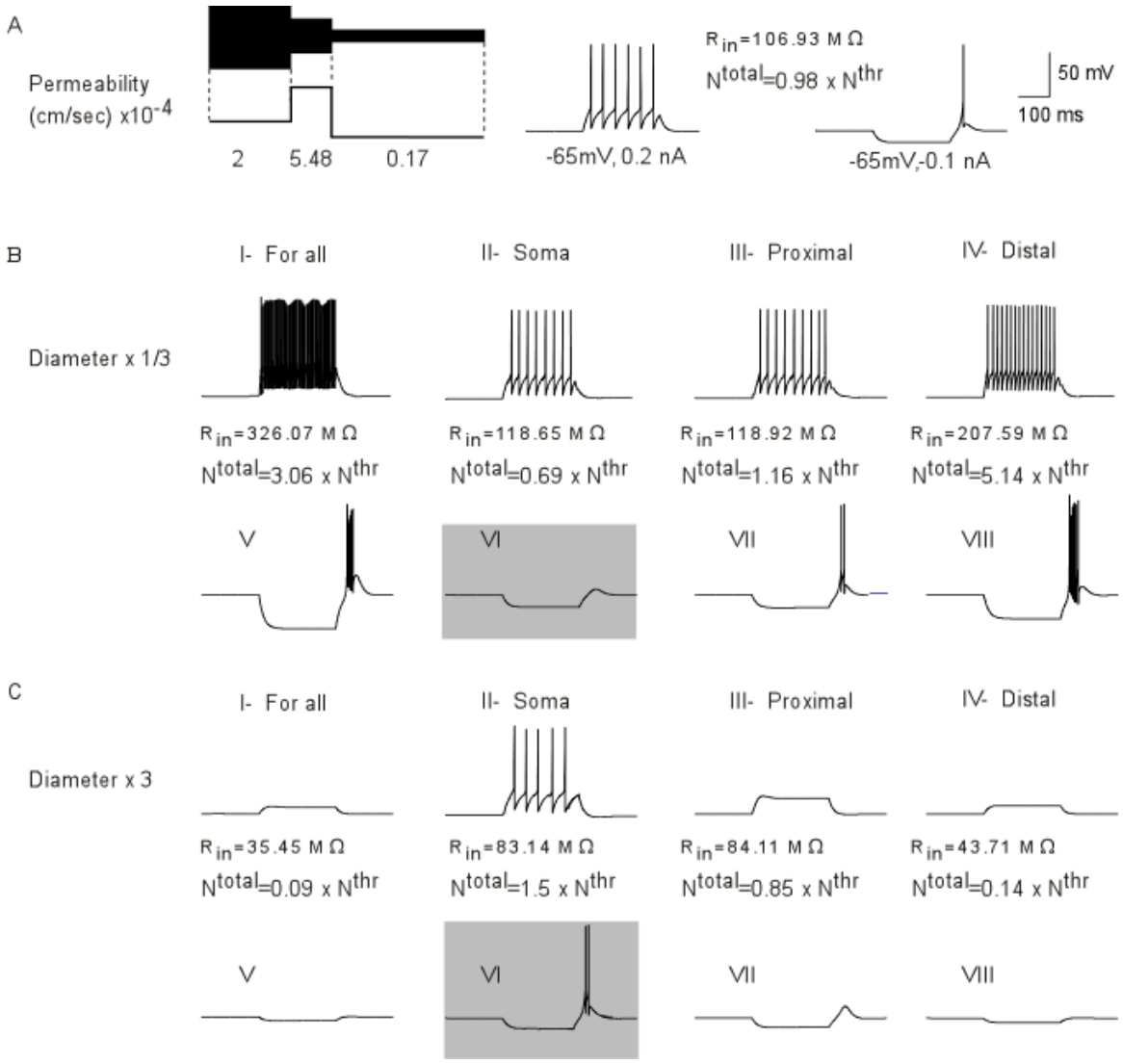

Figure 3-5. Influence of geometry on the response of cell with a higher T-channel density in proximal section. (A) In a control situation (N^{total} = 0.98 x N^{thr}) the model TC cell generates 6 spikes in response to a 0.2 nA depolarizing current pulse and 1 rebound spike in response to a -0.1 nA hyperpolarizing current pulse. (B, C; I - IV) Decreasing/increasing the cell size increases/decreases input resistance of the cell. This causes higher/lower frequency of tonic response to a depolarizing current. (B, C; V, VII, VIII). For a constant density of T-channels, reducing/increasing the size of the cell, or reducing/increasing the dendritic area increased/decreased input resistance as well as N^{total} of the cell. This gives more/less sodium spikes induced by LTS. (B, C; IV) Despite the fact that smaller/larger soma has a higher/lower input resistance, the number of T -channels is also decreased/increased. Therefore, the same hyperpolarized current pulse was found sufficient/insufficient to activate enough T-channels for rebound burst response.

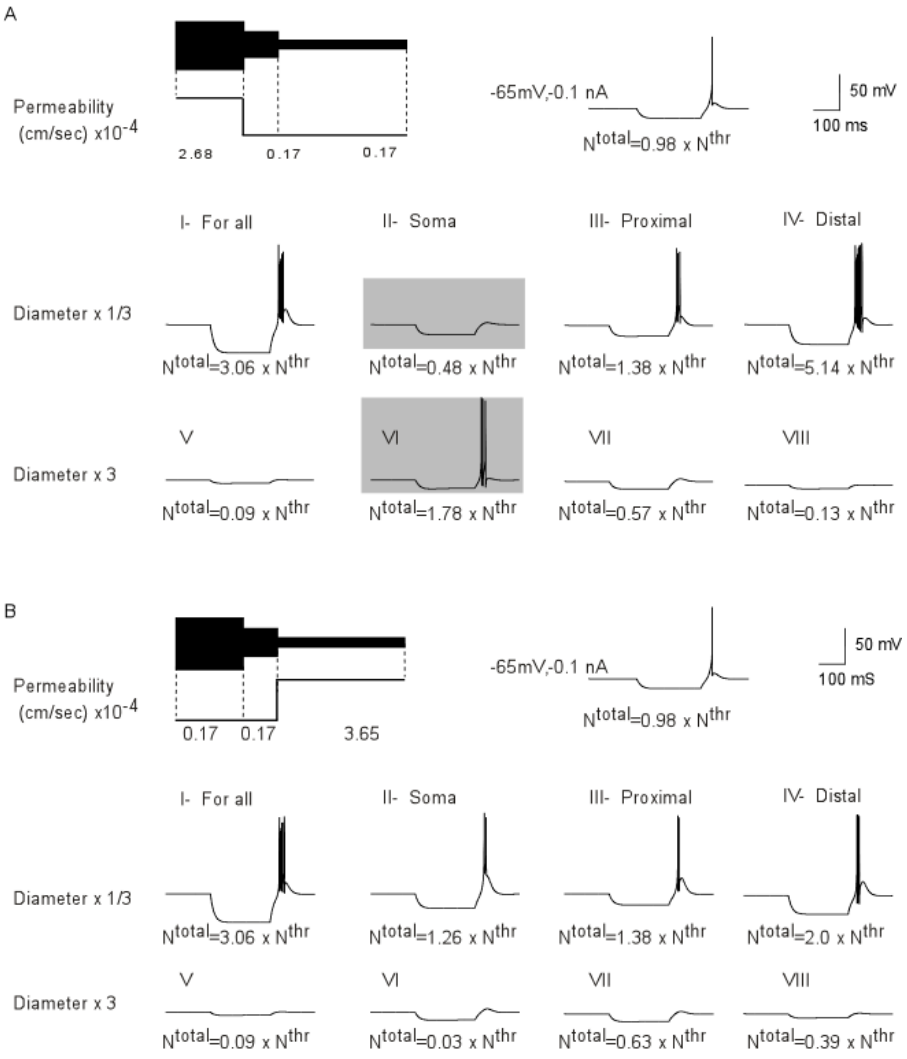

Figure 3-6. Influence of geometry on the response of cell with a higher T-channel density in somatic or distal dendritic sections. (A) LTS response with a higher density of T-channels located in soma. (A I, III and IV) Reducing the size of the cell decreased the total number of T-channels, but still its value was higher than threshold. Thus the model produced an LTS response accompanied with burst firing. (A; V, VII, VIII) Increasing the size of the cell increased the total number of T-channels, which was smaller than threshold. Thus model reproduced a passive response. (A II) Reducing the size of the soma changes the ratio in the number of total to threshold T-channels to the value of 48%. This was not sufficient to generate LTS. (A VI) increasing the size of soma changed the ratio in the channel number to 178%, which leads to a rebound burst. (B) The LTS response with a higher density of T-channels located in distal dendrites. (B I- VIII) Reducing the cell size makes the cell more excitable, which produces a higher frequency for the LTS response. A larger cell has a smaller input resistance and the ratio of N^{total} to N^{thr} of T-channels was found to lie outside of the range of LTS generation.

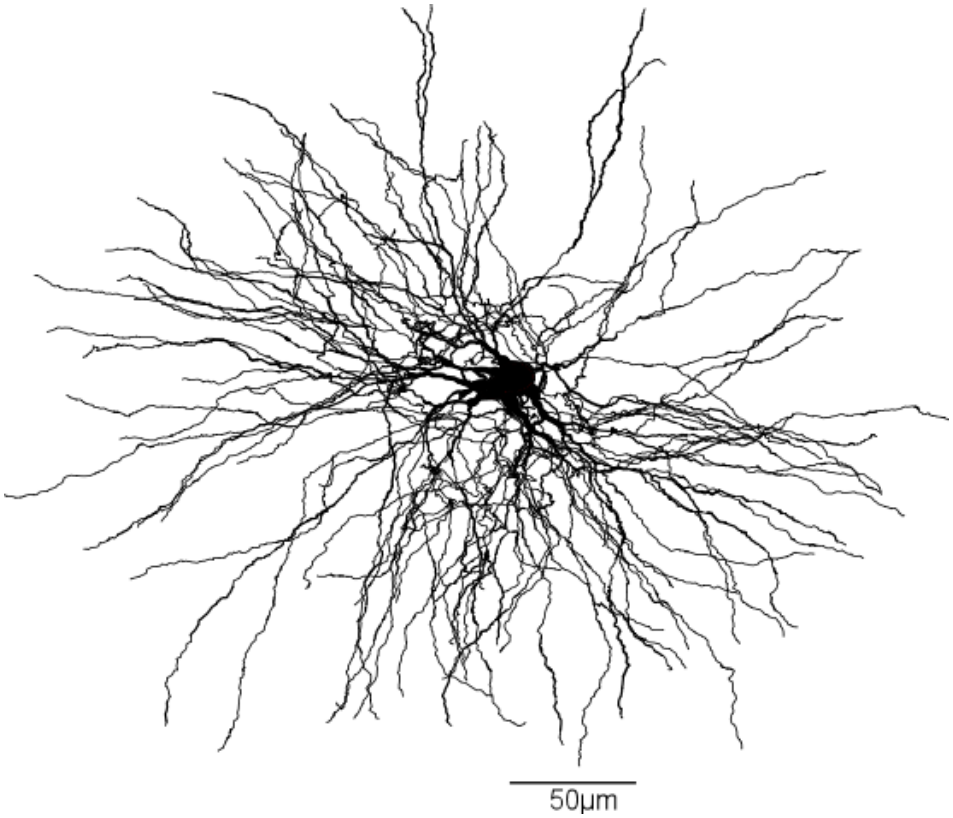

Figure 3-7. Morphology of reconstructed TC cell. Three-dimensional reconstruction of TC cell from VPL nucleus of adult cat. Retrograde tracer (fluorogold) was injected in somatosensory area SI. The complete dendritic arbor was reconstructed from 6 serial sections 80 µm each.

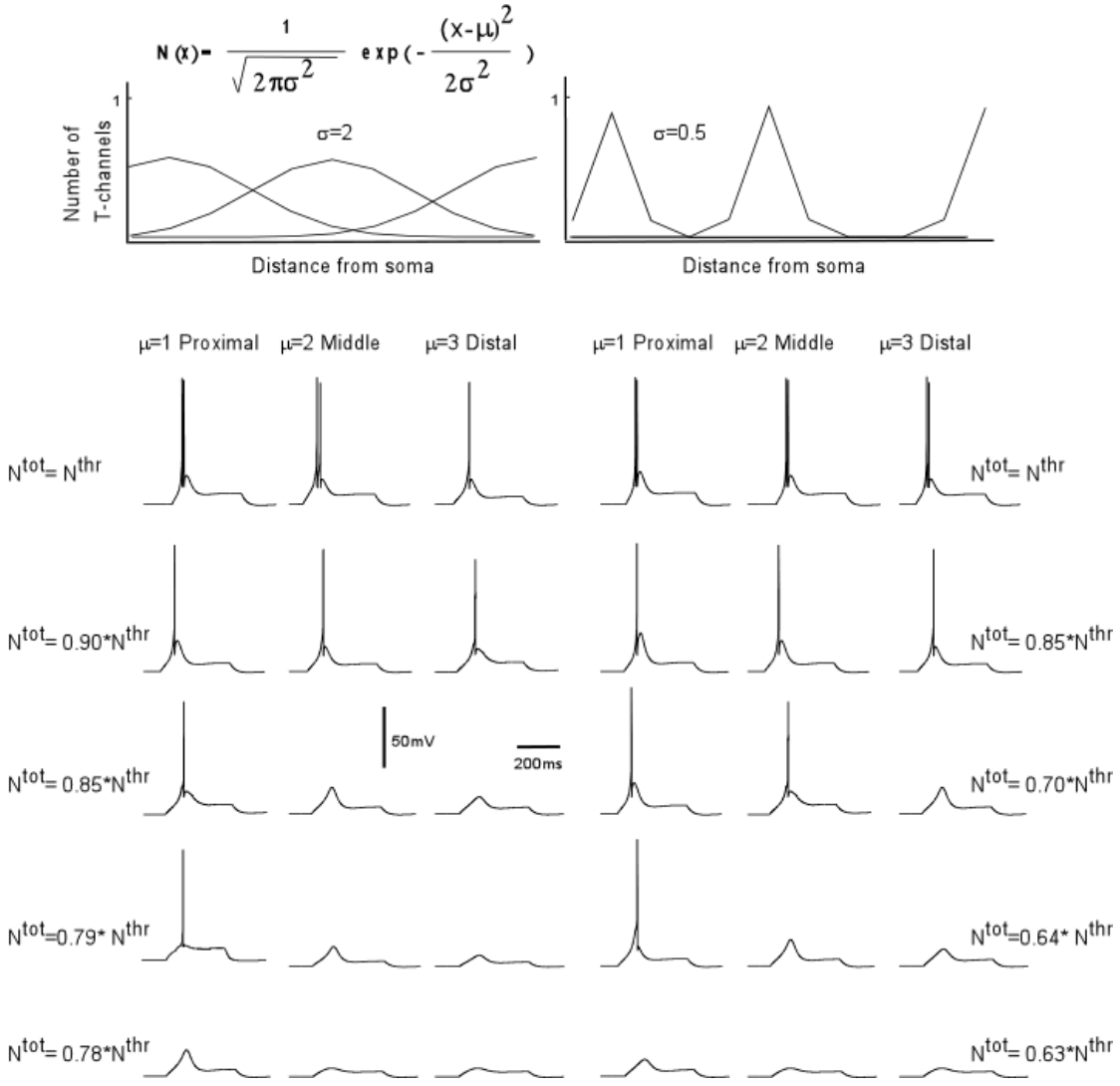

Figure 3-8. T-channel distribution required for LTS generation with minimal number of channels in multi-compartment model. The upper panel shows the shape of T-channel distribution used in the multi-compartment model. In the left column, the maximal channel density slowly decreases from its maximum value. In the right column, the maximal channel density rapidly decreases from its maximum value. Below examples are given for the response of the modeled neuron kept at -75 mV subject to 0.1 nA square current pulses. Note that the lower number of T-channels necessary to generate LTS occurred when the highest channel density was located in proximal dendrites. In addition, a sharp T-channel distribution leads to LTS generation with fewer channels (bottom, right).

4 Influence of morphological parameters on signal propagation efficacy in dendritic tress of thalamocortical neurons

Reza Zomorrodi, Helmut Kröger, Igor Timofeev

4.1 Résumé

Le type spécifique de patron de décharge et l'étendue selon laquelle un potentiel électrique se propage peut être attribué à une forme exclusive de morphologie dendritique d'un neurone. Dans cette étude, nous avons étudié l'influence des paramètres morphologiques sur l'efficacité de propagation du signal dans l'arborisation dendritique des neurones thalamocorticaux (TC) du noyau VPL, lesquels illustrent une grande variabilité de leurs caractéristiques morphologiques. Dans nos simulations, nous avons utilisé des modèles multicompartimentaux basés sur les équations de Hodgkin Huxley pour quatre neurones TC entièrement reconstruits. Nos résultats ont montré que la dépolarisation membranaire dendritique causée par la rétropropagation d'un potentiel d'action a un profil asymétrique. En outre, l'efficacité synaptique de chaque sous-arbre dépend fortement du patron d'arborisation dendritique. Afin d'étudier la relation entre chaque propriété morphologique et l'efficacité de la propagation du signal, nous avons recréé plusieurs modèles artificiels de cellules. Les ramifications dendritiques de ces cellules artificielles représentent la valeur moyenne des paramètres morphologiques des neurones TC. En gardant toutes les propriétés électriques et morphologiques constantes à l'exception qu'un seul paramètre morphologique, nous avons constaté que les paramètres topologiques ainsi que des propriétés géométriques influencent significativement l'amplitude du signal électrique propagé. Toutefois, les paramètres géométriques (longueur, diamètre, ratio géométrique, distribution de la surface membranaire) ont un impact plus élevé que les paramètres topologiques (longueur de parcours moyen et indice d'asymétrie moyen). En outre, notre modèle indique l'influence réciproque des propriétés morphologiques sur le contrôle du taux d'atténuation de la propagation du potentiel dans les sous-arbres voisins.

4.2 Abstract

In this study, we investigated the influence of geometrical (length, diameter, geometrical ratio, distribution of membrane area) and topological (mean path length and asymmetry index) parameters on signal propagation efficacy in dendritic trees of thalamocortical (TC) neurons from the VPL nucleus. We used multicompratment models based on Hodgkin-Huxley type of equations for four fully reconstructed TC neurons. To examine the influence of morphological parameters on signal propagation we assigned equal passive and active electrical properties to all dendritic sections. Our numerical simulations showed that the somatic action potential back propagates to the most distal dendrites with different attenuation rate, which led to diverse level of depolarization on dendritic membrane at equidistance from the soma. The specific form of dendritic arborization of TC neurons caused a high attenuation rate on forward propagation of synaptic inputs. The synaptic efficacy on each subtree showed a strong dependency on the morphological features of that tree. To explore the relation between morphological properties and the efficacy of a signal propagating, we developed several artificial cell models with different dendritic arborization. By keeping all electrical and morphological properties the same, but altering only one morphological parameter, we revealed that geometrical parameters had the higher impact than the topological parameters. Our model predicts a different physiological role, played by each dendritic subtrees of a TC neuron, because of their exclusive and diverse morphological properties. Keywords: thalamus, dendritic morphology, signal propagation, computational model

4.3 Introduction

Complex dendritic arborization with the elaborate mixture of voltage-dependent conductances significantly enhances the computational power of a single neuron (Hausser and Mel, 2003; London and Hausser, 2005). It has been shown that dendritic conductances strongly influence the integration process, synaptic plasticity and signal processing in neuronal circuits (Hausser et al., 2000; Magee, 2000; Johnston et al., 2003; Frick and Johnston, 2005; Magee and Johnston, 2005; Gobel and Helmchen, 2007; Spruston, 2008). In addition, the morphological properties and the synaptic topology of a neuron are critical determinants of neuronal information processing and may directly contribute to various brain functions (Mainen and Sejnowski, 1996; Vetter et al., 2001; Acker and White, 2007; Larkum and Nevian, 2008; Weaver and Wearne, 2008; Chen, 2010; Froemke et al., 2010; van Elburg and van Ooyen, 2010).

Although the primary function of dendritic trees is transferring input information toward the soma, the neurons can send reciprocally the vital information to the input of a neuron about the status of the cell's output via back-propagating action potentials (BP-AP). Experimental data from in vivo and in vitro studies indicated the influence of BP-AP on short/long-term synaptic plasticity, local synaptic feedback and stabilization of growing synapses (for a review, see (Waters et al., 2005)).

Most experimental studies examined BP-AP merely on one dendritic tree, and only few experiments have been performed to measure simultaneously the extent of backpropagation on different dendritic trees of a single neuron (i.e. basal versus apical dendrites)(Antic, 2003; Frick et al., 2003; Waters et al., 2005). Numerical simulations identified the impact of dendritic membrane conductance and neuronal morphology in controlling the efficacy of propagating action potentials in different class of neurons (Hausser et al., 2000; Vetter et al., 2001; Acker and White, 2007; Acker and Antic, 2009). However, it is not clear that whether the morphological diversity between dendritic trees of a single neuron lead to different efficacy for BP-AP or forward propagation of synaptic potentials? If so, which

morphological property has a determinant role in controlling the propagation of an electrical signal within the dendritic tree?

Here, we investigated this issue on a multicompratment model of thalamocortical (TC) neurons, which shows a wide range of morphological features between its dendritic tress (Zomorrodi et al., 2010). First, we examined the extent of BP-AP and forward propagation of synaptic inputs within dendritic trees and second, we studied the distinctive role of the geometrical and topological parameters on efficacy of an electrical potential propagation in several artificial modeled neurons.

Our results showed that given identical biophysical properties, the extent of propagation of an electrical signal was strongly modulated by morphological features of dendritic pathways. Numerical simulations indicated that geometrical parameters have a higher impact on efficacy of electrical signal propagation than topological parameters. In investigated TC neurons the attenuation rate of BP-AP was up to 35-65% at 120μm from the soma and EPSPs originating in these locations were attenuated by 96-99% when recorded at the level of soma.

4.4 Methods

To explore the relation between the efficacy of a signal propagation and dendritic morphology, we used several multicompartmental models based on four 3D reconstructed thalamocortical neurons from the VPL nucleus (Zomorrodi et al., 2010). We examined the influence of topological properties such as mean path length (MPL), asymmetry index (Asym_index) and geometrical parameters such as the total dendritic length, total membrane area and geometrical ratio (GR) at branching points of dendrites. Given a diversity of each dendritic arborization of thalamocortical cells from VPL nucleus (Fig. 1A), and to investigate the impact of each morphological feature, while other parameters were kept constant we constructed several forms of dendritic arborization (artificial dendrites) that captured the ranges of anatomical parameters (Zomorrodi et al., 2010) (Fig. 1 B).

Artificial cell models consisted of 31 sections and a single dendritic branch with 2 main subtrees. In order to examine the influence of two neighbor subtrees on each other, different morphological properties were attributed to the subtree with 12 dendritic tips (ST_{12}) and constant morphological parameters were used for the subtree with 4 dendritic tips (ST_4) (Fig. 1B). We analyzed attenuation rate of BP-AP on ST_4, while another daughter subtree (ST_{12}) had different value of asym_index ranging from 0.09 to 0.91 as well as MPL ranging from 142μm to 225μm. We verified these results for different geometrical parameters on ST_{12} such as total dendritic length, GR and membrane area distributions.

In all multicompratmental models, we used identical membrane resistance (R_m= 27 $K\Omega*cm^2$), membrane capacitance (C_m= 1 $\mu F/cm^2$) and axial resistivity (R_a=173 $\Omega*cm$) in all sections. We also employed Hodgkin-Huxley type equations for fast Na^+/K^+ currents in soma, the low-threshold Ca^{2+} current (IT) and leak current in all compartments (Zomorrodi et al., 2008). To investigate the impact of morphological features on signal propagation within the dendritic tree a uniform passive and active parameters were inserted in all dendritic sections of the models. In order to eliminate any variability in the action potential amplitude and duration, a typical action potential waveform (amp=90 mV, dur =2 msec) was injected as a command in voltage clamp protocol at soma for all models. We also

employed an identical synaptic current (amp=50 pA, dur= 100 msec) to study the efficacy of the forward propagation of postsynaptic potentials.

To investigate the influence of each morphological property on a propagating electrical signal through a dendritic arborization, we analyzed the impact of morphological variability of a subtree (ST_{12}) on its input resistance and its influence on current flow to another neighboring branch (ST_4). Finally, we traced amplitude of propagating action potentials and postsynaptic potentials at equidistance from soma on the dendogram of a dendritic tree and interpreted the attenuation rate of a propagating signal in the soma-dendritic pathway based on geometrical and topological properties.

All equations were solved in NEURON simulation environment (Hines and Carnevale, 1997). To determine the number of necessary compartments in various dendrites (Fig. 2A) the d-lambda method was used (Carnevale and Hines, 2005). All dendritic sections were divided into cylindrical compartments with a maximum length of 5-10 μm. Equal passive properties and a uniform density of low-threshold Ca^{2+} conductance were assigned to all dendritic sections.

4.5 Result

4.5.1 Back-propagation of action potential in dendritic trees of modeled TC neurons

Results of numerical simulations revealed that the propagation of the injected action potential waveform at soma caused different depolarization and attenuation rates on each dendritic pathway. For instance, measuring the dendritic membrane depolarization at 100 μm from soma on different sub-trees indicates a large variation in the amplitude and duration of BP-AP (Fig. 2B). Plotting maximal amplitude reached by the BP-AP shows a dramatic reduction in spike amplitude within first 100 μm (Fig. 2C.) The amplitude of BP-AP on some sub-trees dropped significantly to about 50-60%, while on other sub-trees the attenuation rate was about 20-30%. A polar plot shows the level of dendritic membrane depolarization induced by somatic BP-AP along each dendritic branch (n=137) Fig. 2D. Because of overlapping of several dendritic pathways, we used polar coordinates to demonstrate the pattern of membrane depolarization (Fig .2D). As it is illustrated by color bar, the recorded membrane potential at equidistance from soma shows a wide range of variability and consequently, different attenuation rates for BP-AP in each dendritic pathway.

Similar results were obtained in other investigated neurons (Fig. 3). There was 50±10% average decrease in the action potential amplitude on the proximal and middle regions of dendritic tree (e.g., up to 120μm from soma), and an additional reduction of 15-7% till the end of the dendritic tip (Fig. 3B). The attenuation rate of BP-AP even at the same distance from soma was not similar in different branches. The membrane depolarization of BP-AP at 100 μm from the soma (dotted circle in fig. 3C) reached values from -50 to -5 mV and it was reduced to by 63% to 85% at the end of dendritic tips. The attenuation rates of BP-AP in individual dendrites of the same TC neuron can vary significantly (Fig. 4).

Given that in our model all passive and active conductances were identical in each compartment, we investigated the morphological factors that affect attenuation rate in different dendrites. We explored this dependency in more details for a single subtree (Fig. 5). Figure 5A illustrates a dendritic branch consisted of two main subtrees with 14 dendritic pathways. The dendritic length (x-axis) and a mean diameter (numbers on dendrogram) for each dendritic section are indicated on Figure 5B. In agreement with results shown above, the BP-AP in three separate dendritic branches was attenuated to a different extent (Fig. 5C) and such a pattern was true for all dendritic branches (Fig. 5 D). Numbers correspond to the dendritic pathway (dend-P) as shown in the dendogram. We compared attenuation rates in each compartments of three dendritic branches with dendritic diameter at this compartment and with GR at branching points (Fig. 5E). We found: (I) The amplitude of back propagating signal was decreasing in parallel with a decrease in the diameter of dendrite (see first 25 mm in Fig. 5E and Fig. 10, A [T2]). (II) Although dend-P14 and dend-P9 owns a similar length, the recorded membrane potentials at distal regions show a difference up to 20 mV. (III) While AP had to travel a longer distance on dend-P7 to reach the dendritic tip, its attenuation rate was lower than on dend-P14.

Analyzing the dendritic diameter (Fig. 5E, middle) and GR (Fig. 5E, bottom) versus the distance from the soma indicate approximately the same dendritic diameter along dend_Ps, but violation of 3/2 Rall's power law (Goldstein and Rall, 1974) at branching points(e.g., GR>1), suggesting a decrease in the amplitude of signal after branching point. Morphological analysis shows that dend-P14 owns two branching points with GR very close to one (i.e., GR=1.1, 1.0), dend-P7 has four branching points with GR more than one (i.e., GR=1.1, 1.36, 1.18, 1.53) and dend-P9 possesses six branching points with GR=1.1, 1.36, 1.18, 1.53, 1.66 and 1.27. The higher GR explains the higher attenuation rate on dend-P9 than dend-P7 and dendP14.

4.5.2 Propagation of a synaptic potential in dendritic trees of modeled TC neurons

We explored how morphological properties of a dendritic arborization modulate the forward propagation (FP) of excitatory postsynaptic potentials (EPSPs). Figure 6A, B illustrate the dendritic subtree, its corresponding dendogram and the sites of tested synaptic inputs (colored symbols). In this simulation, we studied the FP of an EPSP, which was generated by injection of a synaptic current (amp=50 pA, dur= 100 msec) at 120 μm from soma. In this dendritic tree, the amplitude of generated EPSP at the site of injection varied from 5 mV to 8 mV. For the three dendritic pathways, the shape of postsynaptic potentials at different distance from soma (i.e., 80 μm and 40 μm) and somatic responses are illustrated in figure 6C. It is clearly seen that the attenuation rate was different in these 3 dend-Ps. It also shows that despite different amplitude of local responses at the site of stimulation, the somatic responses were of similar amplitude. With the used intensity of stimulation, the recording amplitude of somatic EPSP was in the order of 0.1 mV.

In order to compare the influence of dendritic morphology on the FP of a distal EPSP, we measured membrane potential along each dend-Ps and their corresponding diameter and geometrical ratio at each branching points (Fig. 6D). Difference between local geometry at the site of the synaptic input caused variability in the local EPSP (Fig. 6D, upper plot at 120 μm). As the signal propagated toward the some, at proximal regions (~ 50-70 μm from soma) the diameter of dendritic sections suddenly increased (Fig. 6D, middle), and EPSP amplitude encounter amplitude suppression. At branching points, since the average GR value for a forward propagation of signal was well above 1 (Fig. 6 D, (bottom), the EPSPs amplitude underwent dramatic attenuation. For instance, although generated EPSP at 120 μm from soma on the dend-P9 (blue) has larger amplitude than dend-P7 (green) or dend-P14 (brown), the higher values of the geometrical ratio for dend-P9 (i.e., GR=5.8, 7.1) before the proximal region led to a high attenuation rate on this dendritic pathway. From the stimulation points to the dendritic tips the diameter of shown branches was almost constant and accordingly, the attenuation rates were similar.

Dendritic pathway from the soma to the dendritic tip is not the only route that a distal EPSP may travel. It also propagates toward other daughter dendritic pathways. Using the same dendrite as in figure 6, we calculated the amplitude of EPSP versus distance from soma, as it propagated toward soma and toward other dendritic sections. As we showed above, the FP EPSPs were dramatically attenuated at proximal dendritic regions. However, after a branching point, the same EPSP could efficiently propagate and depolarize other connected dendritic branches (Fig. 7). For all 14 dendritic pathways, we plotted maximum depolarization pattern in Fig. 7B.

4.5.3 Influence of morphological parameters on the signal propagation in dendritic trees

In order to specify the influence of each morphological parameter on propagation of an electrical signal in the cell, we used 30 artificial modeled cells. The dendritic arborization of these cells has the same range of the morphological features as TC neurons. All artificial cells consisted of two main subtree, with the one that had identical morphological properties throughout all models and another one in which morphological features such as total dendritic length, area, GR, MPL and Asym_index varied (Fig. 1B). We used this morphological variability to investigate their impact on controlling signal propagation in both subtrees.

All artificial neurons with a uniform passive and active conductance (T-channel) on their dendritic sections can reproduce tonic and low-threshold Ca^{2+} spike (LTS), but with different delay time and frequency (Fig. 4-8B).

4.5.4 Impact of topological properties

Two modeled cells with equal geometrical properties (total area, total dendritic length and equal dendritic diameter) but different topological properties (MPL and Asym_index) of

ST_{12} subtree (Fig. 4-8A), generated tonic and rebound burst in response to depolarized current (0.1 nA) at -65mV and -75 mV, respectively. Cell with higher MPL or Asym_index have shorter time delay and higher frequency response (Fig. 4-8B up and middle) and different attenuation rate on adjacent ST_4 subtree (Fig. 4-8B bottom). It has to be noticed the only source to create such difference between BP-AP and spiking pattern is topological feature of ST_{12}. Higher value of topological parameters on ST_{12} cause lower attenuation rate on ST_4.

For all modeled neurons in fig.1B, we determined the relation between input resistance of ST_{12} and MPL as well as the relation between MPL of ST_{12} and attenuation rate on ST_4. Result shows a strong correlation between MPL of ST_{12} and attenuation rate on daughters ST_4 subtree. In other words, a subtree with higher input resistance direct more current flow to another daughter subtree, and provide an opportunity for propagation potential to reach more distal part of the dendritic tree (Fig. 4-8D).

For a propagating electrical signal on dendritic arborization of a neuron, level of membrane depolarization at any point of subtree depends on amount of axial current and transfer resistance (Jaffe and Carnevale, 1999). In addition, the amplitude of an axial current after branching point depends on resistance of downstream subtree. Therefore, any parameters that affect resistance of a dendritic branch might influence efficacy of propagating signal on daughter subtree.

On artificial models, first we examined the effect of dendritic topology when subtrees had the same geometrical properties, and then we explored the influence of the geometrical features for equal dendritic topology.

To determine the relation between input resistances of ST_{12} subtree and its MPL/asym_index, first, we set an equal dendritic length and diameter (GR=2) for all sections. In addition, density of T-channel was kept to threshold value (P_{ca}=2e-5 cm/sec) to generate single action potential induced by LTS. All artificial models demonstrate a strong correlation between input resistance (R_{in}) and MPL/Asym_index of ST_{12} subtree. Although

varying GR at branching points strongly influenced the value and even altered the sign of the correlation coefficients, distributions of T-channel (e.g. linear increase or decrease from distance of soma) had minor effect on these results (Fig. 4-9A top). However, distribution of T-channel has more significant effect, when the total number of T-channel was slightly more than threshold value (N_T=1.3 N_{thr}) (Fig. 4-9A bottom).

The relation between R_{in} and MPL/Asym_index, for three values of GR (=0.5, 1, 2), uniform and non-uniform T-channel distribution (N_T=N_{thr}) has been shown in Fig. 9B. These graphs indicate that although R_{in} and MPL/Asym_index have a strong correlation, the effect of MPL/Asym_index on R_{in} is considerable only for large value of GR. The slope of the fitted line between R_{in} and MPL/Asym_index has plotted for a wide range of GR (Fig. 4-9C). Our results show that the impact of topological properties on input resistance of a subtree strongly regulated by geometrical properties.

It has been known that the input resistance is a function of inverse total membrane surface (Koch, 1999), but how the distribution of dendritic membrane area, may influence the input resistance is not examined yet. We investigate this possible relationship in a multicopartmental model for an artificial cell with a dendogram as shown in fig. 4-10A.
Numbers on fig. 4-10A indicate dendritic sections and Eq.1-2 in fig. 4-10B shows employed algorithm for area distribution. According to Eq.1, we change the area of one dendritic section, and compensate this variation by all other sections, in order to have ca constant total area. In Eq.2, we only change diameter of the proximal dendrite (i.e., diam(0)), and this variation compensated by another section according to Eq.2 algorithm. As in previous simulation, dendritic tree had uniform electrical properties. We show that for a constant total membrane area, the input resistance dropped significantly by increasing membrane area of section 0 or 8. Increasing area of section 1 or 14 slightly reduced the R_{in}, but for all other sections R_{in} increased by increasing dendritic membrane area (Fig. 4-10C). If distribution of membrane area follows Eq.1, then increasing dendritic membrane area leads to decreasing $R_{in,}$ except for section 8. Increasing diameter of section 8 by 40%, slightly decrease R_{in} and after that the R_{in} increases as the diameter of the section grows up (Fig. 4-10D).

4.5.5 Impact of geometrical properties

We calculated the attenuation rate (=1-V_2/V_1) on several possible dendritic arborizations (Fig. 4-11A). When a dendritic tree did not have any branching points, the attenuation rate depended on membrane area distribution. All dendritic branches indicated by T1, T2, T3 had the same total dendritic area, but the diameter reduced abruptly (T3) or gradually (T2) up to dendritic tip rather than a constant diameter (T1). This specific geometry changed attenuation rate from 89 to 85 and 81 percent on T1, T3 and T2, respectively (Fig. 4-11B). However, attenuation rate had higher value if the dendritic tree possessed only one branching point. T4, T5 and T6 had equal and membrane area identical to T1. Daughter branches in T4 have equal length and diameter, in T5 different lengths and in T6 have different diameters. The attenuation rate on the dendritic pathway was higher for longer dendrite (Fig. 4-11C). If dendritic pathway had equal length (T6), the attenuation rate was lower for dendrite with smaller diameter.

In addition, we examined the impact of a subtree with different topological parameters on the attenuation rate. T8a and T8b have the same diameter and length, which were connected to T7 and T9 as the daughter branch. These dendritic arborizations (T8 and T9 or T8 and T7) have the same area as T1. As fig. 11D shows the level of depolarization on T8a was slightly different from T8b. T9 had higher topological parameters (MPL and Asym_index) rather than T7. Therefore, the attenuation rate of T8 shows the lower value when it was connected to T9. This graph also indicates that the higher attenuation rate happened on the longer dendritic pathway. However, not only dendritic length and area, but also geometrical ratio had a strong effect on attenuation rate. For GR=1/2, 1, 2 at branching point of T10, we determined the attenuation rate and the duration of AP waveform as propagate on the longest dendritic pathway (VII or VIII). Branching point with GR>1 cause transient decrease in the amplitude and those with GR<1 cause transient increase in the amplitude of propagating signal, while at branching point that follows 3/2 Rall's power law (GR=1), the amplitude before and after branching point does not change (Goldstein and Rall, 1974).

Therefore, attenuation rate on the dendritic pathway with GR>1 and GR<1 at branching points shows the higher and lower value rather than GR=1 (Fig. 4-11F). While, duration of a propagating signal compares to GR=1 for GR<1 and GR>1 is lower and higher, respectively (Fig. 4-11G).

4.6 Discussion

Dendrites with diverse morphological and physiological features not only modulated postsynaptic potenti al on their way to the soma (Magee and Cook, 2000; Jarsky et al., 2005; Stuart et al., 2007; Spruston, 2008; Remy et al., 2009), but they also could effectively amplify backpropagation action potential into their dendrites (Stuart et al., 1997; Waters et al., 2005).

The efficacy of Na^+ action potential backpropagation depends to several factors such as firing frequency (Spruston et al., 1995; Golding et al., 2001; Errington et al., 2010), the presence of dendritic potassium conductances (Migliore et al., 1999; Acker and White, 2007), the excitatory and the inhibitory synaptic background activity (Buzsaki et al., 1996; Chen et al., 1997; Stuart and Hausser, 2001), and the branching pattern of the dendrites (Vetter et al., 2001).

In this study, we specifically examined the influence of morphological features on the efficacy of electrical signal propagation through the dendritic arborizations of TC neurons. We constructed multicompartmental model using Hodgkin-Huxley type of equations, based on detailed morphological data of several fully reconstructed thalamocortical neurons.
Our numerical simulations illustrated the pattern of membrane depolarization cause by BP-AP in all dendritic sections and extent to which an EPSP might propagate from distal sites towards the soma or even towards other adjacent dendritic branches. To investigate the effect of morphology, a uniform distribution of passive and active conductance (T-channel) had been inserted in all dendritic sections.

Results of our multicompratment model of TC neurons revealed that (1) membrane depolarization cause by BP-AP on dendritic trees at equidistance from soma gives wide range of amplitudes. (2) While passive and active properties on dendritic trees held identical, the extend of BP-AP and level of membrane depolarization strongly depends on morphological properties of subtree. (3) Dendritic morphology has higher impact on synaptic efficacy than BP-AP. Our simulations showed that morphological properties of a

dendritic pathway prevent effective transfer of a unitary distal EPSP toward the soma. (4) Although most distal EPSP attenuate dramatically on their way to soma, they may efficiently propagate to other adjacent subtrees creating possibility for effective dendritic interactions.

In order to examine the impact of each morphological property on signal propagation we developed several artificial cells. These results indicated that (5) the major impact of morphology on signal propagation comes from geometrical parameters such as dendritic length, geometrical ratio at branching points, total area and its distribution rather than topological parameters such as mean path length and asymmetry index. (6) Morphological feature of a downstream subtree not only controls efficacy of signal propagation within the subtree, but also regulate efficacy on other daughter subtrees.

Our models illustrated that each dendritic tree of TC neuron have special ability to transfer BP-AP and forward propagation EPSP, therefore, each dendritic tree might play different role in processing input information and generated output action potentials. Investigating morphological properties of a dendritic tree simply from a dendogram plot can be first estimation for efficacy of dendritic tree in transferring forward or backward propagation of an electrical potential. Based on our numerical simulation, we can predicate that for a reliable transforming information to thalamocortical neuron, synaptic input should distributed on different dendritic trees instead of converging on a single subtree.

4.7 Acknowledgements

This study was supported by National science and engineering research council of Canada (grant 298475), Canadian Institutes of Health Research (MOP-37862, MOP-67175), and National Institute of Neurological Disorders and Stroke (1R01NS060870 I.T. is Fonds de la recherche en santé du Québec Research Scholar.

4.8 References:

Acker CD, White JA (2007) Roles of IA and morphology in action potential propagation in CA1 pyramidal cell dendrites. J Comput Neurosci 23:201-216.

Acker CD, Antic SD (2009) Quantitative assessment of the distributions of membrane conductances involved in action potential backpropagation along basal dendrites. J Neurophysiol 101:1524-1541.

Antic SD (2003) Action potentials in basal and oblique dendrites of rat neocortical pyramidal neurons. J Physiol 550:35-50.

Bloomfield SA, Sherman SM (1989) Dendritic current flow in relay cells and interneurons of the cat's lateral geniculate nucleus. Proc Natl Acad Sci U S A 86:3911-3914.

Buzsaki G, Kandel A (1998) Somadendritic backpropagation of action potentials in cortical pyramidal cells of the awake rat. J Neurophysiol 79:1587-1591.

Buzsaki G, Penttonen M, Nadasdy Z, Bragin A (1996) Pattern and inhibition-dependent invasion of pyramidal cell dendrites by fast spikes in the hippocampus in vivo. Proc Natl Acad Sci U S A 93:9921-9925.

Carnevale NT, Hines ML (2005) The NEURON book. Cambridge ; New York: Cambridge University Press.

Chen JY (2010) A simulation study investigating the impact of dendritic morphology and synaptic topology on neuronal firing patterns. Neural comput 22:1086-1111.

Chen WR, Midtgaard J, Shepherd GM (1997) Forward and backward propagation of dendritic impulses and their synaptic control in mitral cells. Science 278:463-467.

Errington AC, Renger JJ, Uebele VN, Crunelli V (2010) State-dependent firing determines intrinsic dendritic Ca2+ signaling in thalamocortical neurons. J Neurosci 30:14843-14853.

Frick A, Johnston D (2005) Plasticity of dendritic excitability. J neurobiol 64:100-115.

Frick A, Magee J, Koester HJ, Migliore M, Johnston D (2003) Normalization of Ca2+ signals by small oblique dendrites of CA1 pyramidal neurons. J Neurosci 23:3243-3250.

Froemke RC, Letzkus JJ, Kampa B, Hang GB, Stuart G (2010) Dendritic synapse location and neocortical spike-timing-dependent plasticity. Front Synaptic Neurosci 3:12.

Gobel W, Helmchen F (2007) New angles on neuronal dendrites in vivo. J Neurophysiol 98:3770-3779.

Golding NL, Kath WL, Spruston N (2001) Dichotomy of action-potential backpropagation in CA1 pyramidal neuron dendrites. J Neurophysiol 86:2998-3010.

Goldstein SS, Rall W (1974) Changes of action potential shape and velocity for changing core conductor geometry. Biophys J 14:731-757.

Grewe BF, Bonnan A, Frick A (2010) Back-Propagation of Physiological Action Potential Output in Dendrites of Slender-Tufted L5A Pyramidal Neurons. Front Cell Neurosci 4:13.

Hausser M, Mel B (2003) Dendrites: bug or feature? Curr Opin Neurobiol 13:372-383.

Hausser M, Spruston N, Stuart GJ (2000) Diversity and dynamics of dendritic signaling. Science 290:739-744.

Hausser M, Stuart G, Racca C, Sakmann B (1995) Axonal initiation and active dendritic propagation of action potentials in substantia nigra neurons. Neuron 15:637-647.

Hines ML, Carnevale NT (1997) The NEURON simulation environment. Neural Comput 9:1179-1209.

Jaffe DB, Carnevale NT (1999) Passive normalization of synaptic integration influenced by dendritic architecture. J Neurophysiol 82:3268-3285.

Jarsky T, Roxin A, Kath WL, Spruston N (2005) Conditional dendritic spike propagation following distal synaptic activation of hippocampal CA1 pyramidal neurons. Nat Neurosci 8:1667-1676.

Johnston D, Christie BR, Frick A, Gray R, Hoffman DA, Schexnayder LK, Watanabe S, Yuan LL (2003) Active dendrites, potassium channels and synaptic plasticity. Philos Trans R Soc Lond 358:667-674.

Koch C (1999) Biophysics of computation : information processing in single neurons. New York: Oxford University Press.

Larkum ME, Nevian T (2008) Synaptic clustering by dendritic signalling mechanisms. Curr Opin Neurobiol 18:321-331.

London M, Hausser M (2005) Dendritic computation. Ann Rev Neurosci 28:503-532.

Magee JC (2000) Dendritic integration of excitatory synaptic input. Nat Rev Neurosci 1:181-190.

Magee JC, Cook EP (2000) Somatic EPSP amplitude is independent of synapse location in hippocampal pyramidal neurons. Nat Neurosci 3:895-903.

Magee JC, Johnston D (2005) Plasticity of dendritic function. Curr Opin Neurobiol 15:334-342.

Mainen ZF, Sejnowski TJ (1996) Influence of dendritic structure on firing pattern in model neocortical neurons. Nature 382:363-366.

Martina M, Vida I, Jonas P (2000) Distal initiation and active propagation of action potentials in interneuron dendrites. Science 287:295-300.

Migliore M, Hoffman DA, Magee JC, Johnston D (1999) Role of an A-type K+ conductance in the back-propagation of action potentials in the dendrites of hippocampal pyramidal neurons. J Comput Neurosci 7:5-15.

Remy S, Csicsvari J, Beck H (2009) Activity-dependent control of neuronal output by local and global dendritic spike attenuation. Neuron 61:906-916.

Spruston N (2008) Pyramidal neurons: dendritic structure and synaptic integration. Nat Rev Neurosci 9:206-221.

Spruston N, Schiller Y, Stuart G, Sakmann B (1995) Activity-dependent action potential invasion and calcium influx into hippocampal CA1 dendrites. Science 268:297-300.

Stuart G, Hausser M (1994) Initiation and spread of sodium action potentials in cerebellar Purkinje cells. Neuron 13:703-712.

Stuart G, Spruston N, Häusser M (2007) Dendrites, 2nd Edition. Oxford ; New York: Oxford University Press.

Stuart G, Spruston N, Sakmann B, Hausser M (1997) Action potential initiation and backpropagation in neurons of the mammalian CNS. Trend Neuroscis 20:125-131.

Stuart GJ, Hausser M (2001) Dendritic coincidence detection of EPSPs and action potentials. Nat Neurosci 4:63-71.

Svoboda K, Helmchen F, Denk W, Tank DW (1999) Spread of dendritic excitation in layer 2/3 pyramidal neurons in rat barrel cortex in vivo. Nat Neurosci 2:65-73.

Van Elburg RA, van Ooyen A (2010) Impact of dendritic size and dendritic topology on burst firing in pyramidal cells. PLoS computational biology 6:e1000781.

Vetter P, Roth A, Hausser M (2001) Propagation of action potentials in dendrites depends on dendritic morphology. J Neurophysiol 85:926-937.

Waters J, Helmchen F (2004) Boosting of action potential backpropagation by neocortical network activity in vivo. J Neurosci 24:11127-11136.

Waters J, Schaefer A, Sakmann B (2005) Backpropagating action potentials in neurones: measurement, mechanisms and potential functions. Prog Biophys Mol Biol 87:145-170.

Waters J, Larkum M, Sakmann B, Helmchen F (2003) Supralinear Ca2+ influx into dendritic tufts of layer 2/3 neocortical pyramidal neurons in vitro and in vivo. J Neurosci 23:8558-8567.

Weaver CM, Wearne SL (2008) Neuronal firing sensitivity to morphologic and active membrane parameters. PLoS computational biology 4:e11.

Williams SR, Stuart GJ (2000) Action potential backpropagation and somato-dendritic distribution of ion channels in thalamocortical neurons. J Neurosci 20:1307-1317.

Zomorrodi R, Kroger H, Timofeev I (2008) Modeling thalamocortical cell: impact of ca channel distribution and cell geometry on firing pattern. Front Comput Neurosci 2:5.

Zomorrodi R, Ferecskó AS, Kovács K, Kröger H, Timofeev I (2010) Analysis of morphological features of thalamocortical neurons from ventro postero lateral nucleus of the cat. J Comp Neurol 9999:3541-3556.

4.9 Figures

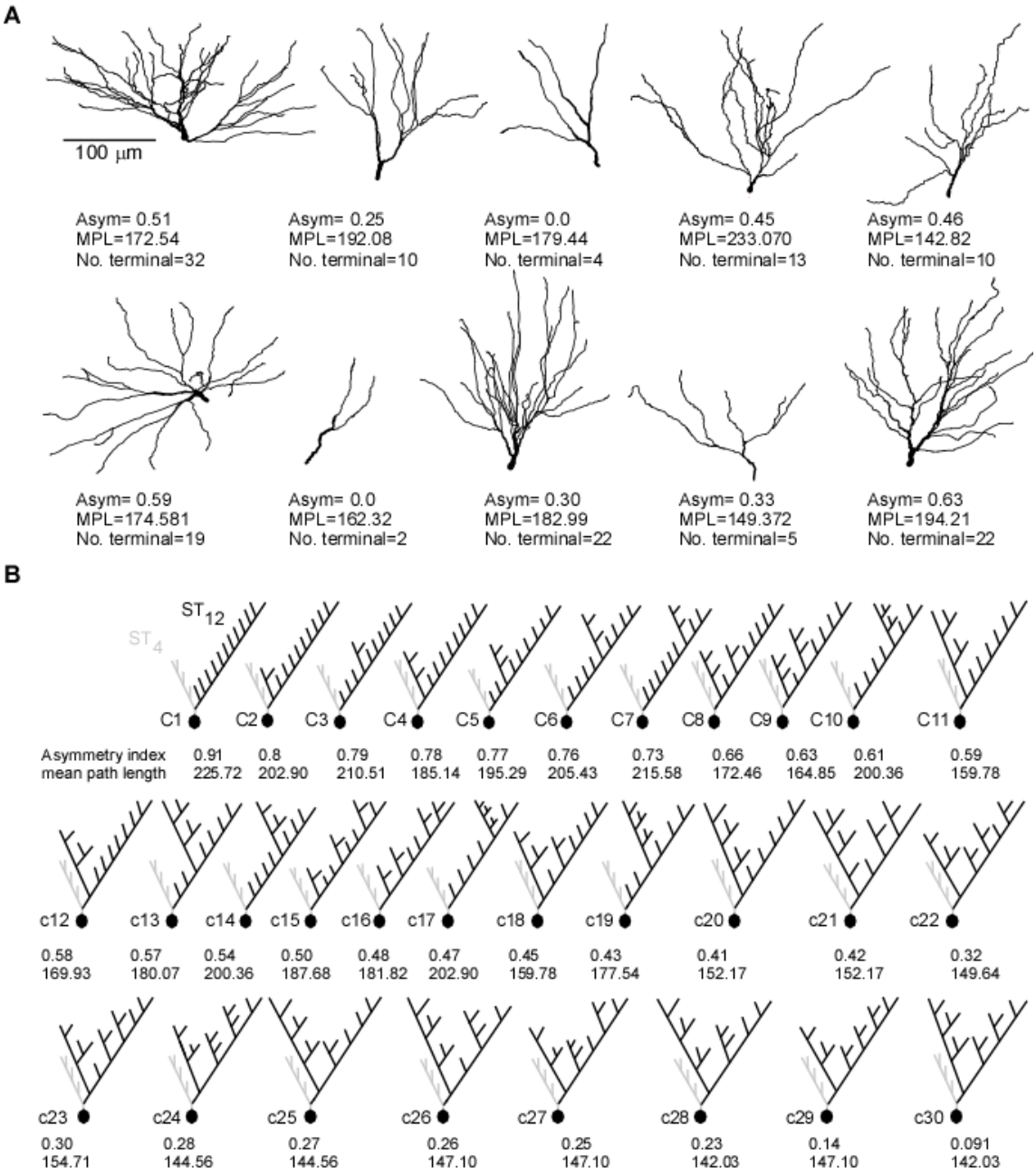

Figure 4-1. Constructed artificial modeled cells based on diverse morphological parameters of TC neurons. Dendritic arborizations in a single TC neuron show a significant variety in the pattern of connectivity between dendritic sections. **(A)** Each dendritic tree illustrates a single dendritic arborization of a several fully reconstructed TC neurons. Numbers indicate asymmetry index (Asym), mean path length (MPL) and number

of terminals (No. terminal). Scale bar=100μm. **(B)** Schematic presentations of modeled neurons with 16-degree topologies, based on the average morphological features of the TC neurons. Each model consists of two main subtrees with constant (gray) and variable (black) morphological parameters throughout the models. In simulations, equal length and electrical properties assigned to all dendritic sections.

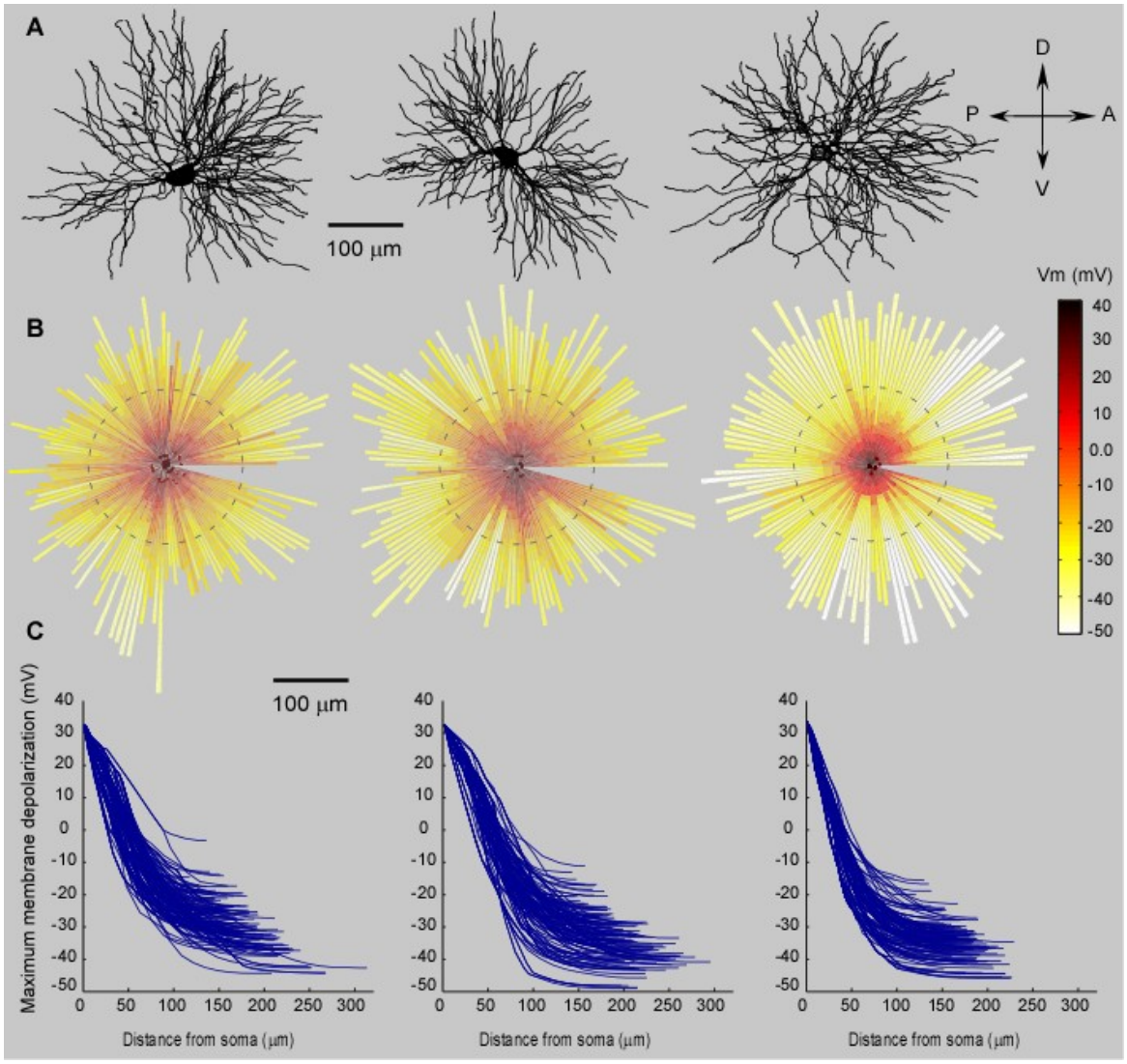

Figure 4-2 Elaborated dendritic arborizations of a TC neuron controls the Level of membrane depolarization on a dendritic branch caused by a backpropagating action potential. (A) Three-dimensional reconstruction of the TC neurons from VPL nucleus in dorsal/ventral-posterior/anterior. **(B)** Depolarization pattern of the back propagating action potential in all dendritic trees in a in multi-compartmental model based on Hodgkin-Huxley equations. **(C)** Graph shows the maximum membrane depolarization during backpropagating action potential generation in each dendrites versus distance from soma.

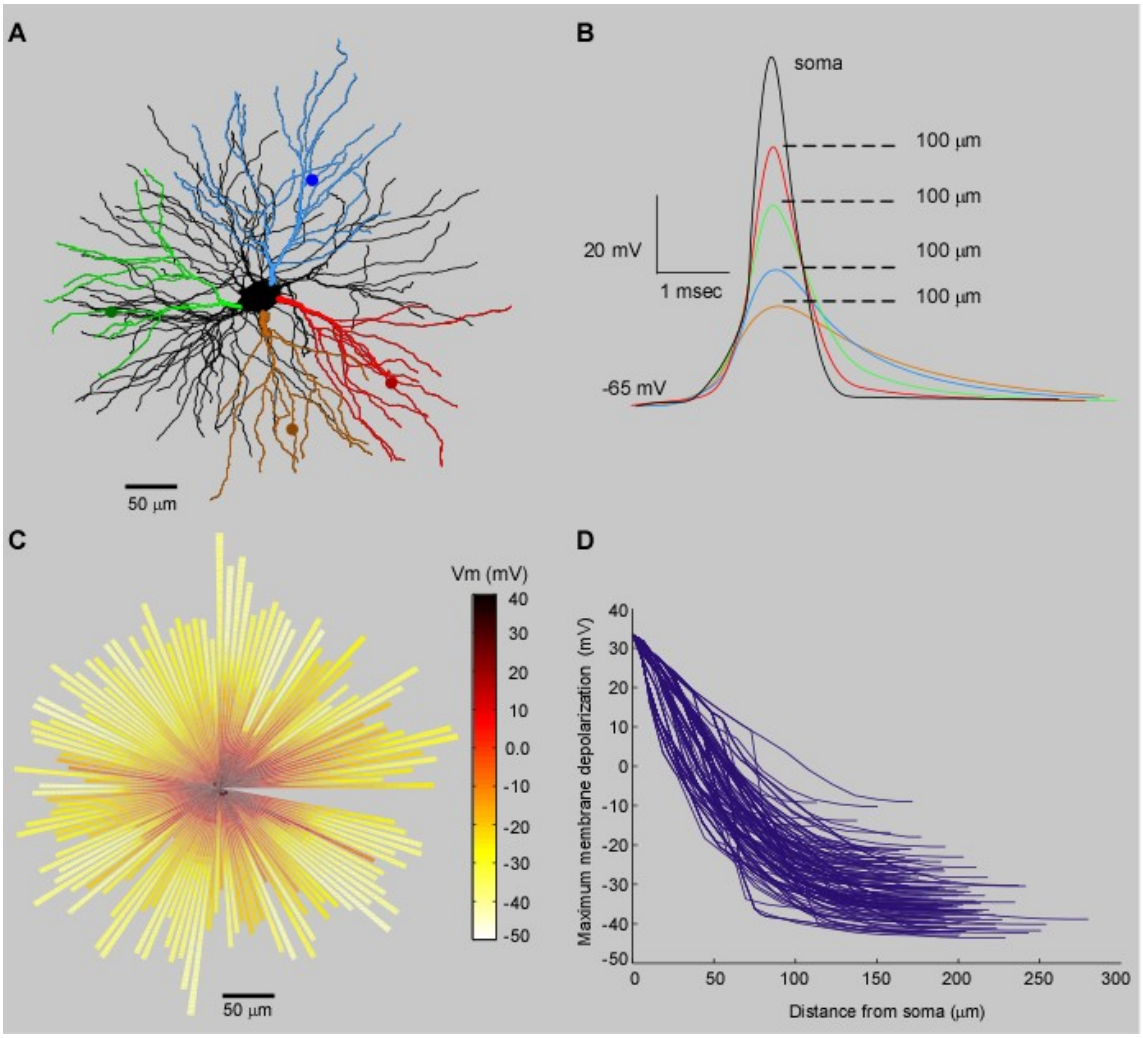

Figure 4-3. Asymmetrical back propagation of an action potential on a symmetrical TC neuron. (A) A fully 3D reconstructed of a typical TC neuron from VPL nucleus. **(B)** Numerical simulation based on a multi-compartmental model with Hodgkin-Huxley type of equations. Graph shows the maximum membrane depolarization pattern during backpropagating action potential in all dendritic trees. All dendritic sections have the same passive and active electrical properties. **(C)** Shape of action potential at soma and at different dendritic trees, but at the same distance from soma. **(D)** Graph shows the maximum membrane depolarization during action potential backpropagation in each dendritic pathway versus distance from soma.

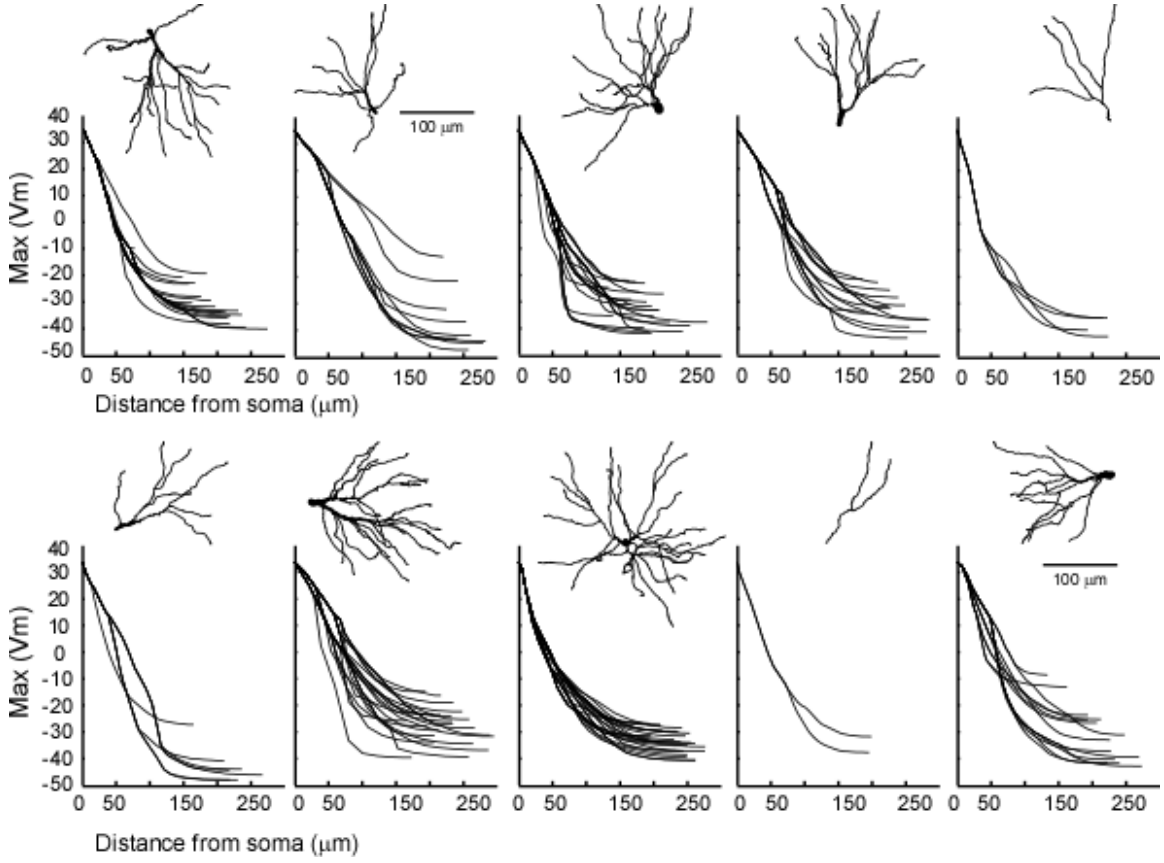

Figure 4-4. The depolarization pattern of a backpropagating action potential depends on morphological features of each subtree. Results of the multi-compartment model of a TC neuron exhibit different attenuation rate of back propagating AP on each dendritic branch. While for all sections had equal passive and active electrical properties, the geometrical and topological properties played important role in regulating the amplitude of backpropagating AP.

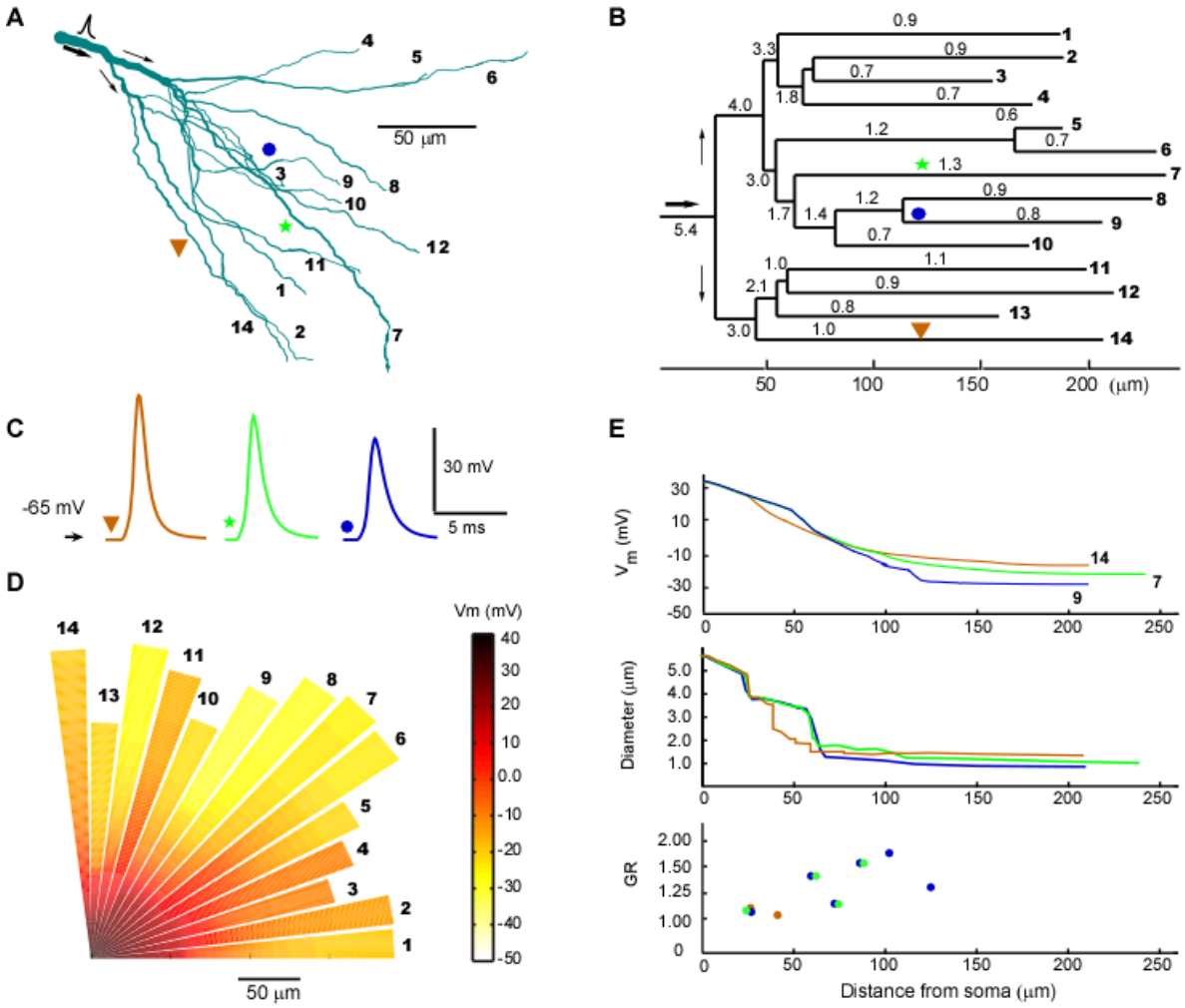

Figure 4-5. Morphological parameters of downstream subtree adjust the amplitude of a backpropagating action potential Morphological parameters of downstream subtree adjust the amplitude of a backpropagating action potential (A) An individual dendritic tree of the fully reconstructed TC neuron (Fig.3A). Number shows the different dendritic pathway. **(B)** Dendrogram of the subtree. Numbers show the mean diameter of dendrites and numbers in right part show different dendritic terminations as the panel A. **(C)** Each waveform indicates the AP at 120 μm from soma on different dendritic segments. On this subtree, the amplitude of back propagating action potential varies from -10 mV to -30 mV. **(D)** Depolarization pattern of the back propagating action potential in the subtree illustrate the level of depolarization in corresponding dendritic pathway versus distance from soma. **(E)** UpperGraph shows the maximum depolarization of membrane potential (Vm), on three

dendritic pathways. Numbers correspond to different dendritic pathways. Middle-bottom: The variation on dendritic diameter and values of geometrical ratio (GR) along each dendritic pathway has been plotted versus distance from soma.

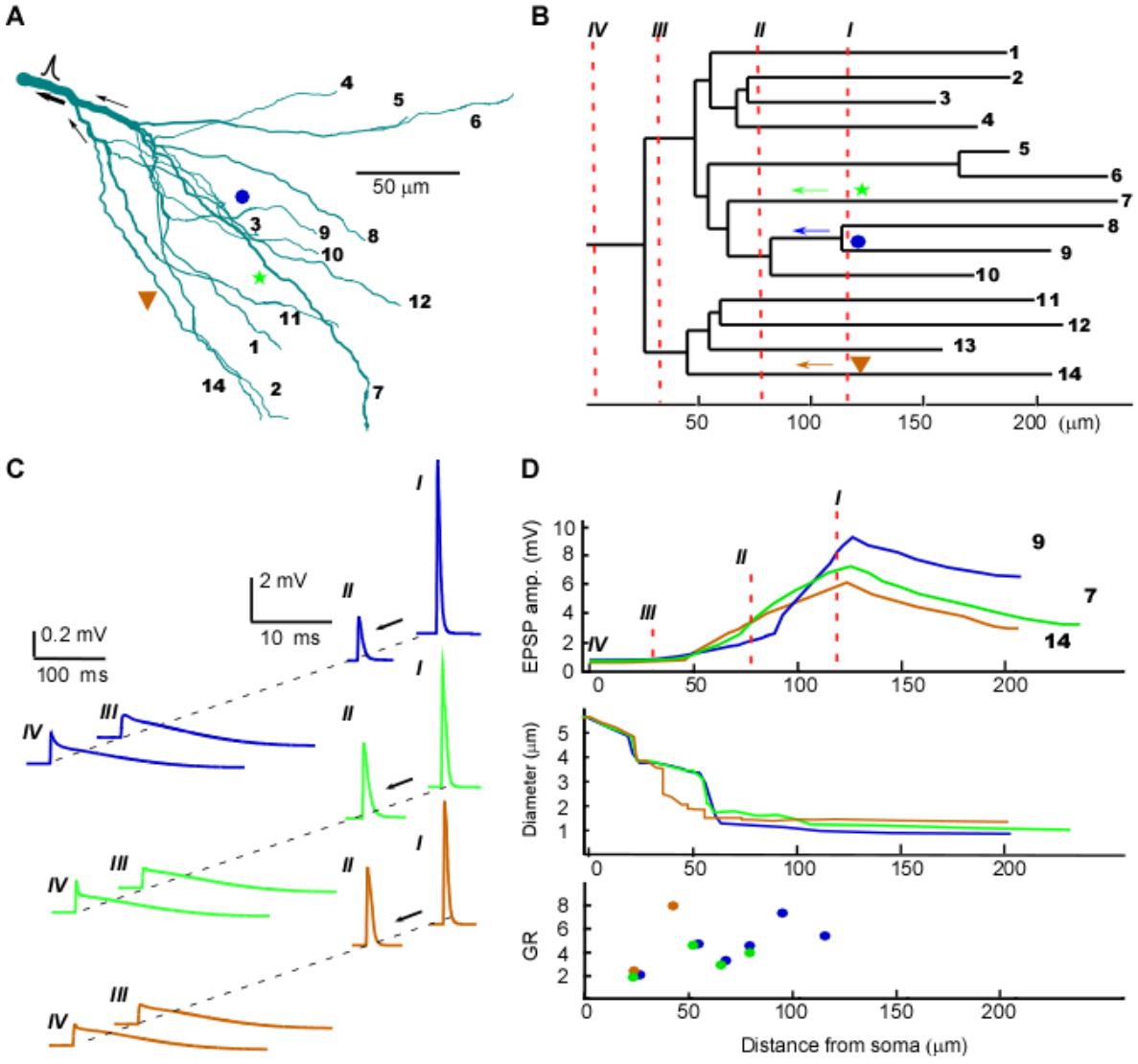

Figure 4-6. Synaptic efficacy of an EPSP depends on the morphological properties of a subtree. **(A)** An individual dendritic tree of the fully reconstructed TC neuron. Numbers show different dendritic pathways and symbols indicates the site of synaptic input. **(B)** Dendogram of the subtree and position of synaptic inputs on dendritic sections. **(C)** EPSP at different sites of synaptic input and at different distance from soma. **(D)** upper: Amplitude of EPSP versus distance from soma on two dendritic pathways. Middle-bottom: variation of diameter of the dendrite and geometrical ratio (GR) at branching points along the dendritic pathway.

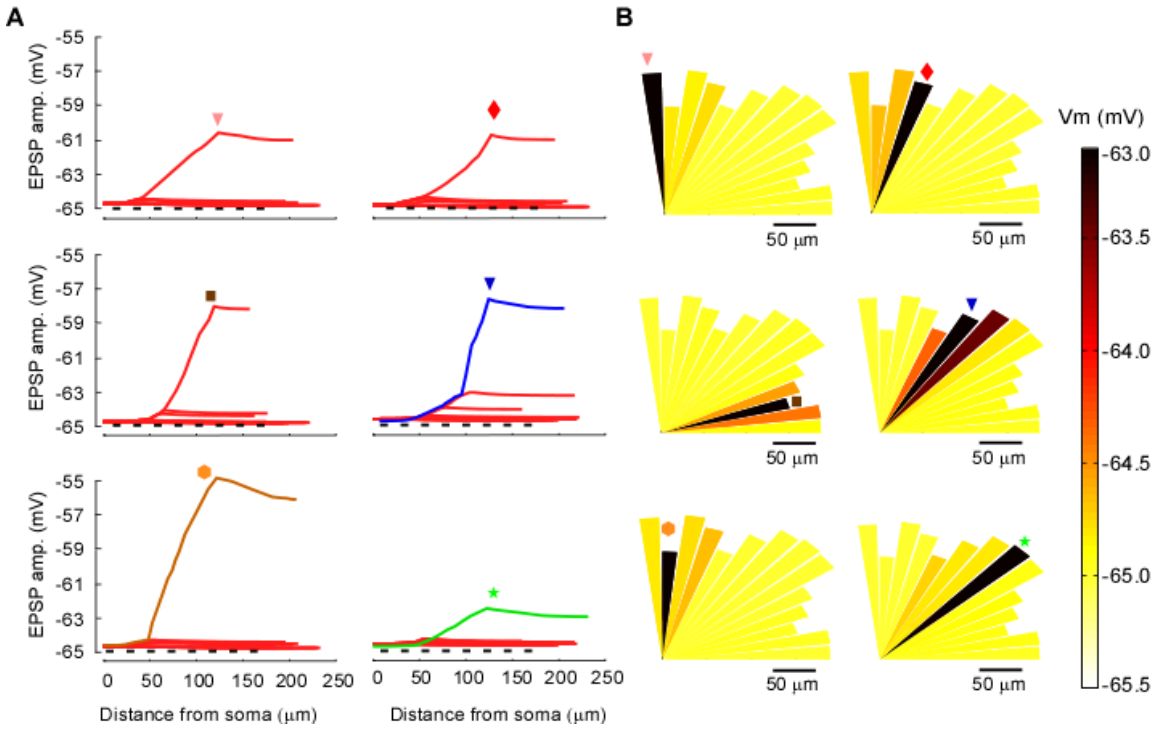

Figure 4-7. Propagating of an EPSP toward soma and other dendritic branches is location-dependent. Graphs show the extent of propagating EPSP toward the soma as well as to other neighboring branches. Color graphs more clearly show the affect of a local synaptic input to other neighboring dendritic sections at 120 μm from soma (Fig.4-6A). Graphs show the amplitude of a propagating EPSP vs. distance from soma and its induced depolarization pattern in the subtree.

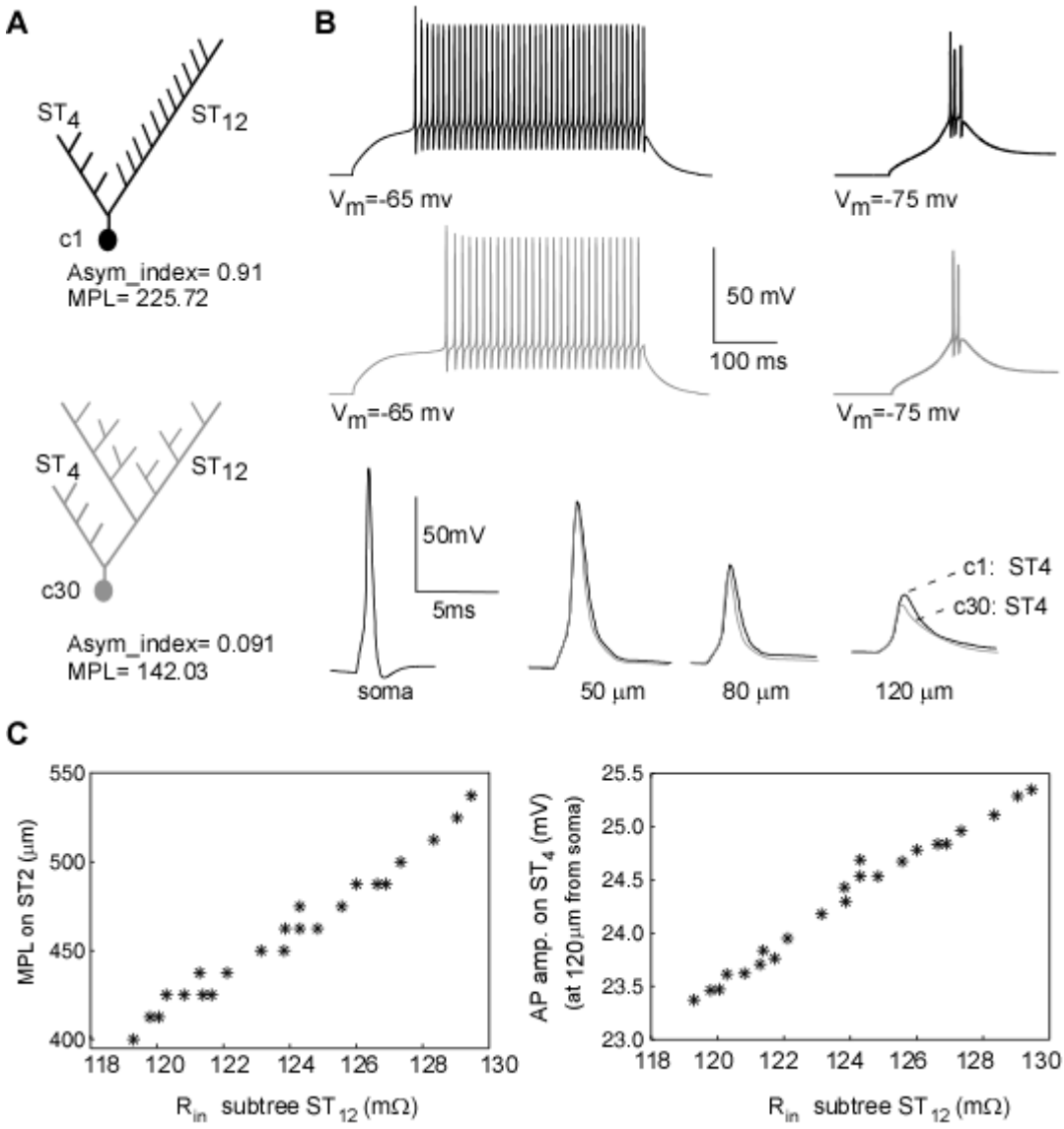

Figure 4-8. Influence of dendritic morphology on firing pattern and back propagation of action potential. (A) Two artificial cell consisted of two main subtrees (ST_4, ST_{12}), which have equal electrical and geometrical properties (total length, total area, GR value at branching points), but the different pattern of connectivity between dendritic sections on ST_{12}. **(B)** Up, middle; the modeled neurons reproduced characteristic electrophysiological responses of TC neuron (tonic and LTS), but with different delay and frequency. Bottom graphs show action potential wave at different distance on ST_4. **(C)** Although, ST_{12} has the same geometrical properties on both modeled neurons, but its specific pattern of connectivity influences the amplitude of propagation AP on the neighboring subtree (ST_4).

Right graph shows the positive correlation between MPL and input resistance of ST_{12} and left graph indicates the positive correlation between input resistance in ST_{12} and the attenuation rate in adjacent dendritic branch (ST_4).

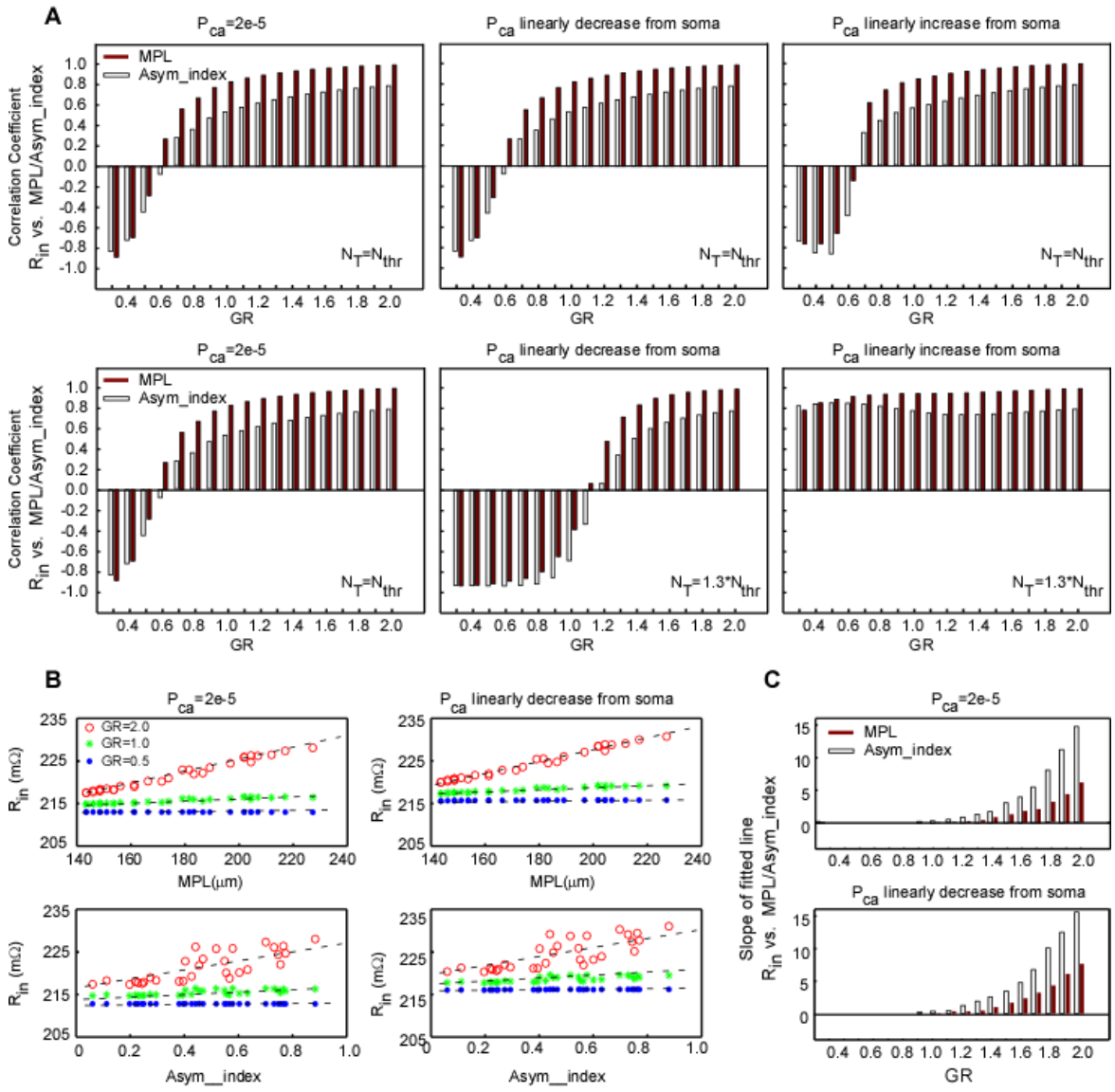

Figure 4-9 . Correlation between input resistance and morphological parameters. For all artificial cells shown in fig. 1B, correlation coefficient between input resistance and mean path length (MPL) and asymmetry index (Asym_index) has been calculated. **(A)** Top panel, shows the correlation coefficient between R_{in} vs. MPL as well as R_{in} vs. Aym_index for different GR value and different form of T-channel distributions. In these simulations, total number of T-channels (N) is equal to the minimum necessary number to generate LTS response (N_T). Bottom panel shows the same type of simulation as the upper panel, but with the different total of T-channel. **(B)** Graphs show the relation between input resistance and morphological parameters for uniform (left-panels) and non-uniform (right-

panels) T-channel distributions. These graphs indicate that the correlation coefficient and slope of the fitted line increase for higher value of GR at branching points. **(C)** Graphs show the slope of the fitted line to pairs of R_{in} and MPl as well as R_{in} and Asym_index. Rate of R_{in} variation versus morphological parameter increases for higher value of GR. Distribution forms of dendritic T-channel do not have significant effect on these results.

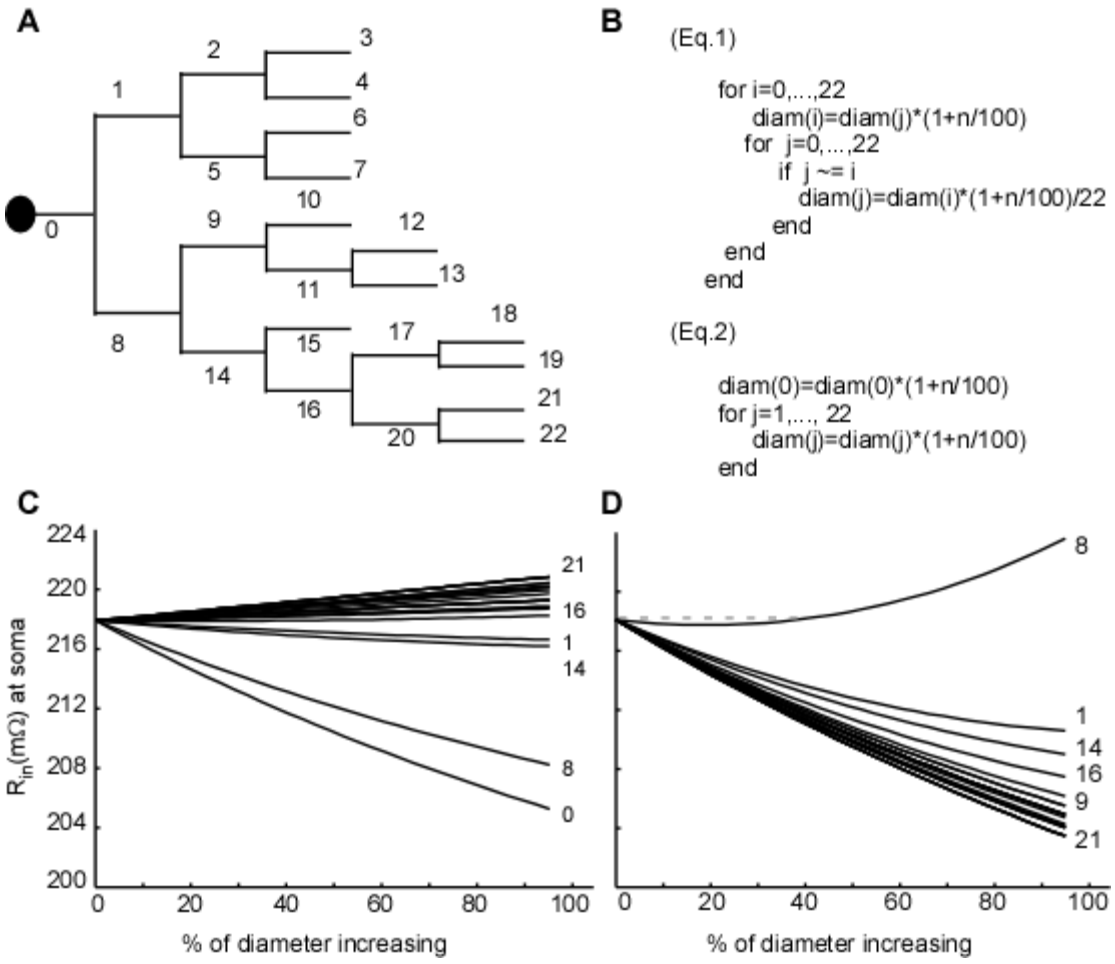

Figure 4-10. Influence of dendritic membrane area distribution on the excitability of a neuron. (A) Schematic presentation of an artificial neuron with 12-degree topologies. All sections have the same length and electrical properties. Numbers only identify the dendritic sections. **(B)** When the total area of the dendritic sections kept constant, the input resistance strongly influenced by the shape of membrane area distribution.Eq.1 and Eq.2 shows the employed algorithm to assign different form of membrane area distribution to the dendritic tree **(C)** Graph shows R_{in} vs. area when the distribution follows eq.1. For this form of area distribution, R_{in} decrease by increasing membrane area of dendritic section indicated by 0, 8, 14 and 1, but cell excitability increase as well as increasing membrane area of other dendritic sections **(D)** shows R_{in} vs. area when the distribution follows eq.2. For this form of area distribution, R_{in} decrease by increasing membrane area of all dendritic sections except the section indicated by 8. Although, increasing diameter of section 8 up to 40% slightly reduce R_{in}, but give rise to cell excitability as its diameter increased more.

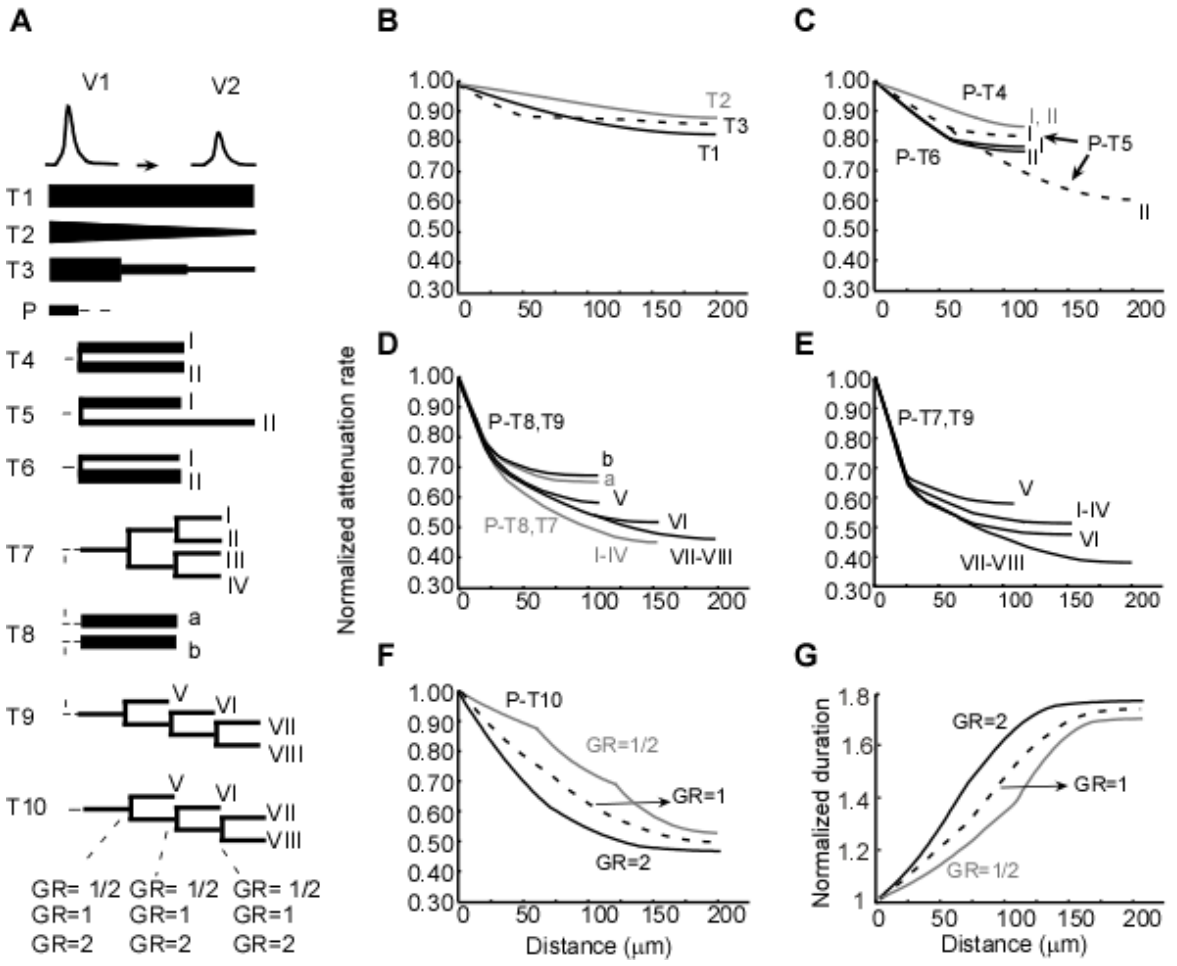

Figure 4-11. Influence of geometrical and topological parameters on attenuation rate of a propagating signal. (A) We examined the normalized attenuation rate (= 1-v2/v1) of a propagation potential on different dendritic trees: Such as a dendritic tree without any branching points, but different membrane area distribution (1-3), one branching point, but different geometrical properties for neighboring dendritic branch (4-6) and several branching points with different morphological parameters for neighboring dendritic branch (7-9). **(B)** Graphs show the variation of the attenuation rate as dendritic morphology alters. Numbers in graph corresponds to dendritic configuration in panel A. **(C), (D)** Graphs demonstrate the effects of the geometrical ratio (GR) on the attenuation of back propagating potentials and duration of action potential, respectively.

5 Conclusion

5.1 Brief summary of the results

In this study, we used histological reconstructions of TC neurons combined with computational modeling approach to study the influence of morphological features and the impact of active dendritic conductance (i.e., T-channel) on the electrophysiological responses of the TC neurons. The results of our study can be summarized as follows:

(a) In chapter 3, in order to propose the possible distribution of the low threshold Ca^{2+} conductance on somato-dendritic membrane of TC neurons, we examined different distribution forms of low-threshold Ca^{2+} channels based on the proposed hypothesis of minimizing metabolic energy consumption. In our numerical simulation, we showed that minimizing energy consumption applied to TC cells with realistic morphology led to a preferred distribution form of dendritic T-channels conductance. Our model predicted a higher density of T-channel on the proximal dendrites than on somatic membrane and distal dendrites. We proposed that this special form of T-channel distribution could be the preferred distribution of these channels on the membrane of TC neurons.

(b) In chapter 4, we examined the morphological properties of TC neurons from eight fully reconstructed cells from VPL nucleus of cat. Analyzing the geometrical ratio (GR) at branching points revealed that TC cells do not follow 3/2 Rall's power law. In addition, we pointed out that the geometrical ratio for forward and backward propagation of an electrical signal owns very different values (about two times higher for forward propagation) suggesting a strong attenuation of signals propagating toward neuronal soma. Furthermore, analyzing the topological parameters showed a wide variability for the asymmetry index (i.e., from fully symmetry to highly asymmetry) and the mean path length among dendritic

arborizations of a TC cell. The pattern of connectivity between dendritic sections of a subtree show a high correlation to the input resistance of the neuron,

(c) In chapter 5, we examined the impact of the morphological properties of TC neurons on the efficacy of forward propagation of EPSPs arriving at the distal dendritic branches and the extent of back propagating electrical signals. We showed that the morphological variability led to different efficacy of back propagating action potentials and forward propagating EPSPs, which depends primarily on the geometrical and secondly topological properties. We indicated that due to distinct morphological features, each dendritic tree of a single TC neuron possesses different efficacy to transfer distal synaptic currents toward the soma, and owns a specific ability to transfer the generated action potential toward dendritic tips.

Although electrophysiological recordings or optical imaging mainly provide information about neuronal activity in the soma or proximal dendrites, using multicompratmental model for TC neurons, we provide new information about the state of activity at all dendritic regions.

5.2 Some limitations

Most of our work was done in computational experiments and some parameters for the model were unknown. Therefore, this could introduce some bias in the obtained results.

(1) The study on optimal distribution of T-channels was done using somatic application of depolarizing currents and results suggested that for optimal energy consumption, the highest density of T-channels should be on proximal dendrites. Therefore, we cannot claim this would be the preferred distribution of T-channel to generate LTS response, when TC neuron receives a complex pattern of spatio-temporal synaptic inputs arriving to dendritic tree.

(2) While our morphological analysis indicated the violation of Rall's power law in dendritic arborization of TC neurons, but it has to be noticed that the calculation of GR was performed based on the assumptions of (i) cylindrical (round) geometry of dendritic sections and (ii) a constant diameter for sections before and after branching points. However, these assumptions could be challenged and corrected by a 3D reconstruction from serial ultra thin sections obtained with fast freezing technique to avoid dehydration. If one can extract such precise data, obviously, the geometrical ratio formula and the one dimensional cable equations have to be modified.

(3) Based on our computational model that indicated the relation between morphological properties and the synaptic efficacy, we can concluded that a TC cell needs fewer numbers of synaptic connections on the dendritic tree with low attenuation rate to transfer input information to the soma, than dendritic tree with high attenuation rate. Therefore, we may hypothesize those synaptic inputs on TC neuron can be optimized by forming synaptic connections on some specific portions of dendritic tree(s). However, our numerical simulations were based on two assumptions: (I) the same type and form of channel distribution on dendritic trees, and (II) no interaction between the back propagating action potential and forward propagating synaptic inputs. Thus, if TC neurons follow a specific democracy rule to have the same number of synaptic inputs on each dendritic tree, then we can hypothesis that the difference between FP efficacies can be adjusted by different form of dendritic voltage dependent channel distributions.

5.3 Final remarks

Regardless of complexity of a physical system, we are encouraged to take the first step toward exploring its behavior by a fundamental theory that stats: Nature is simple and complexity is only a repetition of this simplicity (Mirman, 2006). We have been searching and still looking for the simple and fundamental law that governs the behavior of apparently different physical phenomena. We successfully derived the laws of gravity,

optics, electromagnetism and thermodynamics, which can be presented by few simple equations.

However, in addition to simplicity, Nature follows the optimization principle. This means a natural phenomenon occurs in a way that some physical quantities reach to their extremum value. For instance, all equations of motions in mechanics and behavior of a system in equilibrium thermodynamic can be derived from "the principle of least action" and the "thermodynamics potentials", respectively.

The brain, apparently, has its extremum principle. In the theoretical neuroscience, metabolic cost has been proposed as a principle that governs neuronal biophysics (Hasenstaub et al., 2010). The "metabolic cost principle" not only applied in the neuronal response and action potential generation (Laughlin et al., 1998; Crotty et al., 2006; Zomorrodi et al., 2008; Alle et al., 2009), but also has been used to investigate the neuronal branching pattern and the wiring pattern in neuronal circuits (Mitchison, 1991; Chklovskii et al., 2002; Chen et al., 2006).

The thalamus is the gateway to the cerebral cortex and nearly all sensory information passes through it to the higher level of the brain. Therefore, relay neurons in the thalamus have to be in optimizing conditions in order to execute the input-output function in the efficient way. Spreading dendritic trees in almost all directions and the complex form of the dendritic arborization with diverse ionic channels, give a distinct character to the thalamic relay among other neurons. In addition, specific morphological properties of each dendritic tree give a particular capacity (e.g., different attenuation rate) to relay neurons to process and transfer the input information to the soma.

According to "the metabolic cost principle", synaptic density and patterning must well adjusted to form a proper neuronal circuit. Therefore, for equal active properties on dendritic sections, each relay neuron may have one preferable dendritic tree for the synaptic inputs, and this specific dendritic tree will possess more synaptic connections than other dendritic trees of the relay neuron. Figure 5.1 shows the difference between the somatic

depolarization in response to the four excitatory synaptic inputs at equal-distance from the soma on two dendritic trees. Although these dendritic arborizations look similar, they have quite different synaptic efficacy. Variations in the synaptic efficacy of each subtree can be explained by comparing morphological parameters such as mean path length, asymmetry index, and geometrical ratio. This may also raise another hypothesis that whether a preferable dendritic tree may act as a single functional unit.

In addition, the efficient BP-AP on most dendritic pathways and interaction with oncoming synaptic inputs may induce a change in synaptic efficacy in a specific time windows. Thus, spike-time dependent synaptic plasticity might be another mechanism used by thalamocrtical neurons to perform synaptic integration. However, the rich repertoire of ionic channels of TC neuron (Jones, 2007) may adjust the extent of electrical signal propagation within dendritic trees. Although the distribution of these ionic channels on dendritic tree of TC neurons is not known, we can expect the suppression effect on efficacy of BA-AP by presence of different type of potassium currents.

While we study the brain as a complex structure in the known universe, looking for the fundamental laws that govern its operation not only will extend our knowledge about it organization and function, but also may lead us to a general principle about the brain function. The idea of minimizing consumption energy may be the first principle for this unified theory.

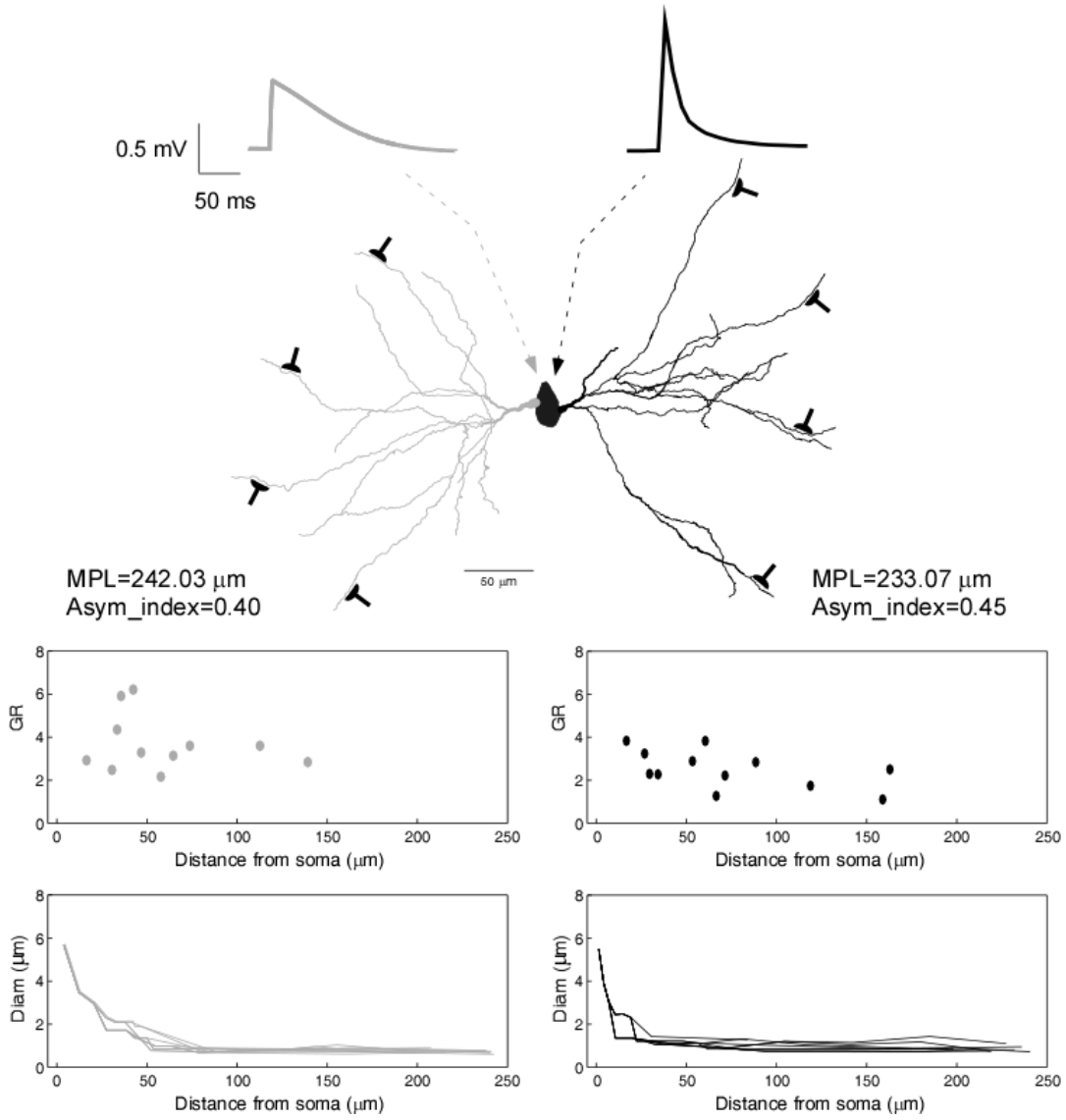

Figure 5.1 Impact of morphological properties of a thalamocortical neuron on the transferring input information to the soma. This graph shows a significant difference between the somatic depolarization in response to the four excitatory synaptic inputs at equal-distance from the soma on two dendritic trees. Difference in somatic response as the result of difference in the synaptic efficacy of each subtree can be explained by comparing morphological parameters such as mean path length, asymmetry index, geometrical ratio or variation of dendritic diameter along each dendritic branch**.**

Bibliography

Abbott LF (2008) Theoretical neuroscience rising. Neuron 60:489-495.

Achard P, De Schutter E (2006) Complex parameter landscape for a complex neuron model. PLoS Comput Biol 2:e94.

Agmon-Snir H, Segev I (1993) Signal delay and input synchronization in passive dendritic structures. J Neurophysiol 70:2066-2085.

Alle H, Roth A, Geiger JR (2009) Energy-efficient action potentials in hippocampal mossy fibers. Science 325:1405-1408.

Amit DJ, Gutfreund H, Sompolinsky H (1985) Spin-glass models of neural networks. Phys Rev A 32:1007-1018.

Ananthanarayanan R, Esser SK, Simon HD, Modha DS (2009) The Cat is Out of The Bag: Cortical Simulations with 10^9 neurons and 10^13 synapses. In: the ACM/IEEE SC2009 Conference on High Performance Networking and Computing. Portland, OR.

Arcelli P, Frassoni C, Regondi MC, De Biasi S, Spreafico R (1997) GABAergic neurons in mammalian thalamus: a marker of thalamic complexity? Brain Res Bull 42:27-37.

Arendt J, Skene DJ (2005) Melatonin as a chronobiotic. Sleep Med Rev 9:25-39.

Badel L, Lefort S, Brette R, Petersen CC, Gerstner W, Richardson MJ (2008) Dynamic I-V curves are reliable predictors of naturalistic pyramidal-neuron voltage traces. J Neurophysiol 99:656-666.

Bloomfield SA, Hamos JE, Sherman SM (1987) Passive cable properties and morphological correlates of neurones in the lateral geniculate nucleus of the cat. J Physiol 383:653-692.

Bluman GW, Tuckwell HC (1987) Techniques for obtaining analytical solutions for Rall's model neuron. J Neurosci Methods 20:151-166.

Bower JM, Beeman D (1995) The book of GENESIS : exploring realistic neural models with the GEneral NEural SImulation System. Santa Clara, Calif.: TELOS.

Brette R, Piwkowska Z, Monier C, Rudolph-Lilith M, Fournier J, Levy M, Fregnac Y, Bal T, Destexhe A (2008) High-resolution intracellular recordings using a real-time computational model of the electrode. Neuron 59:379-391.

Budde T, Mager R, Pape HC (1992) Different Types of Potassium Outward Current in Relay Neurons Acutely Isolated from the Rat Lateral Geniculate Nucleus. Eur J Neurosci 4:708-722.

Budde T, Munsch T, Pape HC (1998) Distribution of L-type calcium channels in rat thalamic neurones. Eur J Neurosci 10:586-597.

Budde T, Meuth S, Pape HC (2002) Calcium-dependent inactivation of neuronal calcium channels. Nat Rev Neurosci 3:873-883.

Bush PC, Sejnowski TJ (1993) Reduced compartmental models of neocortical pyramidal cells. J Neurosci Methods 46:159-166.

Buzsaki G (2010) Neural syntax: cell assemblies, synapsembles, and readers. Neuron 68:362-385.

Cao BJ, Abbott LF (1993) A new computational method for cable theory problems. Biophys J 64:303-313.

Carnevale NT, Hines ML (2005) The NEURON book. Cambridge ; New York: Cambridge University Press.

Castro-Alamancos MA (2003) Thalamocortical dynamics: how do the thalamus and the neocortex communicate during the processing of information?. Rev Neurol 36:643-649.

Castro-Alamancos MA, Connors BW (1997) Thalamocortical synapses. Prog Neurobiol 51:581-606.

Chavis P, Fagni L, Lansman JB, Bockaert J (1996) Functional coupling between ryanodine receptors and L-type calcium channels in neurons. Nature 382:719-722.

Chen BL, Hall DH, Chklovskii DB (2006) Wiring optimization can relate neuronal structure and function. PNAS 103:4723-4728.

Chklovskii DB, Schikorski T, Stevens CF (2002) Wiring optimization in cortical circuits. Neuron 34:341-347.

Cole KS, Hodgkin AL (1939) Membrane and Protoplasm Resistance in the Squid Giant Axon. J Gen Physiol 22:671-687.

Cole KS, Curtis HJ (1941) Membrane Potential of the Squid Giant Axon during Current Flow. J Gen Physiol 24:551-563.

Cole KS, Baker RF (1941) Transverse Impedance of the Squid Giant Axon during Current Flow. J Gen Physiol 24:535-549.

Connor JA, Stevens CF (1971) Prediction of repetitive firing behaviour from voltage clamp data on an isolated neurone soma. J Physiol 213:31-53.

Coulter DA, Huguenard JR, Prince DA (1989) Calcium currents in rat thalamocortical relay neurones: kinetic properties of the transient, low-threshold current. J Physiol 414:587-604.

Cowan WM, Powell TP (1956) A study of thalamo-striate relations in the monkey. Brain 79:364-390.

Crank J (1979) The mathematics of diffusion, 2d Edition. Oxford, [Eng]: Clarendon Press.

Crick F, Koch C (2003) A framework for consciousness. Nat Neurosci 6:119-126.

Crochet S, Petersen CC (2006) Correlating whisker behavior with membrane potential in barrel cortex of awake mice. Nat Neurosci 9:608-610.

Crotty P, Sangrey T, Levy WB (2006) Metabolic energy cost of action potential velocity. J Neurophysiol 96:1237-1246.

Crunelli V, Toth TI, Cope DW, Blethyn K, Hughes SW (2005) The 'window' T-type calcium current in brain dynamics of different behavioural states. J Physiol 562:121-129.

Cuntz H, Borst A, Segev I (2007) Optimization principles of dendritic structure. Theor Biol Med Model 4:21.

Dayan P, Abbott LF (2005) Theoretical neuroscience : computational and mathematical modeling of neural systems, MIT Press pbk. Edition. Cambridge, Mass. ; London: MIT.

De Schutter E (2008) Why are computational neuroscience and systems biology so separate? PLoS Comput Biol 4:e1000078.

De Schutter E (2010) Computational modeling methods for neuroscientists. Cambridge, Mass.: MIT Press.

De Schutter E, Bower JM (1994) An active membrane model of the cerebellar Purkinje cell. I. Simulation of current clamps in slice. J Neurophysiol 71:375-400.

Deschenes M, Madariaga-Domich A, Steriade M (1985) Dendrodendritic synapses in the cat reticularis thalami nucleus: a structural basis for thalamic spindle synchronization. Brain Res 334:165-168.

Deschenes M, Paradis M, Roy JP, Steriade M (1984) Electrophysiology of neurons of lateral thalamic nuclei in cat: resting properties and burst discharges. J Neurophysiol 51:1196-1219.

Destexhe A, Crunelli V (2008) Methods for computational neuroscience. J Neurosci Methods 169:269-270.

Destexhe A, Neubig M, Ulrich D, Huguenard J (1998) Dendritic low-threshold calcium currents in thalamic relay cells. J Neurosci 18:3574-3588.

Donohue DE, Ascoli GA (2008) A comparative computer simulation of dendritic morphology. PLoS Comput Biol 4:e1000089.

Dossi RC, Nunez A, Steriade M (1992) Electrophysiology of a slow (0.5-4 Hz) intrinsic oscillation of cat thalamocortical neurones in vivo. J Physiol 447:215-234.

Druckmann S, Banitt Y, Gidon A, Schurmann F, Markram H, Segev I (2007) A novel multiple objective optimization framework for constraining conductance-based neuron models by experimental data. Front Neurosci 1:7-18.

Economo MN, Fernandez FR, White JA (2010) Dynamic clamp: alteration of response properties and creation of virtual realities in neurophysiology. J Neurosci 30:2407-2413.

Euler T, Detwiler PB, Denk W (2002) Directionally selective calcium signals in dendrites of starburst amacrine cells. Nature 418:845-852.

Evans JD (2000) Analysis of a multiple equivalent cylinder model with generalized taper. IMA J Math Appl Med Biol 17:347-377.

Fellin T, Halassa MM, Terunuma M, Succol F, Takano H, Frank M, Moss SJ, Haydon PG (2009) Endogenous nonneuronal modulators of synaptic transmission control cortical slow oscillations in vivo. PNAS 106:15037-15042.

Feng J (2004) Computational neuroscience: comprehensive approach. Boca Raton: Chapman & Hall/CRC.

Fodor JA, Pylyshyn ZW (1988) Connectionism and cognitive architecture: a critical analysis. Cognition 28:3-71.

Fortune ES, Rose GJ (1997) Passive and active membrane properties contribute to the temporal filtering properties of midbrain neurons in vivo. J Neurosci 17:3815-3825.

Fuentealba P, Crochet S, Timofeev I, Bazhenov M, Sejnowski TJ, Steriade M (2004) Experimental evidence and modeling studies support a synchronizing role for electrical coupling in the cat thalamic reticular neurons in vivo. Eur J Neurosci 20:111-119.

Gerstner W, Kistler WM (2002) Spiking neuron models : single neurons, populations, plasticity. Cambridge, U.K. ; New York: Cambridge University Press.

Gerstner W, Kempter R, van Hemmen JL, Wagner H (1996) A neuronal learning rule for sub-millisecond temporal coding. Nature 383:76-81.

Gimenez-Amaya JM, McFarland NR, de las Heras S, Haber SN (1995) Organization of thalamic projections to the ventral striatum in the primate. J Comp Neurol 354:127-149.

Godwin DW, Vaughan JW, Sherman SM (1996) Metabotropic glutamate receptors switch visual response mode of lateral geniculate nucleus cells from burst to tonic. J Neurophysiol 76:1800-1816.

Gold C, Henze DA, Koch C (2007) Using extracellular action potential recordings to constrain compartmental models. J Comput Neurosci 23:39-58.

Goldstein SS, Rall W (1974) Changes of action potential shape and velocity for changing core conductor geometry. Biophys J 14:731-757.

Grossberg S (1982) Processing of expected and unexpected events during conditioning and attention: a psychophysiological theory. Psychol Rev 89:529-572.

Guido W, Weyand T (1995) Burst responses in thalamic relay cells of the awake behaving cat. J Neurophysiol 74:1782-1786.

Guillery RW (1995) Anatomical evidence concerning the role of the thalamus in corticocortical communication: a brief review. J Anat 187 (Pt 3):583-592.

Gutierrez C, Cox CL, Rinzel J, Sherman SM (2001) Dynamics of low-threshold spike activation in relay neurons of the cat lateral geniculate nucleus. J Neurosci 21:1022-1032.

Guyon A, Leresche N (1995) Modulation by different GABAB receptor types of voltage-activated calcium currents in rat thalamocortical neurones. J Physiol 485 (Pt 1):29-42.

Halliwell JV, Adams PR (1982) Voltage-clamp analysis of muscarinic excitation in hippocampal neurons. Brain Res 250:71-92.

Hasenstaub A, Otte S, Callaway E, Sejnowski TJ (2010) Metabolic cost as a unifying principle governing neuronal biophysics. PNAS 107:12329-12334.

Hecht-Nielsen R, McKenna T (2003) Computational models for neuroscience : human cortical information processing. London ; New York: Springer.

Henneberger C, Papouin T, Oliet SH, Rusakov DA (2010) Long-term potentiation depends on release of D-serine from astrocytes. Nature 463:232-236.

Hikosaka O (2007) Habenula. Scholarpedia 2:2703.

Hille B (2001) Ion Channels of Excitable Membranes. Sunderland, MA: Sinauer Associates, Inc. .

Hines ML, Carnevale NT (1997) The NEURON simulation environment. Neural Comput 9:1179-1209.

Hines ML, Carnevale NT (2001) NEURON: a tool for neuroscientists. Neuroscientist 7:123-135.

Hirsch JC, Fourment A, Marc ME (1983) Sleep-related variations of membrane potential in the lateral geniculate body relay neurons of the cat. Brain Res 259:308-312.

Hodgkin AL (1937) Evidence for electrical transmission in nerve: Part I. J Physiol 90:183-210.

Hodgkin AL, Huxley AF (1945) Resting and action potentials in single nerve fibres. J Physiol 104:176-195.

Hodgkin AL, Huxley AF (1947) Potassium leakage from an active nerve fibre. J Physiol 106:341-367.

Hodgkin AL, Huxley AF (1952a) Movement of sodium and potassium ions during nervous activity. Cold Spring Harb Symp Quant Biol 17:43-52.

Hodgkin AL, Huxley AF (1952b) A quantitative description of membrane current and its application to conduction and excitation in nerve. J Physiol 117:500-544.

Hodgkin AL, Huxley AF (1952c) The components of membrane conductance in the giant axon of Loligo. J Physiol 116:473-496.

Hopfield JJ (1982) Neural networks and physical systems with emergent collective computational abilities. PNAS 79:2554-2558.

Hughes SW, Cope DW, Crunelli V (1998) Dynamic clamp study of Ih modulation of burst firing and delta oscillations in thalamocortical neurons in vitro. Neuroscience 87:541-550.

Huguenard JR (1996) Low-threshold calcium currents in central nervous system neurons. Annu Rev Physiol 58:329-348.

Huguenard JR, Prince DA (1991) Slow inactivation of a TEA-sensitive K current in acutely isolated rat thalamic relay neurons. J Neurophysiol 66:1316-1328.

Huguenard JR, McCormick DA (1992) Simulation of the currents involved in rhythmic oscillations in thalamic relay neurons. J Neurophysiol 68:1373-1383.

Huguenard JR, Prince DA (1997) Basic mechanisms of epileptic discharges in the thalamus. In: Thalamus, vol. 2, Experimental and Clinical Aspects (Steriade M, Jones EG, McCormick DA, eds), pp 295–330. Oxford: Elsevier.

Huguenard JR, Coulter DA, Prince DA (1991) A fast transient potassium current in thalamic relay neurons: kinetics of activation and inactivation. J Neurophysiol 66:1304-1315.

Huxley AF, Stampfli R (1949) Evidence for saltatory conduction in peripheral myelinated nerve fibres. J Physiol 108:315-339.

Huys QJ, Paninski L (2009) Smoothing of, and parameter estimation from, noisy biophysical recordings. PLoS Comput Biol 5:e1000379.

Huys QJ, Ahrens MB, Paninski L (2006) Efficient estimation of detailed single-neuron models. J Neurophysiol 96:872-890.

Izhikevich EM (2003) Simple model of spiking neurons. IEEE Trans Neural Netw 14:1569-1572.

Izhikevich EM (2004) Which model to use for cortical spiking neurons? IEEE Trans Neural Netw 15:1063-1070.

Izhikevich EM, Edelman GM (2008) Large-scale model of mammalian thalamocortical systems. PNAS 105:3593-3598.

Jack JJB, Noble D, Tsien RW (1983) Electric current flow in excitable cells. Oxford: Clarendon Press.

Jahnsen H, Llinas R (1984a) Electrophysiological properties of guinea-pig thalamic neurones: an in vitro study. J Physiol 349:205-226.

Jahnsen H, Llinas R (1984b) Ionic basis for the electro-responsiveness and oscillatory properties of guinea-pig thalamic neurones in vitro. J Physiol 349:227-247.

Johnston D, Wu SM-s (1995) Foundations of cellular neurophysiology. Cambridge, Mass.: MIT Press.

Joksovic PM, Bayliss DA, Todorovic SM (2005) Different kinetic properties of two T-type Ca2+ currents of rat reticular thalamic neurones and their modulation by enflurane. J Physiol 566:125-142.

Jolivet R, Kobayashi R, Rauch A, Naud R, Shinomoto S, Gerstner W (2008) A benchmark test for a quantitative assessment of simple neuron models. J Neurosci Methods 169:417-424.

Jones EG (2002a) Thalamic organization and function after Cajal. Progr Brain Res 136:333-357.

Jones EG (2002b) Thalamic circuitry and thalamocortical synchrony. Philos Trans R Soc Lond 357:1659-1673.

Jones EG (2007) The thalamus, 2nd Edition. Cambridge ; New York: Cambridge University Press.

Jones SW (2006) Are rate constants constant? J Physiol 571:502-502.

Jones SW, Elmslie KS (1997) Transmitter modulation of neuronal calcium channels. J Membr Biol 155:1-10.

Kellems AR, Chaturantabut S, Sorensen DC, Cox SJ (2010) Morphologically accurate reduced order modeling of spiking neurons. J Comput Neurosci 28:477-494.

Keren N, Peled N, Korngreen A (2005) Constraining compartmental models using multiple voltage recordings and genetic algorithms. J Neurophysiol 94:3730-3742.

Keren N, Bar-Yehuda D, Korngreen A (2009) Experimentally guided modelling of dendritic excitability in rat neocortical pyramidal neurones. J Physiol 587:1413-1437.

Koch C (1999) Biophysics of computation : information processing in single neurons. New York: Oxford University Press.

Koch C (2004) The quest for consciousness : a neurobiological approach. Denver, Colo.: Roberts and Co.

Koch C, Poggio T (1985) A simple algorithm for solving the cable equation in dendritic trees of arbitrary geometry. J Neurosci Methods 12:303-315.

Koch C, Segev I (1998) Methods in neuronal modeling : from ions to networks, 2nd Edition. Cambridge, Mass.: MIT Press.

Koch C, Segev I (2000) The role of single neurons in information processing. Nat Neurosci 3 Suppl:1171-1177.

Koch P, Leisman G (2000) Numbers, models, and understanding of natural intelligence: computational neuroscience in the service of clinical neuropsychology. J Int Neuropsychol Soc 6:580-582.

Kovacs K, Sik A, Ricketts C, Timofeev I (2010) Subcellular distribution of low-voltage activated T-type Ca2+ channel subunits (Ca(v)3.1 and Ca(v)3.3) in reticular thalamic neurons of the cat. J Neurosci Res 88:448-460.

Kubota Y, Hatada SN, Kawaguchi Y (2009) Important factors for the three-dimensional reconstruction of neuronal structures from serial ultrathin sections. Front Neural Circuits 3:4.

Landisman CE, Long MA, Beierlein M, Deans MR, Paul DL, Connors BW (2002) Electrical synapses in the thalamic reticular nucleus. J Neurosci 22:1002-1009.

Lapicque L (1907) Recherches quantitatives sur l'excitabilité'électrique des nerfs traitée comme une polarisation. J Physiol Pathol Gen 9:620-635.

Laughlin SB, de Ruyter van Steveninck RR, Anderson JC (1998) The metabolic cost of neural information. Nat Neurosci 1:36-41.

Leonard CM (1972) The connections of the dorsomedial nuclei. Brain Behav Evol 6:524-541.

Leresche N, Jassik-Gerschenfeld D, Haby M, Soltesz I, Crunelli V (1990) Pacemaker-like and other types of spontaneous membrane potential oscillations of thalamocortical cells. Neurosci Lett 113:72-77.

Liu XB, Honda CN, Jones EG (1995) Distribution of four types of synapse on physiologically identified relay neurons in the ventral posterior thalamic nucleus of the cat. J Comp Neurol 352:69-91.

Llinas R, Jahnsen H (1982) Electrophysiology of mammalian thalamic neurones in vitro. Nature 297:406-408.

Llinas R, Ribary U, Contreras D, Pedroarena C (1998) The neuronal basis for consciousness. Philos Trans R Soc Lond B Biol Sci 353:1841-1849.

Llinas RR, Steriade M (2006) Bursting of thalamic neurons and states of vigilance. J Neurophysiol 95:3297-3308.

London M, Hausser M (2005) Dendritic computation. Annu Rev Neurosci 28:503-532.

London M, Roth A, Beeren L, Hausser M, Latham PE (2010) Sensitivity to perturbations in vivo implies high noise and suggests rate coding in cortex. Nature 466:123-127.

Long MA, Landisman CE, Connors BW (2004) Small clusters of electrically coupled neurons generate synchronous rhythms in the thalamic reticular nucleus. J Neurosci 24:341-349.

Maekawa K, Purpura DP (1967) Properties of spontaneous and evoked synaptic activities of thalamic ventrobasal neurons. J Neurophysiol 30:360-381.

Mainen ZF, Sejnowski TJ (1996) Influence of dendritic structure on firing pattern in model neocortical neurons. Nature 382:363-366.

Makarov VA, Panetsos F, de Feo O (2005) A method for determining neural connectivity and inferring the underlying network dynamics using extracellular spike recordings. J Neurosci Methods 144:265-279.

Maltenfort MG, Hamm TM (2004) Estimation of the electrical parameters of spinal motoneurons using impedance measurements. J Neurophysiol 92:1433-1444.

Manor Y, Koch C, Segev I (1991) Effect of geometrical irregularities on propagation delay in axonal trees. Biophys J 60:1424-1437.

Markram H (2006) The blue brain project. Nat Rev Neurosci 7:153-160.

Mazarati A (2007) The best model for a cat is the same cat...or is it? Epilepsy Curr 7:112-114.

McCormick DA (1992a) Cellular mechanisms underlying cholinergic and noradrenergic modulation of neuronal firing mode in the cat and guinea pig dorsal lateral geniculate nucleus. J Neurosci 12:278-289.

McCormick DA (1992b) Neurotransmitter actions in the thalamus and cerebral cortex and their role in neuromodulation of thalamocortical activity. Prog Neurobiol 39:337-388.

McCormick DA, Prince DA (1988) Noradrenergic modulation of firing pattern in guinea pig and cat thalamic neurons, in vitro. J Neurophysiol 59:978-996.

McCormick DA, Pape HC (1990a) Noradrenergic and serotonergic modulation of a hyperpolarization-activated cation current in thalamic relay neurones. J Physiol 431:319-342.

McCormick DA, Feeser HR (1990) Functional implications of burst firing and single spike activity in lateral geniculate relay neurons. Neuroscience 39:103-113.

McCormick DA, Pape HC (1990b) Properties of a hyperpolarization-activated cation current and its role in rhythmic oscillation in thalamic relay neurones. J Physiol 431:291-318.

McCormick DA, Williamson A (1991) Modulation of neuronal firing mode in cat and guinea pig LGNd by histamine: possible cellular mechanisms of histaminergic control of arousal. J Neurosci 11:3188-3199.

McCormick DA, Huguenard JR (1992) A model of the electrophysiological properties of thalamocortical relay neurons. J Neurophysiol 68:1384-1400.

McCormick DA, von Krosigk M (1992) Corticothalamic activation modulates thalamic firing through glutamate "metabotropic" receptors. PNAS 89:2774-2778.

McCormick DA, Bal T (1997) Sleep and arousal: thalamocortical mechanisms. Annu Rev Neurosci 20:185-215.

Meuth S, Pape HC, Budde T (2002) Modulation of Ca2+ currents in rat thalamocortical relay neurons by activity and phosphorylation. Eur J Neurosci 15:1603-1614.

Mikula S, Niebur E (2006) A novel method for visualizing functional connectivity using principal component analysis. Int J Neurosci 116:419-429.

Milescu LS, Yamanishi T, Ptak K, Mogri MZ, Smith JC (2008) Real-time kinetic modeling of voltage-gated ion channels using dynamic clamp. Biophysical journal 95:66-87.

Mirman R (2006) Our Almost Impossible Universe. Lincoln, NE: iUniverse, Inc. .

Mitchison G (1991) Neuronal branching patterns and the economy of cortical wiring. Proc Biol Sci 245:151-158.

Montero VM (1986) Localization of gamma-aminobutyric acid (GABA) in type 3 cells and demonstration of their source to F2 terminals in the cat lateral geniculate nucleus: a Golgi-electron-microscopic GABA-immunocytochemical study. J Comp Neurol 254:228-245.

Mooney R, Madison DV, Shatz CJ (1993) Enhancement of transmission at the developing retinogeniculate synapse. Neuron 10:815-825.

Moran RJ, Stephan KE, Kiebel SJ, Rombach N, O'Connor WT, Murphy KJ, Reilly RB, Friston KJ (2008) Bayesian estimation of synaptic physiology from the spectral responses of neural masses. Neuroimage 42:272-284.

Morton KW, Mayers DF (2005) Numerical solution of partial differential equations : an introduction, 2nd Edition. Cambridge, UK ; New York: Cambridge University Press.

Mukherjee P, Kaplan E (1995) Dynamics of neurons in the cat lateral geniculate nucleus: in vivo electrophysiology and computational modeling. J Neurophysiol 74:1222-1243.

Mulle C, Steriade M, Deschenes M (1985) The effects of QX314 on thalamic neurons. Brain Res 333:350-354.

Nunez A, Curro Dossi R, Contreras D, Steriade M (1992) Intracellular evidence for incompatibility between spindle and delta oscillations in thalamocortical neurons of cat. Neuroscience 48:75-85.

Ohme M, Schierwagen A (1998) An equivalent cable model for neuronal trees with active membrane. Biol Cybern 78:227-243.

Pape HC (1996) Queer current and pacemaker: the hyperpolarization-activated cation current in neurons. Annu Rev Physiol 58:299-327.

Pape HC, Budde T, Mager R, Kisvarday ZF (1994) Prevention of Ca(2+)-mediated action potentials in GABAergic local circuit neurones of rat thalamus by a transient K+ current. J Physiol 478 Pt 3:403-422.

Parnas I, Segev I (1979) A mathematical model for conduction of action potentials along bifurcating axons. J Physiol 295:323-343.

Parri HR, Crunelli V (1998) Sodium current in rat and cat thalamocortical neurons: role of a non-inactivating component in tonic and burst firing. J Neurosci 18:854-867.

Pedroarena C, Llinas R (1997) Dendritic calcium conductances generate high-frequency oscillation in thalamocortical neurons. PNAS 94:724-728.

Pedroarena CM, Llinás R (2001) Interactions of synaptic and intrinsic electroresponsiveness determine corticothalamic activation dynamics. Thalamus and Related Systems 1:3-14.

Popper KR (2002) The logic of scientific discovery. London ; New York: Routledge.

Pospischil M, Piwkowska Z, Bal T, Destexhe A (2009) Extracting synaptic conductances from single membrane potential traces. Neuroscience 158:545-552.

Poznanski RR (1991) A generalized tapering equivalent cable model for dendritic neurons. Bull Math Biol 53:457-467.

Prinz AA, Billimoria CP, Marder E (2003) Alternative to hand-tuning conductance-based models: construction and analysis of databases of model neurons. J Neurophysiol 90:3998-4015.

Rall W (1959) Branching dendritic trees and motoneuron membrane resistivity. Exp Neurol 1:491-527.

Rall W (1960) Membrane potential transients and membrane time constant of motoneurons. Exp Neurol 2:503-532.

Rall W (1962a) Electrophysiology of a dendritic neuron model. Biophys J 2:145-167.

Rall W (1962b) Theory of physiological properties of dendrites. Ann N Y Acad Sci 96:1071-1092.

Rall W (1964) Theoretical significance of dendritic trees for neuronal input-output relations. In: In Neural Theory and Modeling (Reiss RF, ed): Stanford Univ. Press. .

Rall W (1969) Distributions of potential in cylindrical coordinates and time constants for a membrane cylinder. Biophys J 9:1509-1541.

Rall W, Shepherd GM (1968) Theoretical reconstruction of field potentials and dendrodendritic synaptic interactions in olfactory bulb. J Neurophysiol 31:884-915.

Rall W, Rinzel J (1973) Branch input resistance and steady attenuation for input to one branch of a dendritic neuron model. Biophys J 13:648-687.

Rall W, Shepherd GM, Reese TS, Brightman MW (1966) Dendrodendritic synaptic pathway for inhibition in the olfactory bulb. Exp Neurol 14:44-56.

Rall W, Segev I, Rinzel J, Shepherd GM (1995) The theoretical foundation of dendritic function : selected papers of Wilfrid Rall with commentaries. Cambridge, Mass.: MIT Press.

Ramcharan EJ, Gnadt JW, Sherman SM (2000) Burst and tonic firing in thalamic cells of unanesthetized, behaving monkeys. Vis Neurosci 17:55-62.

Reinagel P, Godwin D, Sherman SM, Koch C (1999) Encoding of visual information by LGN bursts. J Neurophysiol 81:2558-2569.

Remy S, Csicsvari J, Beck H (2009) Activity-dependent control of neuronal output by local and global dendritic spike attenuation. Neuron 61:906-916.

Rinzel J (1990) Mechanisms for nonuniform propagation along excitable cables. Ann N Y Acad Sci 591:51-61.

Rinzel J, Rall W (1974) Transient response in a dendritic neuron model for current injected at one branch. Biophys J 14:759-790.

Robinson HP, Kawai N (1993) Injection of digitally synthesized synaptic conductance transients to measure the integrative properties of neurons. J Neurosci Methods 49:157-165.

Rosenfalck P (1969) Intra- and extracellular potential fields of active nerve and muscle fibres. A physico-mathematical analysis of different models. Thromb Diath Haemorrh Suppl 321:1-168.

Rossi DJ, Brady JD, Mohr C (2007) Astrocyte metabolism and signaling during brain ischemia. Nat Neurosci 10:1377-1386.

Roy JP, Clercq M, Steriade M, Deschenes M (1984) Electrophysiology of neurons of lateral thalamic nuclei in cat: mechanisms of long-lasting hyperpolarizations. J Neurophysiol 51:1220-1235.

Rudy B (1988) Diversity and ubiquity of K channels. Neuroscience 25:729-749.

Rulkov NF, Timofeev I, Bazhenov M (2004) Oscillations in large-scale cortical networks: map-based model. J Comput Neurosci 17:203-223.

Schaefer AT, Larkum ME, Sakmann B, Roth A (2003) Coincidence detection in pyramidal neurons is tuned by their dendritic branching pattern. J Neurophysiol 89:3143-3154.

Schierwagen AK (1989) A non-uniform equivalent cable model of membrane voltage changes in a passive dendritic tree. J Theor Biol 141:159-179.

Segev I, Burke RE (1998) Compartmental models of complex neurons. In: Methods in neuronal modeling: From ions to networks, 2nd Edition (Koch C, Segev I, eds), pp 93-136 Cambridge, Mass.: MIT Press.

Sejnowski TJ, Koch C, Churchland PS (1988) Computational neuroscience. Science 241:1299-1306.

Sevush S (2006) Single-neuron theory of consciousness. J Theor Biol 238:704-725.

Sharp AA, Abbott LF, Marder E (1992) Artificial electrical synapses in oscillatory networks. J Neurophysiol 67:1691-1694.

Sharp AA, O'Neil MB, Abbott LF, Marder E (1993) Dynamic clamp: computer-generated conductances in real neurons. J Neurophysiol 69:992-995.

Sherman SM (2006) Thalamus. Scholarpedia 1:1583.

Sherman SM, Guillery RW (1996) Functional organization of thalamocortical relays. J Neurophysiol 76:1367-1395.

Sherman SM, Guillery RW (1998) On the actions that one nerve cell can have on another: distinguishing "drivers" from "modulators". PNAS 95:7121-7126.

Sherman SM, Guillery RW (2002) The role of the thalamus in the flow of information to the cortex. Philos Trans R Soc Lond B Biol Sci 357:1695-1708.

Sherman SM, Guillery RW (2006) Exploring the thalamus and its role in cortical function, 2nd Edition. Cambridge, Mass.: MIT Press.

Sjostrom PJ, Rancz EA, Roth A, Hausser M (2008) Dendritic excitability and synaptic plasticity. Physiol Rev 88:769-840.

Smith GD, Cox CL, Sherman SM, Rinzel J (2000) Fourier analysis of sinusoidally driven thalamocortical relay neurons and a minimal integrate-and-fire-or-burst model. J Neurophysiol 83:588-610.

Spruston N, Jaffe DB, Johnston D (1994) Dendritic attenuation of synaptic potentials and currents: the role of passive membrane properties. Trends Neurosci 17:161-166.

Steriade M (1997) Synchronized activities of coupled oscillators in the cerebral cortex and thalamus at different levels of vigilance. Cereb Cortex 7:583-604.

Steriade M (2000) Corticothalamic resonance, states of vigilance and mentation. Neuroscience 101:243-276.

Steriade M (2001) Impact of network activities on neuronal properties in corticothalamic systems. J Neurophysiol 86:1-39.

Steriade M (2004) Local gating of information processing through the thalamus. Neuron 41:493-494.

Steriade M, Deschenes M (1984) The thalamus as a neuronal oscillator. Brain Res 320:1-63.

Steriade M, Llinas RR (1988) The functional states of the thalamus and the associated neuronal interplay. Physiol Rev 68:649-742.

Steriade M, Timofeev I (1997) Short-term plasticity during intrathalamic augmenting responses in decorticated cats. J Neurosci 17:3778-3795.

Steriade M, Timofeev I (2003) Neuronal plasticity in thalamocortical networks during sleep and waking oscillations. Neuron 37:563-576.

Steriade M, McCarley RW (2005) Brain control of wakefulness and sleep, 2nd Edition. New York: Springer.

Steriade M, Paré D (2007) Gating in cerebral networks. Cambridge ; New York: Cambridge University Press.

Steriade M, Dossi RC, Nunez A (1991) Network modulation of a slow intrinsic oscillation of cat thalamocortical neurons implicated in sleep delta waves: cortically induced synchronization and brainstem cholinergic suppression. J Neurosci 11:3200-3217.

Steriade M, Curro Dossi R, Contreras D (1993a) Electrophysiological properties of intralaminar thalamocortical cells discharging rhythmic (approximately 40 HZ) spike-bursts at approximately 1000 HZ during waking and rapid eye movement sleep. Neuroscience 56:1-9.

Steriade M, McCormick DA, Sejnowski TJ (1993b) Thalamocortical oscillations in the sleeping and aroused brain. Science 262:679-685.

Steriade M, Jones EG, McCormick D (1997) Thalamus. Amsterdam ; New York: Elsevier.

Stuart G, Spruston N, Häusser M (2007) Dendrites, 2nd Edition. Oxford ; New York: Oxford University Press.

Stuart G, Spruston N, Sakmann B, Hausser M (1997) Action potential initiation and backpropagation in neurons of the mammalian CNS. Trends Neurosci 20:125-131.

Stuart GJ, Hausser M (2001) Dendritic coincidence detection of EPSPs and action potentials. Nat Neurosci 4:63-71.

Tennigkeit F, Schwarz DW, Puil E (1998) Modulation of bursts and high-threshold calcium spikes in neurons of rat auditory thalamus. Neuroscience 83:1063-1073.

Tennigkeit F, Schwarz DW, Puil E (1999) Modulation of frequency selectivity by Na+- and K+-conductances in neurons of auditory thalamus. Hear Res 127:77-85.

Thomson AM, Bannister AP (2003) Interlaminar connections in the neocortex. Cereb Cortex 13:5-14.

Timofeev I, Grenier F, Steriade M (2001) Disfacilitation and active inhibition in the neocortex during the natural sleep-wake cycle: an intracellular study. PNAS 98:1924-1929.

Toth TI, Hughes SW, Crunelli V (1998) Analysis and biophysical interpretation of bistable behaviour in thalamocortical neurons. Neuroscience 87:519-523.

Tsodyks M (2008) Computational neuroscience grand challenges - a humble attempt at future forecast. Front Neurosci 2:17-18.

Tuckwell HC, Walsh JB (1983) Random currents through nerve membranes. I. Uniform poisson or white noise current in one-dimensional cables. Biol Cybern 49:99-110.

Van Geit W, De Schutter E, Achard P (2008) Automated neuron model optimization techniques: a review. Biol Cybern 99:241-251.

van Pelt J, Schierwagen A (2004) Morphological analysis and modeling of neuronal dendrites. Math Biosci 188:147-155.

Vasku A, Holla L, Znojil V (1999) The best model of a cat is a cat, especially the same cat. Exp Hematol 27:187-188.

Venance L, Rozov A, Blatow M, Burnashev N, Feldmeyer D, Monyer H (2000) Connexin expression in electrically coupled postnatal rat brain neurons. PNAS 97:10260-10265.

Vetter P, Roth A, Hausser M (2001) Propagation of action potentials in dendrites depends on dendritic morphology. J Neurophysiol 85:926-937.

Wang X-J (2010) Neurophysiological and Computational Principles of Cortical Rhythms in Cognition. Physiol Rev 90:1195-1268.

Weaver CM, Wearne SL (2008) Neuronal firing sensitivity to morphologic and active membrane parameters. PLoS Comput Biol 4:e11.

Weiss TF (1996) Cellular biophysics. Cambridge, Mass.: MIT Press.

Wen Q, Stepanyants A, Elston GN, Grosberg AY, Chklovskii DB (2009) Maximization of the connectivity repertoire as a statistical principle governing the shapes of dendritic arbors. PNAS 106:12536-12541.

Williams SR, Stuart GJ (2000) Action potential backpropagation and somato-dendritic distribution of ion channels in thalamocortical neurons. J Neurosci 20:1307-1317.

Williams SR, Stuart GJ (2003) Role of dendritic synapse location in the control of action potential output. Trends Neurosci 26:147-154.

Wilson JR, Friedlander MJ, Sherman SM (1984) Fine structural morphology of identified X- and Y-cells in the cat's lateral geniculate nucleus. Proc R Soc Lond B Biol Sci 221:411-436.

Wu LG, Borst JG, Sakmann B (1998) R-type Ca2+ currents evoke transmitter release at a rat central synapse. PNAS 95:4720-4725.

Zhan XJ, Cox CL, Sherman SM (2000) Dendritic depolarization efficiently attenuates low-threshold calcium spikes in thalamic relay cells. J Neurosci 20:3909-3914.

Zhan XJ, Cox CL, Rinzel J, Sherman SM (1999) Current clamp and modeling studies of low-threshold calcium spikes in cells of the cat's lateral geniculate nucleus. J Neurophysiol 81:2360-2373.

Zhang Y, Bose A, Nadim F (2009) The influence of the A-current on the dynamics of an oscillator-follower inhibitory network. SIAM J Appl Dyn Syst 8:1564-1590.

Zhou Q, Godwin DW, O'Malley DM, Adams PR (1997) Visualization of calcium influx through channels that shape the burst and tonic firing modes of thalamic relay cells. J Neurophysiol 77:2816-2825.

Zomorrodi R, Kroger H, Timofeev I (2008) Modeling thalamocortical cell: impact of ca channel distribution and cell geometry on firing pattern. Front Comput Neurosci 2:5.